

HYDROCARBON OXIDATION USING MOLECULAR OXYGEN AND
HYDROGEN PEROXIDE CATALYZED BY TRANSITION METAL COMPLEXES

By

ANA ISON

A DISSERTATION PRESENTED TO THE GRADUATE SCHOOL
OF THE UNIVERSITY OF FLORIDA IN PARTIAL FULFILLMENT
OF THE REQUIREMENTS FOR THE DEGREE OF
DOCTOR OF PHILOSOPHY

UNIVERSITY OF FLORIDA

2004

Dedicated to my husband Elon and daughter Mya, my favorite people in the world.

ACKNOWLEDGMENTS

The past 5 years have been full of joy and sadness, success and defeat, determination and loss of hope. There are many people who have helped me look past the hard times. Intentionally or not they were instrumental in pushing me toward reaching my goal.

I will start by thanking my advisor Dr. David E. Richardson. He has been the ideal mentor, always skillfully steering me in the right direction, while making me feel like I was the one figuring everything out. He has always treated me with respect and understanding, and I will always appreciate that. Most importantly I would likely not be writing this if not for Dr. Richardson's encouragement. He has always understood why this process was so difficult for me, but he never let me quit.

Dr. Khalil Abboud has been a great mentor and friend over the years. I very much appreciate the opportunity to spend 2 years working with him at the x-ray crystallography lab. Dr. Abboud has always been there to lend a helping hand or a word of encouragement.

I extend my appreciation to Dr. Michael Gonzalez for giving me the opportunity to participate in a joint project with the EPA during my last year.

During my time at UF, I have met some really fine people. I will never forget my Serbian brethren (Ivana Bozidarevic, Nebojca Ciric, Tamara Blagojevic, Ksenija Glusac-Haskins, Aleksa Jovanovic and many others). Besides helping me perfect my native language, these folks have been good friends and great company.

Richardson lab members past and present have provided for an interesting work environment. Dr. Ken Weakley was my southern conservative foe. I hated to see him leave, but I could not wait to get Rush off the radio! As much as our opinions differed on many fronts, we got along great. Ken is truly a one-of-a-kind guy, and I appreciate his help in getting started in the lab. Dr. Deon Bennett has continued to be a good friend even after leaving the lab. Celeste Regino and “The Guys” (Dan Denevan, Andy Burke and Mike Mitchell) have definitely brought some good laughs to the lab. I give special thanks to “The Guys” for putting up with my more moody days.

Most of all, I have to thank my family. My father and mother, Ivan and Duska Bitanga, I thank for providing for me over the years. My mom especially has always encouraged me not to give up on my graduate studies. My brother, Tom Bitanga and his family I thank for their continued support.

My husband Elon has probably been one of the most influential people in my life. He has been my best friend and my harshest critic. Without him by my side, I would never have been able to finish this endeavor. Although I didn’t always appreciate his insistence that I need to finish what I started, I have to admit that he was right.

Finally I have a debt of gratitude to pay to my sweet little girl Mya. She was born into this world just as Elon and I were beginning our graduate careers and she has made it through along with us. It wasn’t always easy for her when mommy and daddy were too tired to play, or read that extra book. She has helped to keep me sane during my darkest hours, and always managed to put a smile on my face when I needed it most. I love her more than anything in this entire world, and I can only hope that she never forgets that.

TABLE OF CONTENTS

	<u>page</u>
ACKNOWLEDGMENTS	iii
LIST OF TABLES	viii
LIST OF FIGURES	x
ABSTRACT.....	xiv
 CHAPTER	
1 INTRODUCTION	1
Molecular Oxygen as Terminal Oxidant	1
Free-Radical Autoxidation	1
Metal-Catalyzed Peroxide Decomposition.....	3
Electron-Transfer Mechanism.....	8
Metal-Mediated Molecular Oxygen Activation	11
Hydrogen Peroxide as Terminal Oxidant	14
Alkene Epoxidation by Early Transition-Metal Catalysts.....	14
Metal Porphyrin Catalysts	16
The Mn-Salen Assymmetric Catalysts	18
The Mn ²⁺ /HCO ₃ ⁻ /H ₂ O ₂ Catalyzed Alkene Epoxidation	18
Scope of the Dissertation	20
 2 IRON (II) α,α' -DIIMINE CATALYZED HYDROCARBON AUTOXIDATION ...	 22
Introduction.....	22
Results and Discussion	26
Catalyzed Cumene Autoxidation.....	26
Catalyzed Cumyl Peroxide Decomposition.....	30
Proposed Mechanism.....	32
Solvent Dependence	42
Oxygen Pressure and Temperature Dependence	44
Metal Concentration Dependence	45
Ligand Dissociation Studies	47
Precursor Degradation	50
Co-oxidation by Reaction Products.....	51
Active Catalyst Lifetime.....	55

	Ligand variation studies	55
	Conclusions.....	59
3	HYDROCARBON OXIDATION CATALYZED BY FeL_2X_2 COMPLEXES.....	61
	Introduction.....	61
	Results and Discussion	63
	Cumene Oxidation.....	69
	Solution-state studies of Fedmp	71
	Conclusions.....	77
4	COMPARISON OF FeL_3X_2 TO KNOWN AUTOXIDATION CATALYSTS.....	79
	Introduction.....	79
	Results and Discussion	79
	Fe and Co Acetylacetonates	79
	Fe Complexed by Macrocyclic Ligands.....	80
	Fe Complexed by Hexa and Tetra Coordinating Pyridyl Ligands	81
	Poly-Nuclear Iron Complexes	88
	Conclusions.....	90
5	ALKENE EPOXIDATION CATALYZED BY TRANSITION METAL COMPLEXES USING BICARBONATE-ACTIVATED PEROXIDE (BAP)	91
	Sulfonated Styrene Epoxidation with Mn(II) porphyrin/BAP	91
	Introduction.....	91
	Results and Discussion	92
	Styrene Epoxidation with Jacobson's Catalyst/BAP	96
	Introduction.....	96
	Results and Discussion	98
	Conclusions.....	103
6	SUMMARY.....	104
7	EXPERIMENTAL.....	107
	General.....	107
	Materials	107
	Kinetic Modeling.....	108
	Oxidation Experiments	108
	Peroxide Decomposition Experiments	108
	Sulfonated Styrene Epoxidation	109
	HPLC Analysis	109
	Styrene Epoxidation.....	109
	Synthesis.....	110
	APPENDIX-VARIATIONS IN RATE CONSTANTS.....	114

LIST OF REFERENCES.....	119
BIOGRAPHICAL SKETCH	125

LIST OF TABLES

<u>Table</u>	<u>page</u>
2-1. Catalyzed oxidation of cumene.....	28
2-2. Effects of ROOH and H ₂ O on induction period	29
2-3. Experimental and calculated oxygen equivalents accounted for in products ROOH, ROH and RO.	36
2-4. Simulated and experimental results for uncatalyzed cumene autoxidation.	42
2-5. Solvent effects on cumene oxidation catalyzed by 1	42
2-6. Variation of ligand equivalents.....	47
2-7. Cumene oxidation catalyzed by Ru analogue of 1	48
2-8. Counter ion effects.....	50
2-9. Co-oxidation studies	52
2-10. Catalysis by products in the absence of 1	54
2-11. Bond dissociation energies.	55
2-12. Cumene oxidation and peroxide decomposition data of reactions catalyzed by FeL ₃ X ₂ complexes.	58
3-1. Cyclohexane oxidation catalyzed by Fedmp.	66
3-2. Products from cyclohexane oxidation catalyzed by 1 and Fedmp.....	68
3-3. Cumene oxidation catalyzed by Fedmp.....	69
3-4. Cumene oxidation catalyzed by Fephen ₂ X ₂ complexes.....	76
4-1. Cumene oxidation catalyzed by Fe and Co acetyl acetonates.	80
4-2. Cumene oxidation catalyzed by Fe(II)Pc and Fe(II)cyclam.	81
4-3. Cumene autoxidation catalyzed by Co and Fe complexes.....	83

4-4.	Cumene oxidation catalyzed by μ -oxo Fe complexes.	89
4-5.	Catalytic activity of di-nuclear Fe complexes in cyclohexane oxidation.	90
5-1.	Styrene oxide yields using different solvent systems.	98
5-2.	Experimental epoxide conversion.....	98
5-3.	Determination of enantiomeric selectivity.....	101
5-4.	Epoxidation data	103

LIST OF FIGURES

<u>Figure</u>	<u>page</u>
1-1. Radical steps for uncatalyzed hydrocarbon autoxidation.	3
1-2. Haber-Weiss cycle.	4
1-3. Proposed catalytic cycle for the activation of molecular oxygen and oxygen transfer to alkanes in cytochrome P-450.....	7
1-4. Mid-Century process for terephthalic acid synthesis.....	8
1-5. Electron transfer mechanism in $\text{Co}(\text{OAc})_2$ catalyzed mechanism of p-xylene oxidation.	9
1-6. Examples of metal-molecular oxygen binding modes.....	11
1-7. Selective ethylene epoxidation over a supported silver catalyst.....	12
1-8. Proposed catalytic cycle for oxygen transfer to $\text{P}(\text{Ph})_3$	13
1-9. Selective oxygen transfer to pendant ligand.	14
1-10. Epoxidation of propylene by high valent, early transition metal complexes.....	15
1-11. Active oxidant in MTO-catalyzed epoxidation reactions.	16
1-12. Proposed mechanism of epoxidation co-catalyzed by imidazole.	17
1-13. Equilibrium formation of peroxycarbonate.	19
1-14. Mn^{2+} /BAP catalyzed oxidation of alkenes.....	20
2-1. $[\text{Fe}(\text{4,7-diphenyl-1,10-phenanthroline})_3]^{2+}(\text{CF}_3\text{SO}_3^-)_2$ (1).....	23
2-2. tetra-(pentafluorophenyl)-porphyrin iron(III) chloride (2)	25
2-3. Products of metal-catalyzed cumene autoxidation.	26
2-4. Formation of CO and CO_2 over time in cumene oxidation catalyzed by 1	27
2-5. Cumene oxidation catalyzed by 1	28

2-6.	Oxygen uptake curves for 1 and 2 catalyzed oxidation.	29
2-7.	Metal-catalyzed peroxide decomposition.	31
2-8.	Plots of $\ln [\text{ROOH}]$ vs. time	31
2-9.	Mechanism of metal catalyzed cumene autoxidation	34
2-10	Disproportionation pathways of alkyl tetroxide.	35
2-11.	Simulation of cumene oxidation catalyzed by 1	38
2-12.	Simulation of cumyl peroxide decomposition catalyzed by 1	39
2-13.	Simulation of cumene oxidation catalyzed by 2	39
2-14.	Simulation of cumyl peroxide decomposition catalyzed by 2	40
2-15.	Simulation of ROOH initiated cumene oxidation catalyzed by 1	40
2-16.	Simulation of ROOH initiated cumene oxidation catalyzed by 2	41
2-17.	GC trace of sample after 5h of uncatalyzed reaction.	41
2-18.	Oxygen uptake curves in cumene oxidation catalyzed by 1 in different solvents.	43
2-19.	Dependence of rate of oxygen uptake on oxygen pressure.	44
2-20.	Temperature effects on product selectivity for cumene oxidation catalyzed by 1	45
2-21.	Experimental and calculated dependence of catalyst concentration on rate of oxygen uptake.	46
2-22.	Formation of FeL_2X_2 from 1 in the presence of LiCl.	49
2-23.	Spectral changes of 1 at 60 °C in the presence of ROOH.	51
2-24.	Product formation and oxygen uptake in cumene oxidation catalyzed by 1 in the presence of α -methyl styrene.	53
2-25.	Proposed mechanism of α -methyl styrene formation.	54
2-26.	Comparison of oxygen uptake curve during cumene oxidation catalyzed by 1 and a curve predicted by simulation using proposed mechanism.	55
2-27.	Numbering scheme for the phen ligand.	56

2-28.	Oxygen uptake curves during cumene autoxidation catalyzed by FeL_3X_2 complexes.	58
3-1.	Proposed mechanism for the activation of O_2 by FeL_2X_2	62
3-2.	Examples of radical traps.....	62
3-3.	$[\text{cis-Fe}(\text{2,9-dimethylphenanthroline})_2(\text{H}_2\text{O})_2](\text{SO}_3\text{CF}_3)_2$ (Fedmp).	63
3-4.	Products of the air oxidation of cyclohexane.....	64
3-5.	GC trace after 4h of cyclohexane oxidation catalyzed by Fedmp.	65
3-6.	Oxygen uptake curves for Fedmp catalyzed cyclohexane oxidation.....	66
3-7.	GC trace of cyclohexane oxidation in 50/50 cyclohexane/DCB	67
3-8.	Oxygen uptake curves for cyclohexane oxidation catalyzed by 1 and Fedmp.....	68
3-9.	Oxygen uptake curve during cumene oxidation catalyzed by Fedmp at 60 °C.	70
3-10.	GC trace of sample taken after 2 h of cumene oxidation catalyzed by Fedmp.	70
3-11.	Top; 2,9-dimethylphenanthroline (dmp), Bottom; Fedmp in d_6 -acetone.	71
3-12.	Variable temperature ^1H -NMR spectrum of Fedmp in d_6 -acetone.....	73
3-13.	^1H -NMR spectrum of $\text{Fephen}_2\text{CN}_2$	75
3-14.	Oxygen uptake curves during cumene oxidation catalyzed by $\text{Fephen}_2\text{X}_2$ complexes.	77
4-1.	Structures of macrocyclic ligands.....	80
4-2.	Structures of tpa and tpen ligands.....	83
4-3.	Comparison of oxygen uptake curves during cumene oxidation.....	84
4-4.	Proposed mechanism of α,α -dimethyl benzyl methyl ether formation.....	84
4-5.	Cumyl peroxide (ROOH) decomposition catalyzed by Fetpa.	85
4-6.	^1H -NMR spectra in acetonitrile- d_3	86
4-7.	Oxygen uptake curve in cumene oxidation catalyzed by $\text{Fe}(\text{SO}_3\text{CF}_3)_2$	87
4-8.	Structure of complex 3 and 4	88
4-9.	Structures of di-nuclear iron complexes.	89

5-1.	Equilibrium formation of peroxy carbonate.	92
5-2.	Mn(III) meso-tetrakis(4N-methylpyridinium)porphyrin (MnTMPyP).....	93
5-3.	MnTMPyP/BAP catalyzed room temperature epoxidation of sulfonated styrene.	93
5-4.	¹ H-NMR spectrum after 60 min of reaction.	94
5-5.	HPLC trace of reaction solution after 6 min.....	95
5-6.	ln[SS] vs. time plots.....	95
5-7.	Fast decomposition of MnTMPyP in the presence of BAP.....	96
5-8.	Proposed mechanism of Mn(III)-salen catalyzed epoxidation.	97
5-9.	Jacobson's catalyst.....	98
5-10.	Pseudocontact shift equation.....	99
5-11.	¹ H-NMR spectrum of a standard styrene sample (top) and styrene in the presence of a shift reagent (bottom).....	100
A-1.	Variation in k_1 ($RH \rightarrow R\cdot$)	114
A-2.	Variation in k_2 ($ROO\cdot + RH \rightarrow ROOH + R\cdot$)	115
A-3.	Variation in k_3 ($2 ROO\cdot \rightarrow 2 RO\cdot + O_2$).....	115
A-4.	Variation k_4 ($2 ROO\cdot \rightarrow ROOR + O_2$).....	116
A-5.	Variation in k_5 ($RO\cdot + RH \rightarrow ROH + R\cdot$).....	116
A-6.	Variation in k_6 ($RO\cdot + ROOH \rightarrow ROH + ROO\cdot$)	117
A-7.	Variation in k_7 ($RO\cdot \rightarrow R'O + Me\cdot$)	117
A-8.	Variation in k_{12} ($ROOH + M^{III} \rightarrow ROO\cdot + H^+ + M^{II}$).....	118
A-9.	Variation in k_{13} ($ROOH + M^{II} \rightarrow RO\cdot + HO^- + M^{III}$).	118

Abstract of Dissertation Presented to the Graduate School
of the University of Florida in Partial Fulfillment of the
Requirements for the Degree of Doctor of Philosophy

HYDROCARBON OXIDATION USING MOLECULAR OXYGEN AND
HYDROGEN PEROXIDE CATALYZED BY TRANSITION METAL COMPLEXES

By

Ana Ison

August 2004

Chair: David E. Richardson
Major Department: Chemistry

The catalytic activity of coordination complex [Fe(4,7-diphenyl-1,10-phenanthroline)₃](SO₃CF₃)₂ (**1**) has been investigated in the autoxidation of cumene in the presence of molecular oxygen. Reaction products include 2-phenyl-2-propanol, cumyl hydroperoxide, acetophenone, and traces of dicumyl peroxide. Parallel experiments were done comparing the catalytic activity of **1** to that of a fluorinated iron porphyrin (tetra-pentafluorophenylporphyrin iron(III) chloride (**2**), and the catalytic activities of **1** and **2** are comparable. Our detailed kinetic studies and UV-visible spectrophotometry support a radical autoxidation mechanism, in which the catalytic decomposition of alkyl hydroperoxides generates free-radical autoxidation chain carriers as described previously for halogenated porphyrin catalysts. The kinetics of the disproportionation of cumyl hydroperoxide were determined, and the catalytic rate constants for **1** and **2** were incorporated into a complete kinetic model that fits both autoxidation and peroxide-decomposition data. The inactivity of the Ru analog of **1** and

other experiments suggest that ligand dissociation is crucial in the activation of **1**.

Related FeL_3X_2 , FeL_2X_2 (L=substituted 1,10-phenanthroline; X=anionic counter-ion), and FeL_nX_n (L=tetra,penta,hexa-dentate nitrogen donor ligands) were also investigated and their catalytic reactivity examined in the context of the metal catalyzed peroxide decomposition mechanism.

The advantages of using bicarbonate activated peroxide (BAP) versus H_2O_2 alone as the oxidant in the presence of known epoxidation catalysts were investigated. The room-temperature epoxidation of sulfonated styrene in water was catalyzed by Mn(III)porphyrin/BAP, and resulted in formation of the epoxide with high conversion and selectivity. The rate of epoxidation catalyzed by Mn(III)porphyrin/BAP was found to be comparable to the free Mn^{2+} /BAP system, suggesting catalyst decomposition. The MnTMPyP degraded quickly under the reaction conditions, releasing free Mn^{2+} into the solution. Presumably the resulting epoxide was formed through the well-known free manganese-catalyzed pathway.

Asymmetric epoxidation of styrene catalyzed by Jacobson's catalyst using BAP as an oxidant was also studied. Moderate enantioselectivity was achieved in a biphasic solvent system. Other anionic salts such as AcO^- resulted in similar product enantioselectivity, suggesting that (unlike in the free Mn^{2+} /BAP system), peroxymonocarbonate (peroxy acid formed in the BAP system) was not essential in forming the active catalytic species.

CHAPTER 1 INTRODUCTION

Molecular Oxygen as Terminal Oxidant

The use of molecular oxygen as a terminal oxidant in metal catalyzed oxidation of hydrocarbons has been an area of vigorous and intense research mainly because of the environmental and economic advantages of using dioxygen in place of peroxides, peracids or iodoarenes. The ultimate goal is to develop a catalytic system that mimics the enzyme-mediated activation of molecular oxygen and results in the low temperature, highly selective oxygen transfer to a substrate. The various mechanisms by which metals catalyze autoxidation of hydrocarbons can be separated into three broad categories: 1) metal catalyzed decomposition of intermediate peroxide, 2) direct attack on the substrate by the metal complex, 3) direct activation of molecular oxygen by the metal complex.^{1,2} The mechanism is dependent on the solvent system, ligands surrounding the metal and the substrate. Examples of each mechanism type are described next.

Free-Radical Autoxidation

The importance of molecular oxygen in oxidation was realized as far back as the 18th century with Lavoisier's explanation of combustion.¹ Later observations suggested that the deterioration of many organic materials (such as rubber and natural oils) results from oxygen absorption. Further studies lead to the recognition that organic peroxides were the primary products of these oxidative processes, and the free-radical chain theory of autoxidation that was established in the 1940s^{3,4} The liquid-phase autoxidation of hydrocarbons has been studied extensively since that time, and the well-established

radical mechanism is shown in Figure 1-1. Autoxidation reactions are recognized for having long induction periods, because of the thermodynamically unfavorable C-H bond cleavage in the first step. The direct reaction between RH and O₂ is spin forbidden. Molecular oxygen has two unpaired electrons in the ground state and is paramagnetic. The highest occupied molecular orbitals are two degenerate π^* orbitals; therefore, electron pairing is energetically unfavorable. Molecular oxygen is in a triplet state, whereas the substrate is in a singlet state. The spin-conservation rule forbids the interaction of the two species in the ground state. Despite the difference in multiplicity, hydrocarbons are oxidized in the presence of molecular oxygen mainly due to the presence of peroxidic impurities.

The initial radical-forming step k_i is thought to occur through hydrogen abstraction from RH by trace peroxidic impurities. The addition of molecular oxygen to the R· radical is diffusion controlled ($>10^9 \text{ M}^{-1}\text{s}^{-1}$), even below atmospheric pressure. The radical-propagation step k_p involves hydrogen abstraction by the alkyl peroxy radical (ROO·) to form alkyl hydroperoxide and chain carrying ROO· radical. Termination of peroxy radicals occurs through a bimolecular reaction, to form secondary oxidation products. Step k_t is an oversimplification of a complex series of steps leading to both radical and nonradical products. The precise steps are substrate dependent, and can include the formation of alcohols, ketones, epoxides, carboxylic acids, aldehydes, CO, CO₂ and other products. Once the concentration of alkyl hydroperoxide is high enough, k_p becomes rate limiting. This marks the end of the induction period and the start of rapid substrate oxidation. Since the primary products such as peroxide, alcohol and

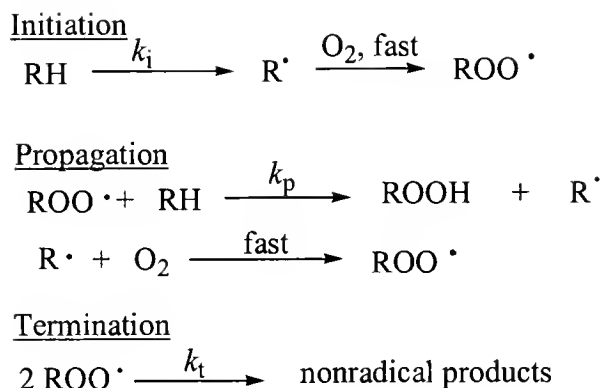


Figure 1-1. Radical steps for uncatalyzed hydrocarbon autoxidation

ketone are more oxidizable than the substrate, secondary reactions of those products are common, resulting in poor selectivity. The utility of synthesis of useful products from saturated hydrocarbons under autoxidizing conditions is limited because of the high reaction temperatures needed to overcome the long induction period, and poor selectivity. The addition of metal salts in catalytic amounts was observed to shorten the induction period and allow for lower reaction temperatures and increased selectivity.^{1,5} This discovery prompted interest in developing autoxidation catalysts capable of autoxidizing hydrocarbons selectively.

Metal-Catalyzed Peroxide Decomposition

Many of the early investigations used low concentrations of Mn, Fe, Co, and Cu acetates, naphthanates, and phthalocyanines to allow for a shorter induction period, lower reaction temperatures, and increased selectivity.^{1,6-8} Although the addition of such catalysts does lead to some desired results, the selectivity of the reactions remains poor unless the conversion is kept low. Nonetheless, metal-catalyzed autoxidation in neat hydrocarbon is used in major industrial processes, for the synthesis of adipic acid from cyclohexane. The autoxidation of cyclohexane to form ketone and alcohol (K/A oil) is done at 150-160°C and catalyzed by Co-naphthenate.⁹ The cobalt catalyst used is soluble

in neat cyclohexane, and does not require the use of co-solvent. High selectivity (ca. 70%) toward K/A oil is maintained by removing the products at a low conversion (ca. 10%). Further direct oxidation of the K/A oil with HNO_3 forms adipic acid, a monomer in the synthesis of nylon 6,6.^{1,2}

The widely accepted mechanism of metal-catalyzed autoxidation carried out neat or in non-polar solvent, occurs through the metal catalyzed decomposition of alkyl peroxides. The presence of a metal catalyst leads to an increase in the rate of formation of chain-carrying radicals.^{1,5,8,10} Therefore, the radical-chain mechanism describing uncatalyzed autoxidation (Figure 1-1) is unchanged other than the addition of metal-catalyzed peroxide decomposition steps referred to as the Haber-Weiss mechanism (Figure 1-2).¹

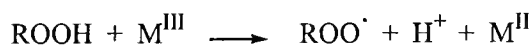
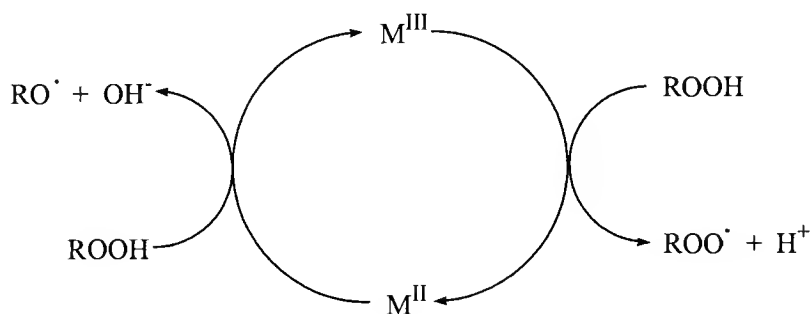


Figure 1-2. Haber-Weiss cycle

Many early investigations of metal-catalyzed autoxidation attempted to develop a more detailed description of the metal-peroxide interaction.^{1,2,11} Numerous active species, such as peroxy metal complexes, substrate adducts and dimers have been

proposed to explain the complex kinetic dependence on metal concentration; however, none have been unambiguously characterized.¹¹

Another important feature of metal-catalyzed autoxidation reactions is the presence of a maximum rate of oxidation.^{1,12} The maximum theoretical rate of oxidation is dependent on the substrate and is determined by the propagation and termination rate constants. Equation 2-1 is used to calculate the maximum rate,

$$-dO_2/dt = \frac{k_p^2 [RH]^2}{2 k_t} \quad (2-1)$$

where k_p and k_t are the propagation and termination rate constants, respectively.¹²

Equation 2-1 holds true in the presence of metal catalysts, as long as they do not catalyze the propagation and termination steps. Because the major function of the catalyst is to decompose the intermediate peroxide while the uncatalyzed steps remain unchanged, the rate of oxidation cannot exceed that inherently governed by the substrate. Hence the rate of metal-catalyzed autoxidation can be increased only up to a limiting value when the steps in Figures 1-1 and 1-2 apply.

For a number of years, the most active autoxidation catalyst used in hydrocarbon media was Co-naphthenate in the industrial oxidation of cyclohexane. More recently Fe(III) halogenated porphyrin complexes were shown to catalyze the air oxidation of saturated C-H bonds at room temperature.¹³⁻¹⁵ Initial interest in using iron porphyrins arose from the desire to mimic highly selective room-temperature oxidation using molecular oxygen as exhibited by mono and dioxygenases. The porphyrins especially have generated much interest because of their function in hemoproteins, and because they

are known to participate in oxygen transport (hemoglobin, myoglobin), electron transport (cytochrome c), and redox chemistry (cytochromes P-450 and peroxidases).¹

Cytochrome P-450 in particular catalyzes the activation and insertion of molecular oxygen into many substrates. The highly selective hydroxylation carried out by P-450 is proposed to be carried out by the high oxidation state oxoiron(IV) heme(protoporphyrin IX)⁺. The general scheme used to describe the mechanism of P-450 hydroxylation is shown in Figure 1-3.¹ The electrons and protons needed by the enzyme to complete the catalytic cycle are provided by cofactors such as NADP and ascorbate. Because of the similarity of the porphyrin ligand to that found in P-450, the initially proposed mechanism of Fe(III)porphyrin catalyzed air oxidation of alkanes was that of activation of molecular oxygen to form the high oxidation oxometal species.¹³ Further investigation by Labinger et al.^{16,17} showed that a radical peroxide decomposition mechanism was more suitable to describe the reactivity of the Fe(III) halogenated porphyrins. Although the Fe(III) halogenated porphyrins have similar characteristics as enzymatic systems that clearly does not necessarily lead to the same kind of reactivity. The ligand environment in the enzyme is highly controlled, and the substrate is isolated at the active site.¹⁸ Although radicals are often formed in enzymatic systems, radical-chain reactions are less favored, compared to reactions catalyzed by simple metal complexes. Furthermore the cycle described in Figure1-3 is difficult to imagine in the absence of coupled proton and electron donors.

An interesting example of a catalytic system employing reducing agents as found in enzymatic oxidations is the Gif family of catalysts. Barton et al.^{19,20} developed a system for oxidation and oxidative functionalization of alkanes under mild conditions.

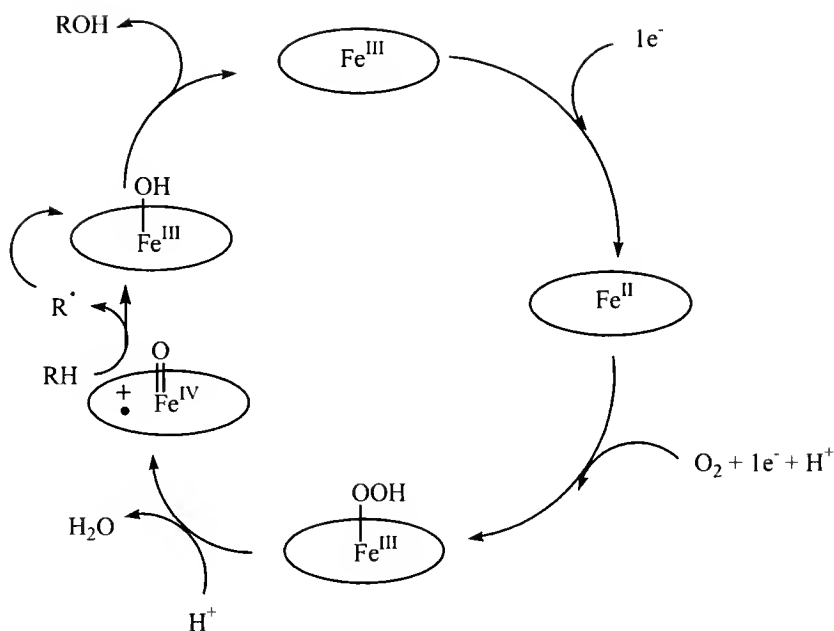


Figure 1-3. Proposed catalytic cycle for the activation of molecular oxygen and oxygen transfer to alkanes in cytochrome P-450

The reactions use pyridine as solvent in the presence of an organic acid (acetic acid), and are catalyzed by mainly Fe complexes in the presence of a reductant (Zn^0 , Fe^0 , Cu^0). Simple sources of iron were used such as FeCl_2 , FeCl_3 , or trinuclear oxo-centered complexes such as $[\text{Fe}_3\text{O}(\text{O}_2\text{CCH}_3)_6(\text{py})_3]^{3+}$.²¹ The primary reaction products are ketones; and C-H bond selectivity follows the unusual order of $2^\circ > 3^\circ > 1^\circ$, based on adamantane oxidation. There is disagreement whether the mechanism is a free-radical chain reaction or nonradical metal-centered catalysis.^{22,23} Product profiles and KIE values obtained from the catalytic oxidation of a number of substrates are not in full agreement with a purely radical mechanism or the involvement of a high oxidation oxometal species.

Oxidation of olefins leads mainly to ketone products and not epoxides as would be expected in case of a selective metal-centered mechanism.²⁴ The details of the Gif mechanism are largely a topic of debate, and are not completely understood. The Gif

reactions are an example of the dramatic effects solvent and additives can have on a mechanism.

Electron-Transfer Mechanism

The Co catalyzed oxidation of p-xylene is an industrially important reaction used in the production of terephthalic acid, a starting material in polymer synthesis.⁵ The Mid-Century process where the reaction is carried out in acetic acid in the presence of relatively high concentrations of Co(OAc) (~0.1M) is shown in Figure 1-4.

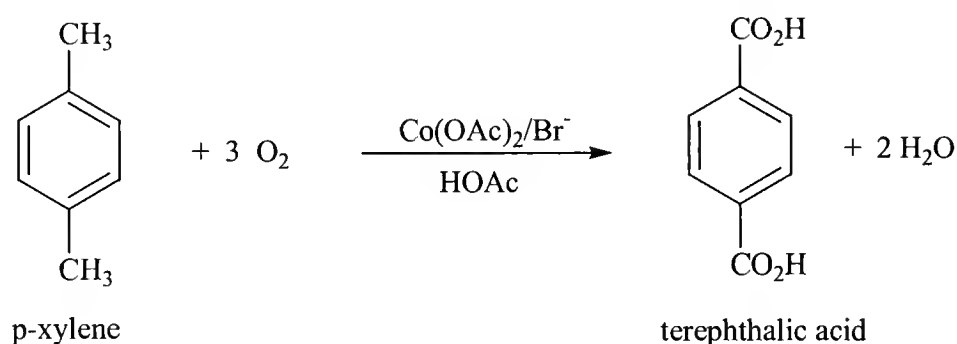
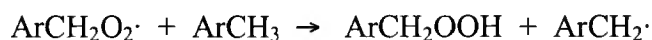


Figure 1-4. Mid-Century process for terephthalic acid synthesis

Strong oxidants such as Co(OAc)₃ are able to abstract an electron from the substrate resulting in the formation of a resonance-stabilized radical cation, followed by loss of a proton to form a benzyl radical. Under autoxidizing conditions, the benzyl radical is trapped by oxygen to form a benzylperoxy radical followed by reaction with another equivalent of the catalyst to form an aldehyde. Further oxidation to the carboxylic acid occurs easily under the reaction conditions (Figure 1-5).^{1,10} High concentration of the catalyst is needed for Co(II) to trap the benzylperoxy radical and circumvent the usual radical chain reaction of alkylperoxy radicals shown below.



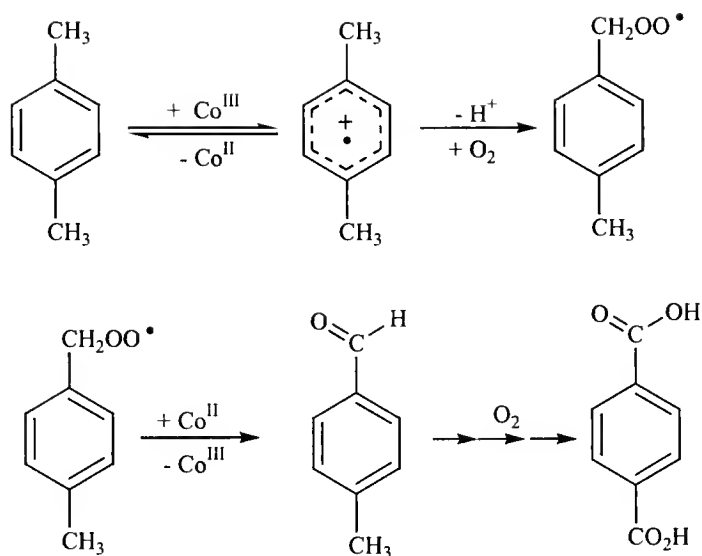
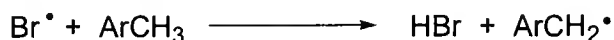


Figure 1-5. Electron transfer mechanism in $\text{Co}(\text{OAc})_2$ catalyzed mechanism of p-xylene oxidation

The rate of electron-transfer reactions is governed by the ionization potential of the substrate; therefore, the complete oxidation to terephthalic acid is retarded because of the significantly higher ionization potential of the intermediate p-toluic acid. Additives such as halide salts are often used to promote the complete oxidation to terephthalic acid as is the case in the Mid-century process (Figure 1-4).¹ Reaction of the $\text{Co}(\text{OAc})_2$ with Br^- results in the formation of bromine atoms that become the chain transfer agents in place of the $\text{Co}(\text{III})$ as shown below.



The abundance and low cost of butane make it a major feedstock for acetic acid production. The oxidation of n-butane at 100-125°C in the presence of large amounts of $\text{Co}(\text{OAc})_2$ and promoter in acetic acid results in 80% conversion of n-butane with 83% selectivity to acetic acid.⁵ The active catalyst is proposed to be a $\text{Co}(\text{III})$ species responsible for electron transfer from the substrate. Details of the mechanism are similar to those of p-xylene oxidation described above, although the mechanism is more

complicated because C-C bond cleavage occurs along with C-H bond cleavage. High concentration of the Co(III) species is maintained by the presence of promoters such as ozone, methyl ethyl ketone, and 2-butanone. Ozone is a strong oxidant and the two ketones easily form radicals that are responsible for oxidizing the Co(II).¹

Selective single-step oxidation of cyclohexane to form adipic acid has been a major goal in industry because the acid is an important intermediate in the production of nylon.⁵ The selective oxidation of cyclohexane can be achieved under conditions similar to those described above. Oxidation using high concentrations of Co(II) acetate in acetic acid at 80-100°C leads to 80% conversion of cyclohexane and the formation of adipic acid with 75% selectivity.²⁵ Such high selectivities are unusual in a free-radical mechanism; therefore, an electron transfer mechanism was proposed. The reactions exhibited an induction period that ended with the conversion of Co(II) to Co(III) in solution. Therefore, direct attack of the metal complex on the substrate is suggested. Adding radical-forming initiators such as acetaldehyde, cyclohexanone, and AIBN can shorten the induction period. Another observation supporting an electron-transfer mechanism is decrease in selectivity upon a decrease in the catalyst concentration. Presumably the free-radical mechanism becomes predominant, as the catalyst at low concentrations is unable to trap the alkylperoxy radicals before they enter radical chain propagation. However, despite the reasonably high selectivity achieved by this system, the industrial method for adipic acid synthesis is a two-step process the first of which is based on free-radical chemistry as described in the previous section. Weaker oxidants such as Mn(III), Pb(IV), Ce(IV), Cu(II), Pd(II) acetates can also be used as catalysts for

the oxidation of aromatic hydrocarbons in the presence of strong acids such as triflic acid and sulfuric acid.

Metal-Mediated Molecular Oxygen Activation

There are numerous examples of both reversible and irreversible complexation of molecular oxygen by metal complexes. Metals with two available oxidation states mainly form short-lived superoxo adducts, and combine to form μ -peroxo complexes (Figure 1-6). Co(II) salen complexes were shown to form μ -peroxo dimers; however, there are some examples of stable suproxo complexes that did not dimerize.¹ In the case where the metal can undergo a $2e^-$ oxidation, the preferred binding mode is side on, forming a peroxo species such as Vaska's complex.²⁶

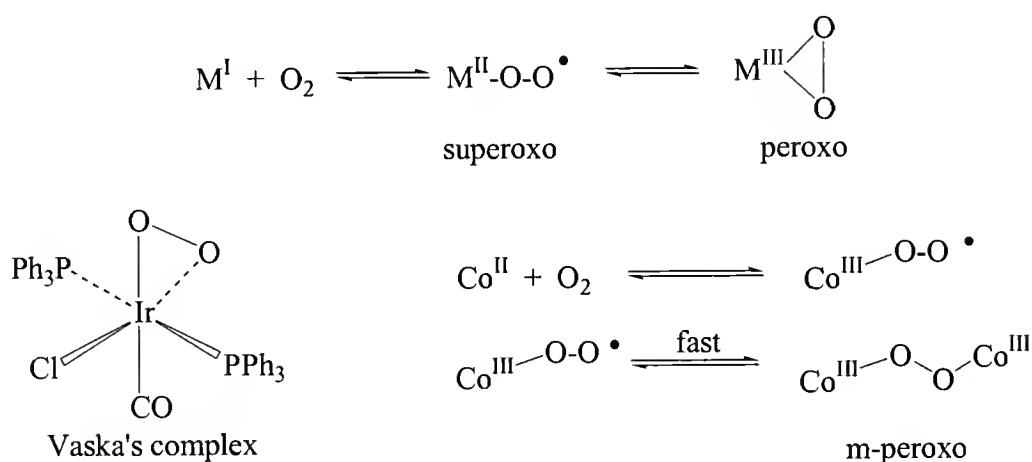


Figure 1-6. Examples of metal-molecular oxygen binding modes

The best known example of molecular oxygen activation by a metal complex resulting in selective oxygen transfer is the industrially important gas-phase oxidation of ethylene over a supported silver catalyst, where a silver peroxo complex is implicated in oxygen transfer.^{1,2,5} However, the catalyst does not catalyze the selective epoxidation of higher alkenes because of participation of radical pathways.

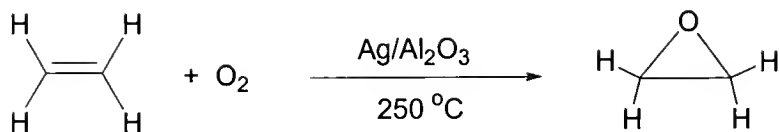


Figure 1-7. Selective ethylene epoxidation over a supported silver catalyst.

The tendency of hydrocarbons to contain trace peroxides and the efficiency of metal complexes to decompose them offers the greatest obstacle to selective non-radical oxidation in the presence of molecular oxygen.

A number of heme protein mimics such as Co, Fe, and Mn porphyrin dioxygen adducts have been isolated and characterized, however none have shown selective oxygen transfer to hydrocarbons.^{27,28} The ability of proteins to transfer molecular oxygen selectively to a substrate stems from their ability to form high-oxidation metal-oxo complexes, and also from the highly controlled environment surrounding the substrate that prevents the propagation of radical chains. Such control is difficult to achieve in simple model systems as is revealed by the lack of synthetic enzyme mimics able to carry out selective oxidation of hydrocarbons using molecular oxygen as a terminal oxidant.^{1,2,5} An example of a synthetic Fe porphyrin complex shown to activate molecular oxygen resulted in oxygen transfer to P(Ph)_3 . Oxygen transfer from a high oxidation (porphyrin) $\text{Fe}^{\text{IV}}\text{O}$ complex has been suggested based on experiments where an independently synthesized (porphyrin) $\text{Fe}^{\text{IV}}\text{O}$ complex oxidized P(Ph)_3 in a stoichiometric reaction. The proposed catalytic cycle is shown in Figure 1-8.¹ Attempts to achieve similar results using alkanes or alkenes resulted in radical products.

Recent investigations of metal mediated activation of dioxygen lead to interesting results worth mentioning. Itoh and coworkers²⁹ investigated oxygen transfer by

bis(μ -oxo)dicopper(II) complex $[\text{Cu}_2^{\text{III}}(\text{L})_2(\mu\text{-oxo})]^{2+}$ where

$\text{L}=\text{N-ethyl-N-[2-(2-pyridyl)ethyl]-2-phenylethylamine}$. Benzylic hydroxylation of the ligand side arm occurred with 46% conversion after 20 h at 25°C, in acetone under a pure dioxygen atmosphere. Reactions carried out using $^{18}\text{O}_2$ confirmed that the oxygen found in the product originated from molecular oxygen. One of the proposed pathways shown in Figure 1-9 suggests that oxygen transfer could occur through a concerted pathway with no radical formation. The second possibility is the formation of a short-lived carbon-centered radical that rebounds at a fast rate recapturing the hydroxy group. Similar mechanistic pathways have been proposed for oxygenases responsible for selective hydroxylation in biological systems. Several other examples of ligand hydroxylation by copper complexes and oxygen have been reported; however, similar oxygen transfer to uncoordinated alkane or alkene substrates has not been observed.^{30,31}

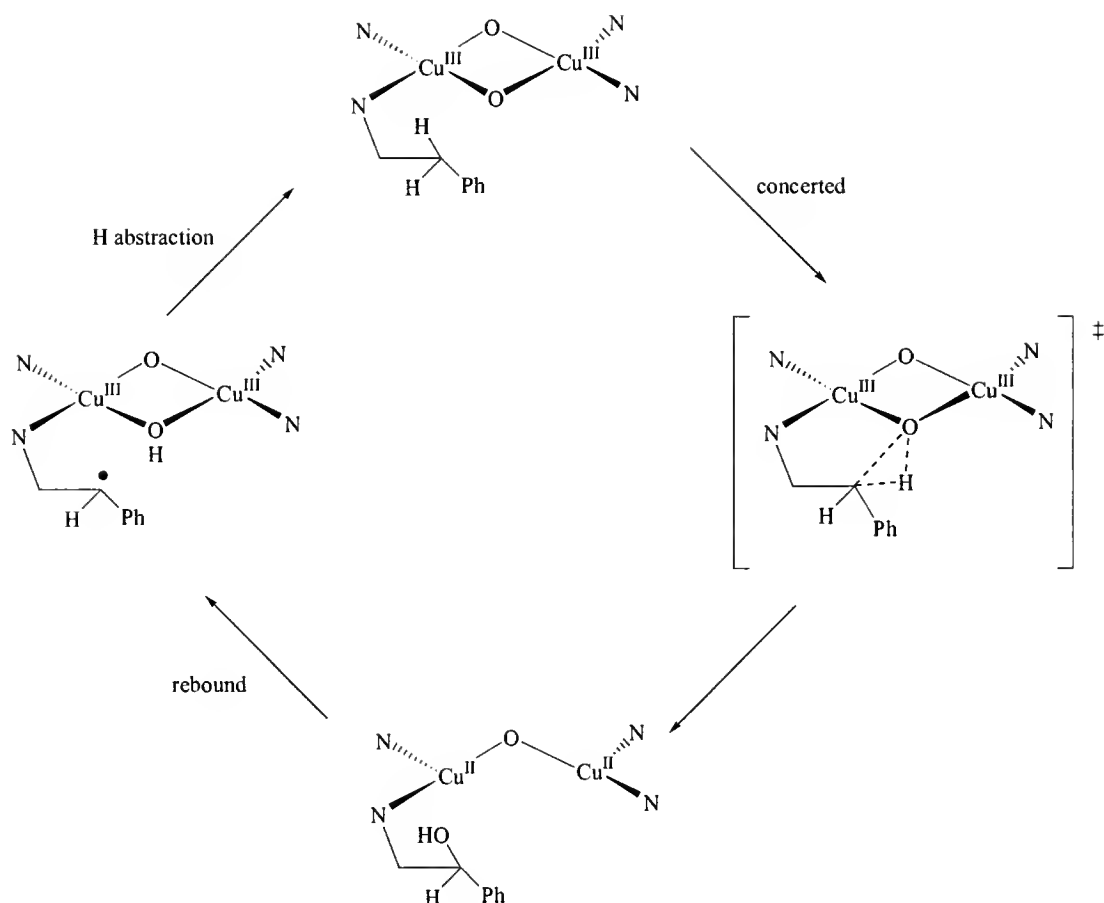


Figure 1-9. Selective oxygen transfer to pendant ligand

Hydrogen Peroxide as Terminal Oxidant

The search for efficient, selective, and clean oxidation processes for the epoxidation of alkenes is a high priority for industrial applications and for bridging the gap between synthetic catalysts and enzymatic systems. In particular, the use of H_2O_2 has been explored, because it is an economical oxidant giving only water as a byproduct.

Alkene Epoxidation by Early Transition Metal Catalysts

The significance of catalyzed epoxidation in industry cannot be overstated. One million tons of propylene is converted to propylene oxide annually catalyzed by compounds of high-valent early transition metals such as Mo^{VI} , W^{VI} , V^{V} , or Ti^{IV} in the presence of alkylperoxide. The active catalyst is a metal-peroxo adduct resulting in a

concerted transfer of oxygen to the substrate.³² The metal does not undergo a change in oxidation state, but behaves as a Lewis acid and withdraws electron density from the O-O bond. The electrophilic character of the coordinated peroxide O-O bond is increased, ensuring the concerted transfer of oxygen to the substrate (Figure 1-10).

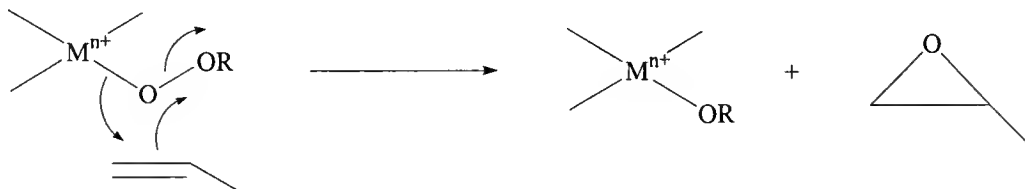


Figure 1-10. Epoxidation of propylene by high-valent, early transition metal complexes

The early transition metal complexes used are suitable for this chemistry because they are strong Lewis acids and weak oxidants. One-electron oxidants such as Fe or Co would lead to radical products and loss of selectivity. Although H_2O_2 undergoes the same type of reaction as alkylperoxides, the usually aqueous solutions of hydrogen peroxide lead to catalyst inhibition by H_2O .³²

The strong drive to find an effective catalyst using H_2O_2 as an oxidant has led to the discovery of a number of active and selective epoxidation systems.

Titanium(IV)-silicalite (TS-1) supported catalyst uses 30% H_2O_2 , and is very effective in epoxidizing linear olefins.³³ The hydrophobic nature of the silicalite support prevents inhibition of the catalyst by water, and absorbs only the hydrophobic substrate. The major limitation of TS-1; however, is the small pore size of the support, allowing only straight-chain alkenes to access the micropores of the silicalite. Attempts to increase pore size and maintain high activity were met with limited success.

First reports by Herrmann et al.³⁴ of methyltrioxorhenium (MTO) catalyzed epoxidation called for the use of anhydrous H_2O_2 in t-butanol. Cyclohexene oxide was

obtained in 90% yield at 10°C over a 5 h reaction time. The reaction was further improved by including heterocyclic bases (pyridine, pyrazole) in a CH₂Cl₂ solvent.^{35,36} High selectivities were obtained with a variety of olefins using 35% H₂O₂ and 0.05% MTO. The proposed mechanism involves a diperoxorhenium(VII) complex shown in Figure 1-11. The drawbacks of MTO catalyzed epoxidation are the low stability of MTO in the presence of H₂O₂, the difficult and expensive synthesis of the rhenium complex, and ring opening of acid-sensitive epoxides under the acidic conditions.

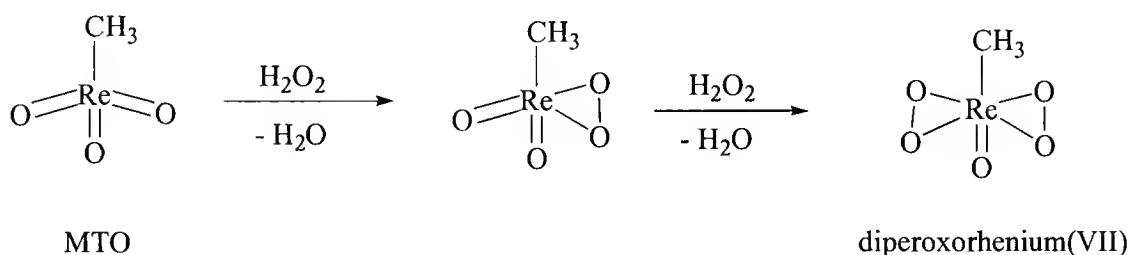


Figure 1-11. Active oxidant in MTO-catalyzed epoxidation reactions

Metal Porphyrin Catalysts

Similar to cytochrome P-450, simple Fe and Mn porphyrin complexes catalyze the selective oxygen transfer to alkenes using iodosylbenzene (PhIO), m-chloroperbenzoic acid (MCPBA), or hypochlorite as oxidants.³⁷⁻³⁹ However, similar selectivities were not observed when using oxygen donors containing O-O bonds, such as alkyl peroxides and H₂O₂. The mechanistic reason for low selectivity is the propensity for homolytic bond cleavage of the O-O bond resulting in alkoxy radicals as active species, instead of the high oxidation state (porphyrin)⁺Fe^{IV}=O or (porphyrin)Mn^V=O.⁴⁰ Another significant problem is the presence of competing pathways leading to dismutation of H₂O₂, and catalyst destruction. Further investigation showed that the efficiency and selectivity of oxygen transfer can be greatly improved by using imidazole as cocatalyst.

The dramatic effect of added imidazole was that epoxide yield increased from 2% for [Mn(5,10,15,20-tetrakis(2',6'-dichlorophenyl)porphyrin)]Cl (Mn(TDCPP)Cl) in the absence of imidazole, to as much as 72% of cyclooctene when the cocatalyst was added.⁴¹ The proposed active species in the Mn(TDCPP)Cl-H₂O₂-imidazole system is the high oxidation state (porphyrin)Mn^V=O based on comparisons using PhIO as oxygen donor. The cis/trans ratios of three different substrates were the same using either H₂O₂ or PhIO as oxygen transfer agent, suggesting that the same active species was formed in both cases. However, product yields were somewhat lower in the Mn(TDCPP)Cl-H₂O₂-imidazole system, presumably because of the parallel peroxide dismutation pathway preventing the efficient transfer of all the oxygen equivalents to the substrate. The proposed function of imidazole is both as an axial ligand and base catalyst. The proposed catalytic cycle is shown in Figure 1-12.⁴¹

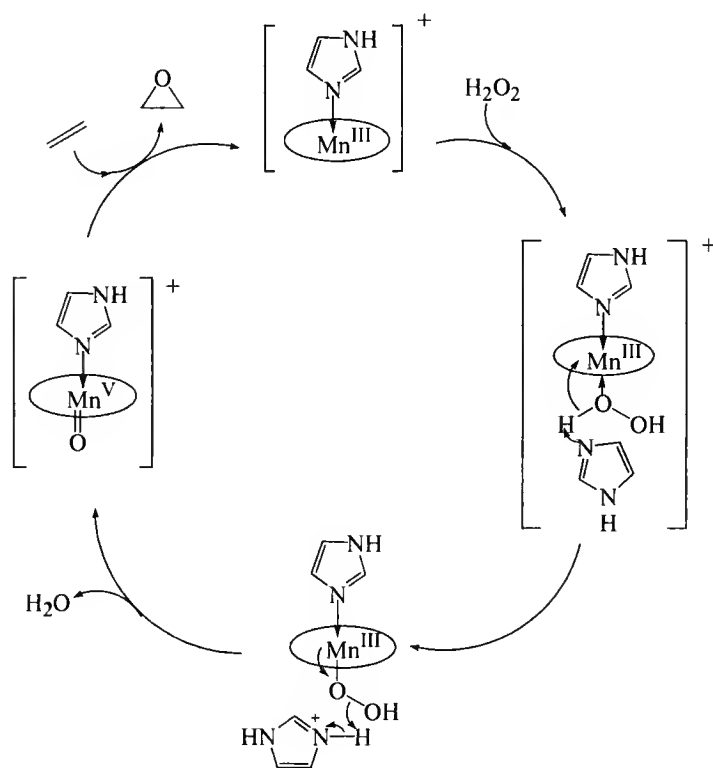


Figure 1-12. Proposed mechanism of epoxidation co-catalyzed by imidazole

The axial coordination of imidazole may aid in the heterolytic bond cleavage of H_2O_2 and prevent the formation of free radicals. Similarly, the base catalyst function of the cocatalyst favors the formation of the high-oxidation state $\text{Mn}^{\text{V}}=\text{O}$ species by the removal of H_2O .

The Mn-Salen Asymmetric Catalysts

Since their discovery, chiral Mn(III)-salen (N,N'-bis(salicylideneamino)ethane) complexes have proven to be highly effective in the asymmetric epoxidation of virtually every class of unfunctionalized conjugated olefins.⁴² The popularity of Mn(III)-salen complexes stems from facile catalyst preparation, high enantiomeric excess (EE) of the products, and the use of cheap oxidants. The preferred oxidants are hypochlorite and iodosylbenzene.^{43,44} Catalytic conditions can be optimized by including nitrogen heterocycles such as imidazoles, pyridines, tertiary amine N-oxides, and carboxylate anions. The additive is thought to function as an axial ligand stabilizing the high oxidation state $\text{Mn}(\text{V})=\text{O}$ species.

An additional function of the more lipophilic N-oxides may be as a phase transfer agent for HCO^- transport to the organic phase in biphasic solvent systems. Additives such as heterocyclic amines and carboxylates have also improved the effectiveness of H_2O_2 as an oxygen transfer agent. High yields (86%) and EE (92%) were achieved in the epoxidation of cyanochromene using Jacobsen's catalyst with ammonium acetate and 30% H_2O_2 .⁴⁵ Such high EE has not been observed with a wide variety of substrates, hence further studies must be completed to further improve the Mn-salen/ H_2O_2 system.

The $\text{Mn}^{2+}/\text{HCO}_3^-/\text{H}_2\text{O}_2$ Catalyzed Alkene Epoxidation

Alkene epoxidation catalyzed by simple transition metal salts using aqueous H_2O_2 and bicarbonate salt was investigated by Richardson et al.⁴⁶ as well as by Burgess and

coworkers.⁴⁷ The room temperature epoxidation of sulfonated styrene in aqueous solution was catalyzed by μM levels of Mn^{2+} resulting in rate enhancement of at least an order of magnitude. No epoxide was obtained in the absence of bicarbonate ion, and trace amounts of epoxide were found when H_2O_2 and HCO_3^- were used after removal of trace metal ions by chelation. Kinetic studies reveal a mixed-order dependence on bicarbonate concentration, suggesting that more than one equivalent of bicarbonate is present in the transition state. Previous studies by Drago et al. and Richardson et al.^{46,48} have shown equilibrium formation of the peroxycarbonate ion in solutions containing H_2O_2 and HCO_3^- (Figure 1-13). Other anionic salts such as NaOAc do not catalyze the epoxidation, nor do they form a peroxy acid species in equilibrium with H_2O_2 , suggesting that the active epoxidizing agent can only be formed in the presence of the peroxycarbonate ion.

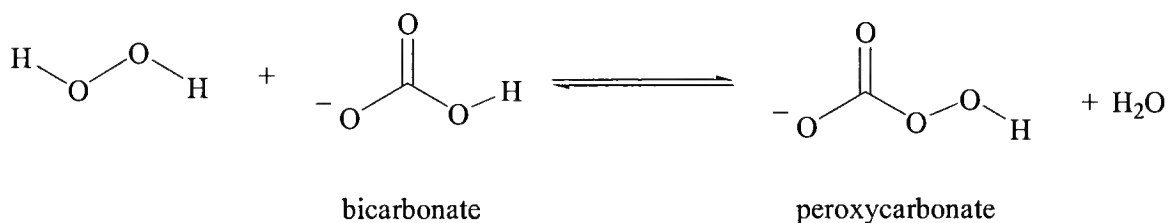


Figure 1-13. Equilibrium formation of peroxycarbonate

Alkene epoxidation carried out in mixed solvents illustrates the scope of the Mn^{2+} /BAP system (Figure 1-14). More than 30 d-block and f-block metal salts were screened and only Cr^{2+} and Fe^{3+} showed moderate activity, with Mn^{2+} being the most active.⁴⁷ Seventeen alkenes were screened, and results showed that aryl-substituted, cyclic and trialkyl-substituted alkenes were epoxidized in high yields (63-94%), while terminal alkenes were unreactive. The large-scale reactions were carried out in DMF or

t-BuOH solvent at room temperature with slow addition of an aqueous solution of $\text{H}_2\text{O}_2/\text{HCO}_3^-$ over a 16 h period.

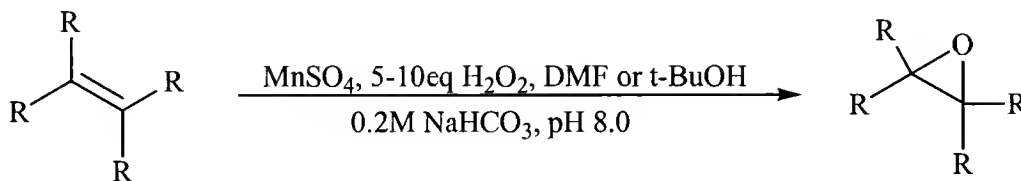


Figure 1-14. Mn^{2+} /BAP catalyzed oxidation of alkenes

The observation that most alkenes converted cleanly to the epoxide, and that no differences in the product profiles were seen if the reaction was carried out in the absence of air, suggests that $\text{HO}\cdot$, and $\text{HOO}\cdot$ are likely not the primary epoxidation species. Furthermore, EPR studies show signals characteristic of Mn^{4+} species formed in the presence of $\text{H}_2\text{O}_2/\text{HCO}_3^-$.⁴⁷ The simplicity, high activity and selectivity of the Mn^{2+} /BAP system make it a unique and convenient method for the epoxidation of a variety of alkenes.

Scope of the Dissertation

Chapter 2 deals with the Fe^{II} diimine catalyzed autoxidation of cumene at moderate temperatures. This particularly active family of Fe catalysts is an important addition to the existing literature because most of the highly active autoxidation catalysts, except for (porphyrin) Fe^{III} , are based on Co^{2+} or Co^{3+} complexes. The function of the catalyst as a peroxide decomposition agent is explored and rationalized based on product selectivities, peroxide decomposition studies as well as catalyst concentration, oxygen pressure and solvent polarity dependencies. We present a detailed mechanistic scheme consistent with the peroxide decomposition mechanism that enables us to model product profiles over time for the catalyzed autoxidation of cumene at 60 °C. The scheme provides good fits to our experimental data even when the system is perturbed by adding small mounts

of products at the beginning of the reaction. The identity of the active catalyst was explored by ligand variation and counter-ion studies.

The interest in further understanding the effect of ligand dissociation on the formation of the active autoxidation catalyst from Fe(II)diimine (FeL_3)²⁺ complexes, lead to the studies presented in Chapter 3. A family of bis-Fe(II)diimine (FeL_2X_2) complexes were investigated and their activity in cumene and cyclohexane autoxidation examined. The complexes were chosen following the observation that loss of one diimine ligand from FeL_3^{2+} is likely the first step toward the active catalyst formation. Effects of X^- ligand field strength on catalytic activity were investigated and rationalized.

The catalytic activity of FeL_3X_2 complexes is compared to known autoxidation and peroxide decomposition catalysts in a polar solvent. The importance of the ligand in the formation of the active catalyst is explored in Chapter 4.

In the realm of metal catalyzed alkene epoxidation, the use of an affordable and clean oxidant such as H_2O_2 to attain high selectivity is a desirable achievement. Chapter 5 reports on the application of an $\text{H}_2\text{O}_2/\text{HCO}_3^-$ system as an oxygen transfer agent with previously known manganese epoxidation catalysts. We discuss the catalyzed epoxidation of styrene using a water soluble Mn-porphyrin complex and the asymmetric epoxidation of styrene using Jacobsen's catalyst. The effects of the $\text{H}_2\text{O}_2/\text{HCO}_3^-$ system on catalyst stability and activity are discussed and compared with previously published literature.

CHAPTER 2

IRON (II) α,α' -DIIMINE CATALYZED HYDROCARBON AUTOXIDATION

Introduction

The tendency of hydrocarbons to form radicals in the presence of oxygen has been exploited for the synthesis of important hydrocarbon oxidation products through the use of simple metal salts (Cr, Mn, Fe, Co, Ni, Cu).¹ Transition metal salts are thought to catalyze the reaction by increasing the rate of radical formation by decomposing the intermediate alkyl hydroperoxide. The formation of terephthalic acid from p-xylene and the oxidation of cyclohexane to cyclohexanone and cyclohexanol (K/A oil) are two key industrial processes using this chemistry.^{1,9}

Halogenated iron porphyrin catalysts, first described by Lyons et al.,^{13,15,49-51} are among the most active hydrocarbon-soluble catalysts for the autoxidation of neat alkanes at low temperatures. The complexes catalyze the oxidation of alkanes at room temperature in the presence of molecular oxygen. The unusually high reactivity of the iron porphyrin complexes was attributed to the ability of the halogenated ligands to stabilize the energetically unfavorable Fe(II) porphyrin species by increasing the electrode potential for the Fe(III/II) couple. It was also shown that catalytic activity increases as the degree of halogenation of the porphyrin ring increases.⁵¹ Although the complexes were developed in an attempt to mimic the oxidative activity of cytochrome P-450, it has been established that the mechanism does not mimic that of the enzyme active site. Instead, these reactions primarily follow the long established radical autoxidation mechanism, in which catalytic decomposition of alkyl hydroperoxides

generates chain propagating radicals $\text{ROO}\cdot$ and $\text{RO}\cdot$ (Figure 1-1).^{11,13-17,50-54} The proposed mechanism is supported by the experimental observation that the rate of substrate oxidation increases with increasing catalyst efficiency toward disproportionation of the corresponding alkyl hydroperoxide.⁵¹ Lyons et al.¹⁵ and Labinger et al.¹⁷ have contributed much of the evidence for the radical mechanism through their investigations of the room temperature oxidation of isobutene and other substrates catalyzed by halogenated iron porphyrins. The series of mechanistic steps and rate constants proposed by Labinger et al.¹⁷ closely model the final product concentrations of catalyzed isobutane oxidation as reported by Lyons et al.⁵³

We have investigated the mechanism of hydrocarbon autoxidation catalyzed by an iron(II) tris-diimine coordination complex, $[\text{Fe}(\text{DPP})_3](\text{SO}_3\text{CF}_3)_2$ (DPP=4,7-diphenyl-1,10-phenanthroline) **1** and related complexes, which have catalytic activity^{55,56} comparable to that of halogenated iron porphyrins.^{13-15,50,51}

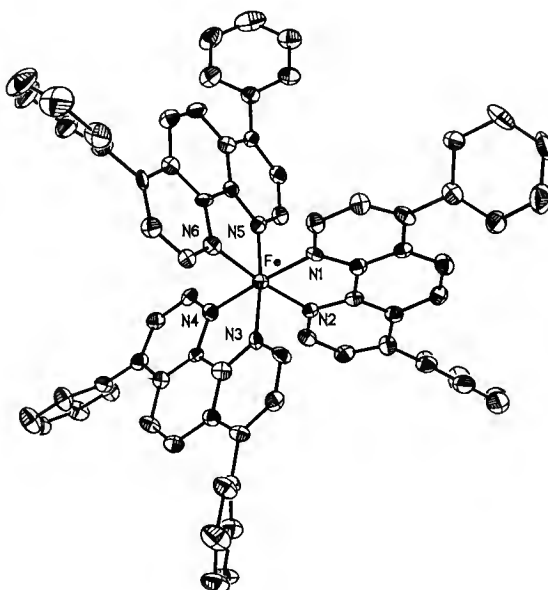


Figure 2-1. $[\text{Fe}(\text{4,7-diphenyl-1,10-phenanthroline})_3]^{2+}(\text{CF}_3\text{SO}_3^-)_2$ (**1**) X-ray structure of the FeL_3^{2+} cation showing 50% probability ellipsoids⁵⁵

Such reactivity is notable, since **1** lacks halogenated ligands unlike the highly active iron porphyrins. Hence, halogenated ligands are not a prerequisite to a highly active autoxidation catalyst.

Prior work by Richardson et al.⁵⁵⁻⁵⁸ and Drago et al. showed **1** to be active in catalyzing cyclohexane autoxidation. There have been no prior reports of using $\text{Fe(L)}_3\text{X}_2$ (L=diimine) complexes as autoxidation catalysts. The use of $\text{Fe(1,10-phenanthroline)}_3^{2+}$ in the presence of H_2O_2 in the hydroxylation of phenol in acidic aqueous solution has been reported.⁵⁹ The proposed oxidants are $\text{HO}\cdot$ and the in-situ formed $\text{Fe(1,10-phenanthroline)}_3^{3+}$ complex. Related $\text{Fe(L)}_2\text{X}_2$ complexes have been reported for their activity in oxygenating hydrocarbons in the presence of molecular oxygen, and the proposed mechanism was that of oxygen activation by the metal complex.^{60,61}

The goal of this work is to show that metal-catalyzed peroxide decomposition is the major catalytic pathway in the autoxidation of cumene catalyzed by precursor **1**.

For our kinetic studies, cumene was chosen as the substrate because of its high boiling point, its tertiary C-H bond, and the stability of cumyl hydroperoxide. Early investigations of metal-catalyzed cumene oxidation reported the catalytic properties of Mn, Co and Cu acetates, acetylacetonates, and Co and Fe phthalocyanines.⁶²⁻⁶⁴ In the case of hydrocarbon-soluble metal salts, solvents such as o-dichlorobenzene or acetonitrile were employed; however, the less soluble salts required the use of a polar protic solvent such as acetic acid. Although there has been some disagreement on the subject in the past, Blanchard et al. showed that when using simple metal salts the role of the metal was to decompose peroxide and not activate oxygen.⁶⁴ More recent examples of cumene autoxidation include catalysis by heterogeneous catalysts such as

iron-aluminum oxides⁶⁵ and polymer supported⁶⁶⁻⁶⁸ simple Cr, Mn, Fe, Co, and Ni salts. The studies mentioned suggested the primary mechanism was that of metal-catalyzed peroxide decomposition and radical-chain propagation.

To provide direct comparisons to the porphyrin catalysts,^{13-17,50,51,53,54,69} tetra-(pentafluorophenyl)-porphyrin iron(III) chloride (**2**) was used in parallel experiments (Figure 2-3). In this investigation, we successfully used a mechanism based on that proposed by Labinger et al.¹⁷ to model the product distribution over time for cumene autoxidation catalyzed by precursors **1** and **2**. A series of FeL_3X_2 complexes were synthesized by varying the substituents on the 1,10-phenanthroline ligands, and the effects of those substituents on the activity of the catalysts was studied. Ligand dissociation studies and spectral investigations were done to elucidate the identity of the active catalyst. Temperature, solvent, pressure and catalyst concentration dependencies were also investigated.

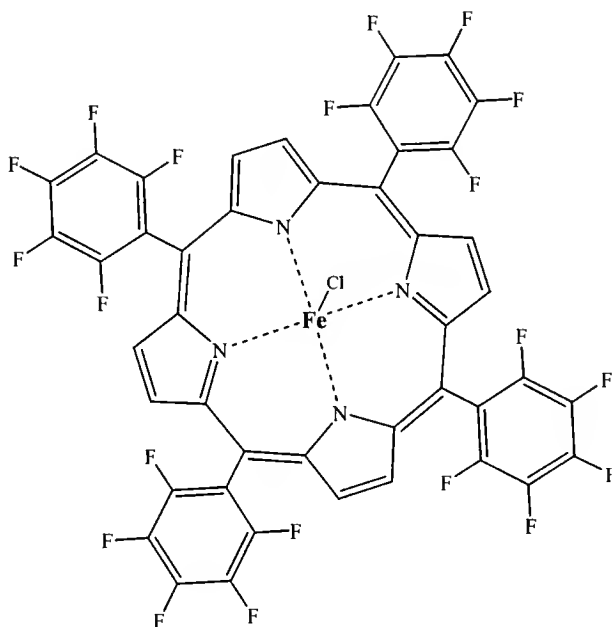


Figure 2-2. Tetra-(pentafluorophenyl)-porphyrin iron(III) chloride (**2**)

Results and Discussion

Catalyzed Cumene Autoxidation

The major products of catalyzed cumene oxidation are 2-phenyl-2-propanol (ROH), acetophenone (R'O), cumyl hydroperoxide (ROOH) and small amounts of dicumylperoxide (ROOR) as shown in Figure 2-3. Additional products detected were trace amounts of α -methylstyrene, as well as overoxidation products CO, CO₂ and H₂O. Although not determined quantitatively, the formation of CO and CO₂ was confirmed by GC/TCD. GC traces in Figure 2-4 show the analysis of the headspace vapor inside the reactor. The buildup of CO and CO₂ over time is clearly observed.

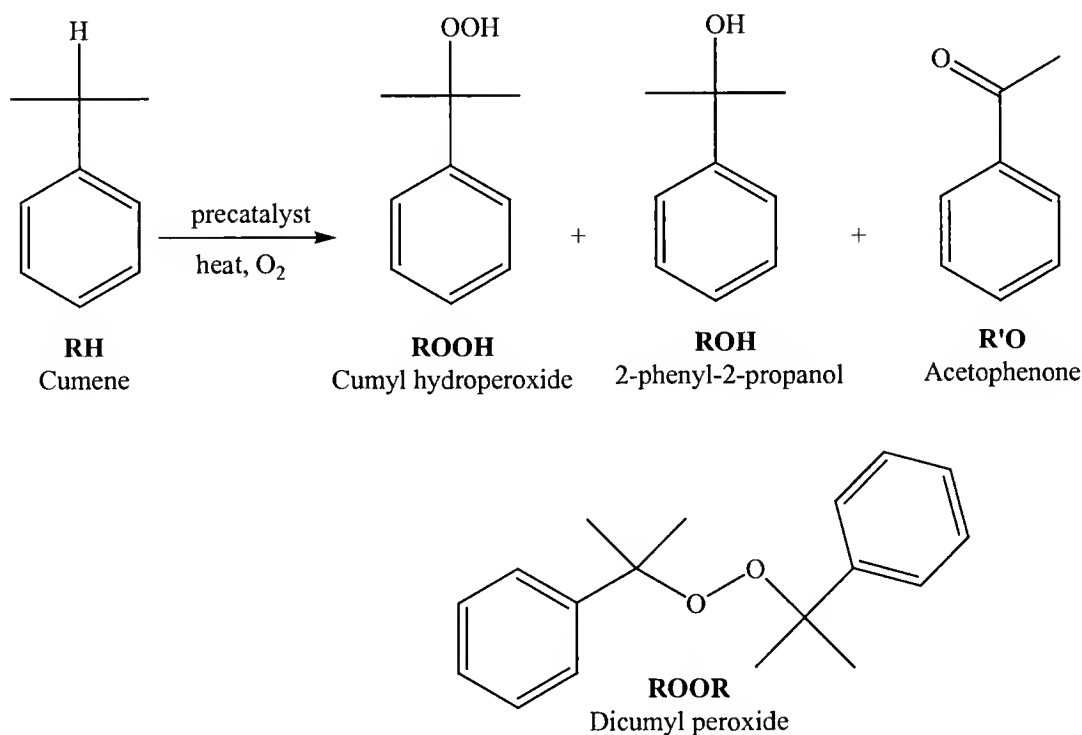


Figure 2-3. Products of metal-catalyzed cumene autoxidation

Figure 2-5 shows the time dependent formation of the three major products during cumene oxidation catalyzed by precursor **1**. Slow initial formation of ROOH is followed by the buildup of ROH and R'O over time as the ROOH concentration reaches a steady

state. Product conversions reported in Table 2-1 show precursors **1** and **2** have comparable activities in catalyzing substrate oxidation by O_2 , with differences in the cumyl hydroperoxide and acetophenone selectivities. The catalytic activities of the two precursors are comparable even at long reaction times, and after 38h of reaction the oxygen uptake was ~ 0.14 mol for both **1** and **2**. The induction periods are ~ 35 min for **1** and ~ 70 min for **2** catalyzed oxidation reactions. The oxygen uptake curves in Figure 2-6 clearly show the differences in the length of induction periods for **1** and **2** catalyzed reactions. Oxygen uptake begins immediately with addition of small amounts (0.04 M) of cumyl hydroperoxide (Table 2-2).

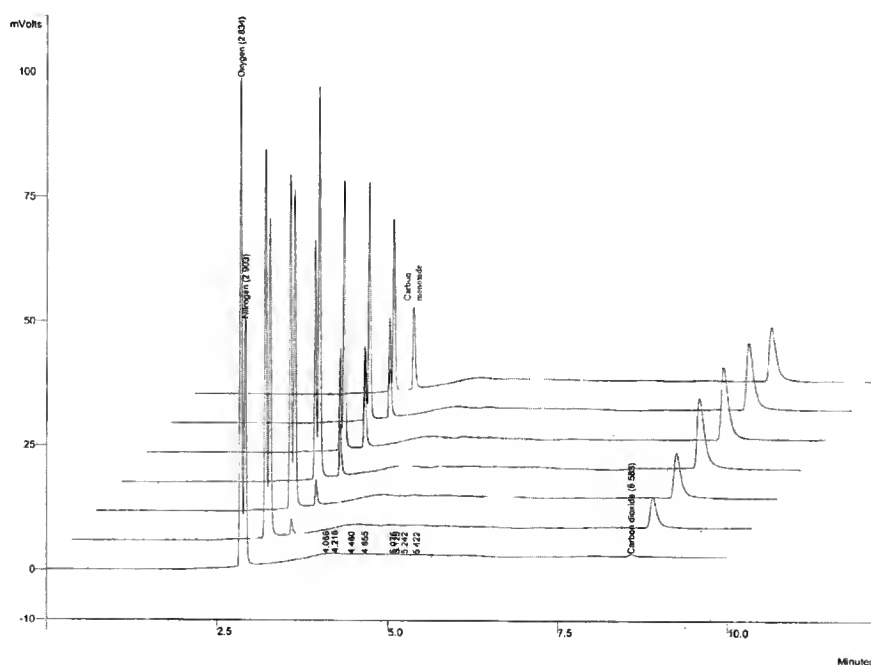


Figure 2-4. Formation of CO and CO₂ over time in cumene oxidation catalyzed by **1**

Table 2-1. Catalyzed oxidation of cumene

	1 ^a	2 ^a	Co-nap ^b	Uncatalyzed ^a
% Conversion	15.1±1.2	15.8±1.8	10	Trace
% ROOH	14.8±1.5	4.6±0.4	Trace	Trace
% ROH	73.1±0.6	78.2±1.4	80	Nd
% R'O	11.9±0.9	17.2±1.3	20	Nd
% ROOR	~2	~2	-	Nd
O ₂ uptake(mol)	0.039±0.001	0.047±0.005	0.05	Trace

^a Reactions done at 60° C and 60 psi of constant O₂ pressure; catalyst = 57 μM; 50 mL cumene; 50 mL benzene; reaction time=5 h; Results and errors calculated from at least 5 experiments for each catalyst. Nd =not detected.

^bT=100° C; 6μl Co-naphthanate (57μM Co metal); over oxidation products detected (not characterized).

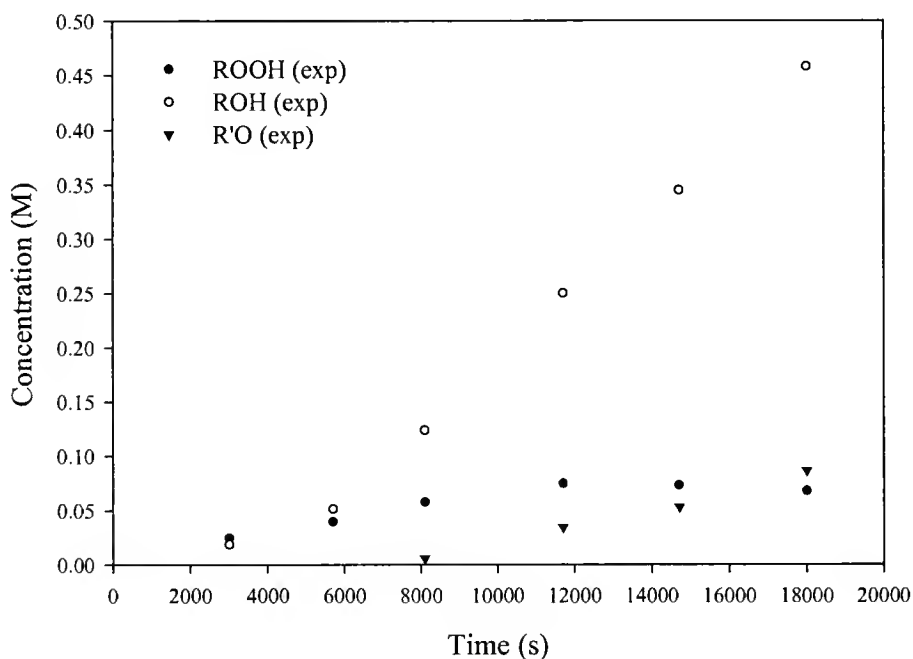


Figure 2-5. Cumene oxidation catalyzed by 1

Water (0.5 M) also decreases the induction period in the case of **2** only.⁷⁰ The observation that ROOH and H₂O eliminate the induction period suggests that active catalyst formation is dependent on the concentration of ROOH or H₂O in the case of both **1** and **2**. Presumably, the small amount of ROOH produced by the background (uncatalyzed) reaction is enough to convert the catalyst precursor to an active species.

The uncatalyzed reaction (no metal complex added) produces only trace amounts of ROOH (Table 2-1).

Co-naphthanate is used industrially as a catalyst for cyclohexane autoxidation and was used for comparison in the present work. The Co catalyzed reaction yielded only trace amounts of products under our reaction conditions, and even at $T=100^{\circ}\text{C}$ the conversion was only 10% (Table 2-1). Co-naphthanate was observed to be highly active in the autoxidation of cyclohexane at a temperature of 135°C (Appendix). Presumably the Co complex becomes highly catalytic only at very high temperatures.

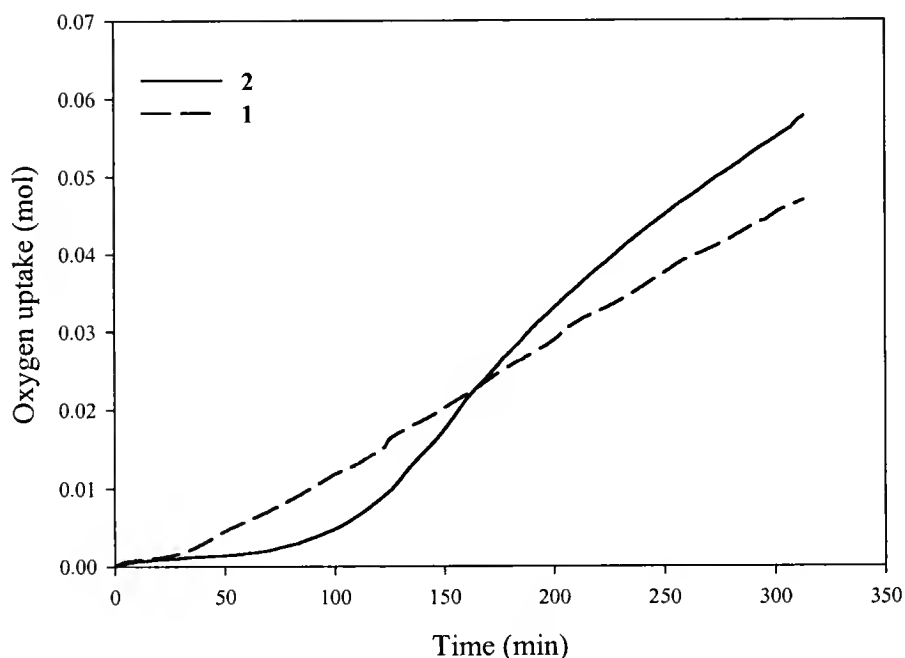


Figure 2-6. Oxygen uptake curves for 1 and 2 catalyzed oxidation

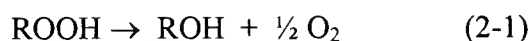
Table 2-2. Effects of ROOH and H_2O on induction period

	% Conversion	% ROOH	% ROH	% R'O
1 + ROOH ^a	19	15	74	11
2 + ROOH ^a	20	4	78	18
2 + H_2O ^b	25	4	72	24

Cumyl hydroperoxide or water was added to cumene/ benzene initially to observe the effect on induction period. Induction period was not present in any of the above experiments. [precursor] = $57\ \mu\text{M}$, ^a [ROOH] = $4 \times 10^{-2}\ \text{M}$, reaction time = 3hr 35min. ^b [H_2O] = 0.5 M, reaction time = 5hr

Catalyzed Cumyl Peroxide Decomposition

Peroxide decomposition under an inert atmosphere was done to determine the catalytic activity of **1** and **2** toward decomposition of the peroxide in the absence of substrate. The peroxide decomposition activity of each complex is expected to parallel its cumene oxidation activity. The major products of cumyl peroxide decomposition were ROH, O₂ and small amounts of the cleavage product R'O. The stoichiometry of the peroxide decomposition reaction (not including the cleavage product R'O) follows the net reaction shown in equation 2-1.



Experimental evidence for the stoichiometric relationship shown in equation 2-1 is shown in Figure 2-7. As expected, oxygen was formed in approximately half the amount of the formed ROH. Plots of $\ln [\text{ROOH}]$ vs. time are linear suggesting a first order dependence in $[\text{ROOH}]$. Plots of $\ln [\text{ROOH}]$ vs. time give experimental k_{obs} values for the decomposition by **1** and **2** (both 57 μM) as $4.8 \pm 0.3 \times 10^{-4} \text{ s}^{-1}$ and $1.5 \pm 0.1 \times 10^{-3} \text{ s}^{-1}$, respectively (Figure 2-8). Under the conditions of the peroxide decomposition experiments activity begins with no induction since ROOH was been added in high concentrations in order to monitor its disappearance.

Although complex **2** is approximately 3-fold more active as a peroxide decomposition agent compared to **1**, the two complexes appear to have similar activities in terms of conversion to ROOH, ROH and R'O after a specified period of time (Table 2-1). However, the induction period exhibited by **2** is approximately twice as long as that of **1**. Although **2** is a more efficient peroxide decomposition agent, the significantly

shorter induction period of **1** results in the formation of approximately the same amount of ROOH, ROH and R'O as **2**.

Co-naphthanate catalyzed cumyl peroxide decomposition gave only traces of decomposition products at 60°C, and this observation is consistent with the low catalytic activity toward cumene oxidation at this temperature.

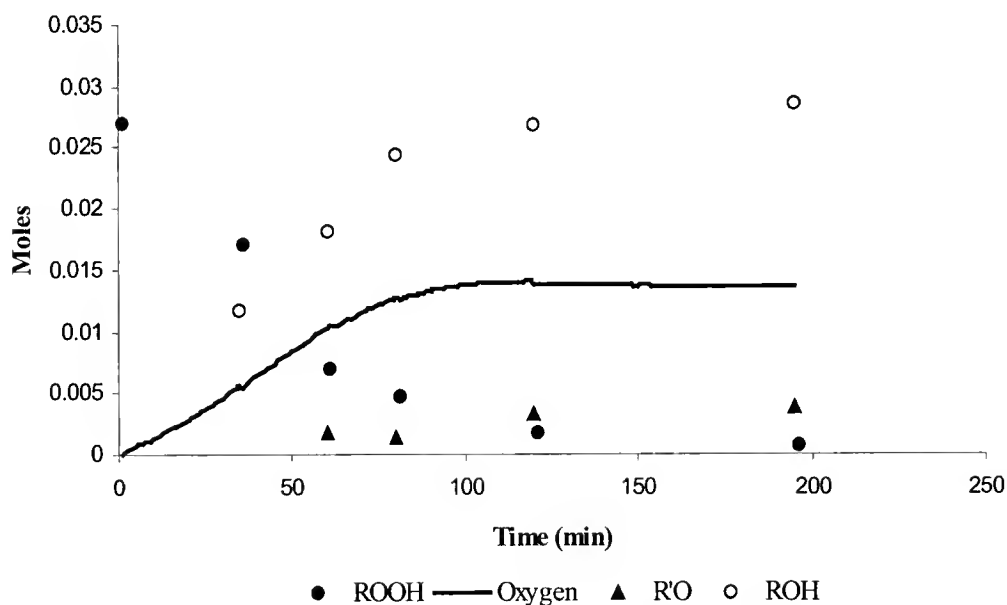


Figure 2-7. Metal-catalyzed peroxide decomposition

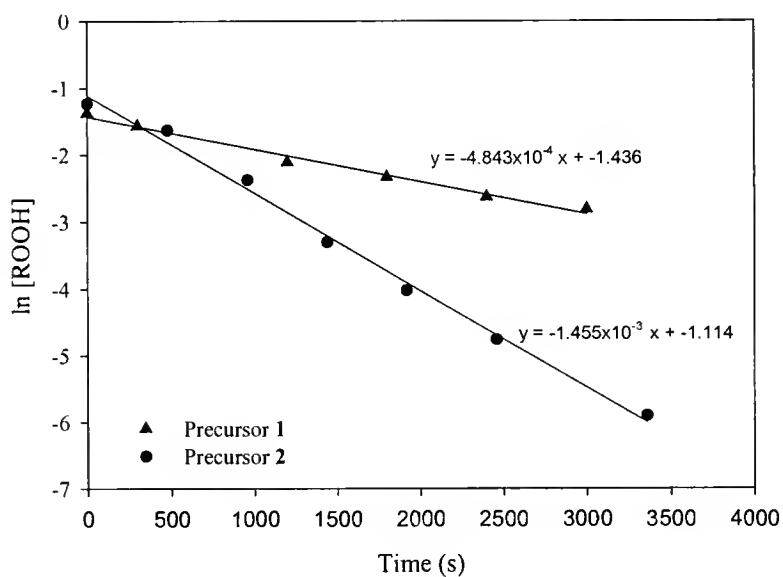


Figure 2-8. Plots of ln [ROOH] vs. time

Proposed Mechanism

As discussed in Chapter 1, the general mechanism of uncatalyzed autoxidation is shown in Figure 1-1. The termination step (k_t) in particular lacks much of the detail present in a complete radical autoxidation mechanism. Figure 2-9 represents the mechanism and rate constants used to obtain the numerical fits to our experimental results. Using a numerical modeling program, the steps and rate constants in Figure 2-9 were used to obtain good fits to the experimentally determined product yields for both autoxidation and peroxide decomposition experiments. The origins and detailed descriptions of the specific steps and rate constants are discussed below.

Steps 1-8, 12 and 13 are based on a mechanism proposed by Labinger et al.¹⁷ for the Fe(III) halogenated-porphyrin catalyzed autoxidation of isobutane. Since both isobutane and cumene have only one tertiary C-H bond we expect the same radical steps to be applicable here. However, the rate constants used in the Labinger study could not be applied here since the reported values correspond to reactions at 30°C. The rate constants shown in Figure 2-9 were taken from literature and/or estimated from fits to both oxidation and peroxide decomposition results.

The initiation step rate constant $k_1 = 10^{-10} \text{ s}^{-1}$ has not been experimentally measured, but is a value used most often in literature to describe the very slow initiation step responsible for the long induction periods.¹⁷ It is noteworthy that variation of the k_1 value ($10^{-10} - 10^{-7} \text{ s}^{-1}$) has little impact on the results suggesting the reaction is not carried by the initiation step (Appendix-A, Figure A-1). The reported experimental rate constant k_2 at 60 °C is in the range of $0.93\text{-}1.0 \text{ M}^{-1}\text{s}^{-1}$.^{71,72} Rate constants k_3 and k_4 are comparable to the published estimated values of 3.8×10^5 and $4.1 \times 10^4 \text{ M}^{-1}\text{s}^{-1}$, respectively.⁷² Experimental values for k_5 and k_6 have not been reported in the literature; however, the

rate constants used in our model are reasonable based on the values reported for analogous steps in isobutane (30 °C; $k_5=8 \times 10^4 \text{ M}^{-1}\text{s}^{-1}$; $k_6=6 \times 10^6 \text{ M}^{-1}\text{s}^{-1}$) and cyclohexane (150 °C; $k_5=7 \times 10^7 \text{ M}^{-1}\text{s}^{-1}$; $k_6=8 \times 10^7 \text{ M}^{-1}\text{s}^{-1}$) autoxidation.¹⁷ The rate constant used in step 7 was tuned according to the experimental yields of R'O since its value varies for different systems. All of the steps indicated as 'fast' are diffusion controlled under our conditions and a rate constant of $1 \times 10^{10} \text{ M}^{-1}\text{s}^{-1}$ was used. Rate constants for the catalyst activation steps k_9 , k_{10} , and k_{11} were determined by numerical fitting to data from reactions initiated by adding ROOH or H₂O (Table 2-2). Since water did not decrease the induction period when using **1** as a catalyst, this step was not included in the mechanism. Finally, the metal catalyzed peroxide decomposition steps k_{12} and k_{13} were obtained by fitting oxidation and peroxide decomposition data.

The sensitivity of the kinetic curves to changes in the values of rate constants is illustrated in Appendix-A.

Initiation by the direct reaction of most hydrocarbons with molecular oxygen is thermodynamically and kinetically unfavorable, and chain initiation (Step 1) in the absence of added initiators usually occurs through substrate attack by peroxidic impurities present in the substrate. The addition of oxygen to R• is diffusion controlled under atmospheric pressure, and the predominant radical species in solution is the alkylperoxy radical (ROO•). The ROO• radical is relatively stable and approximately as selective as Br•, and ROO• abstracts the most weakly bound hydrogen from the substrate. In the case of cumene, the weakest bond is the benzylic tertiary C-H bond.

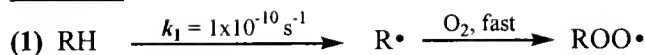
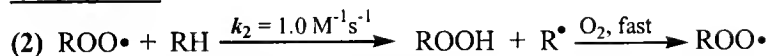
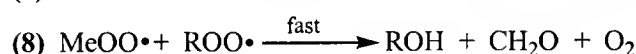
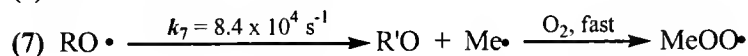
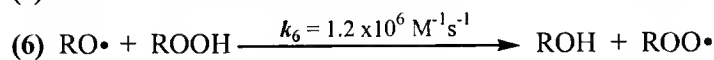
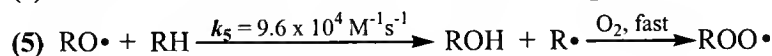
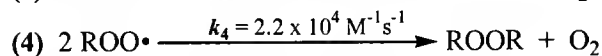
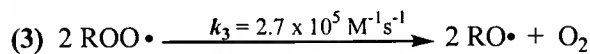
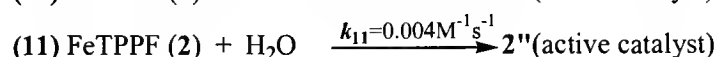
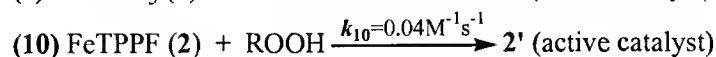
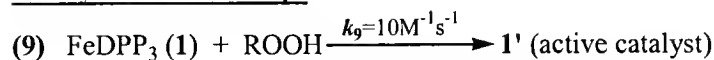
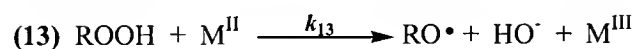
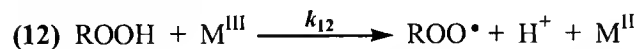
Initiation**Propagation****Radical chain and termination steps****Catalyst activation steps****Catalytic steps**

Figure 2-9. Mechanism of metal catalyzed cumene autoxidation with average rate constants used in the simulation experiments

The C-H bond cleavage is likely to be rapid if the bond energy of ROO-H is at least as strong as the broken C-H bond of the substrate. The cumene tertiary C-H bond energy is 84 kcal mol^{-1} compared to the estimated ROO-H bond strength of 90 kcal/mol .¹

The primary termination pathway for ROO• radicals is through the formation of the intermediate tetroxide as shown in Figure 2-10. The tetroxide disproportionates either through the in-cage formation of ROOR (Step 4) or the diffusion of RO• out of the cage (Step 3).¹²

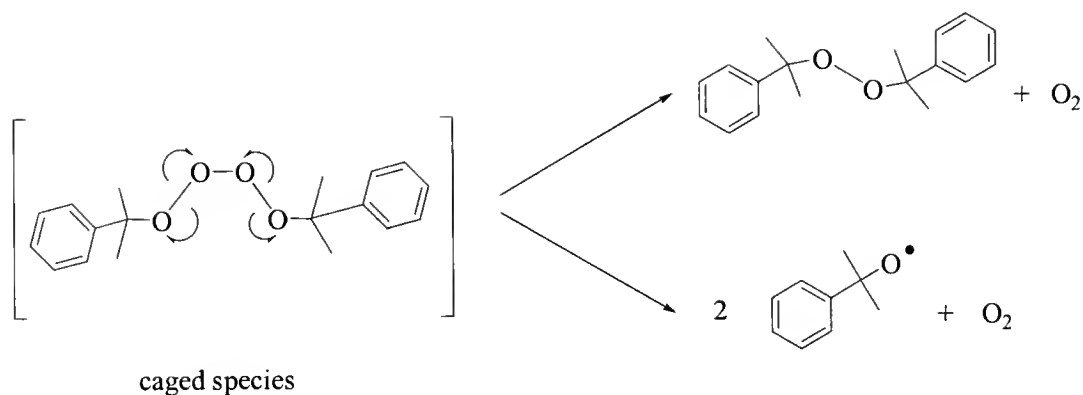


Figure 2-10. Disproportionation pathways of alkyl tetroxide

The relative rates of the two pathways are dependent on the substrate and reaction conditions. In our system, the pathway leading to escape of $\text{RO}\cdot$ out of the cage is slightly favored. Once formed, the $\text{RO}\cdot$ radical can enter one of three different pathways, two leading to the formation of ROH and the third leading to $\text{R}'\text{O}$. Steps 5 and 6 involve hydrogen abstraction from both RH and ROOH resulting in the formation of ROH as well as the propagating radical $\text{ROO}\cdot$. An alternate pathway for the $\text{RO}\cdot$ radical is β -scission to form $\text{Me}\cdot$ radical and $\text{R}'\text{O}$. The termination of the $\text{MeOO}\cdot$ radical is described by step 8 and results in the formation of ROH , CH_2O (formaldehyde) and O_2 . Although CH_2O was not detected as a product, we did observe the formation of CO and CO_2 both of which are oxidation products of CH_2O (Figure 2-4). Furthermore, the proposed model predicts a comparable amount of oxygen equivalents accounted for in products ROOH , ROH and $\text{R}'\text{O}$ relative to the amount of oxygen uptake as is shown by experiment. Table 2-3 shows the comparison between experimental and calculated moles of oxygen uptake and moles of oxygen accounted for in the three products.

Steps 9-11 were added to the mechanism in view of elimination of the induction period by ROOH and H_2O addition. We propose that prior to catalyzed ROOH decomposition each complex must be converted to the active form of the catalyst by

reaction with ROOH (or H₂O in the case of **2**⁷³) produced initially by the slow metal free autoxidation step 2 in Figure 2-9. The rate constants k_9 , k_{10} , and k_{11} were estimated by fitting the experimental data from ROOH and H₂O initiated experiments (Table 2-2).

Table 2-3. Experimental and calculated oxygen equivalents accounted for in products ROOH, ROH and R'O

	1 (exp) ^a	1 (calc)	2 (exp) ^a	2 (calc)
O ₂ uptake (mol)	0.039±0.01	0.036±0.02	0.047±0.01	0.048±0.03
Moles of O ₂ in products ^b	0.029±0.01	0.028±0.01	0.033±0.06	0.035±0.02
% O ₂ in products ^{b,c}	74±2	79±1	69±5	73±1

^a From oxygen uptake curves at time=5h of experiments described in Table 2-1; ^b Products ROOH, ROH and R'O only; ^c Calculated from the ratio of O₂ uptake and moles of O₂ accounted for in products.

According to the mechanism, the primary function of the catalyst is to decompose the intermediate alkyl hydroperoxide (ROOH), and generate chain-propagating radicals RO• and ROO• through steps 12 and 13, where one of the steps is diffusion controlled and the other is rate determining. UV-visible spectra of the catalysts in-situ confirm that Fe(II) and Fe(III) species are the resting states for **1** and **2**, respectively. The weakly oxidizing catalyst precursor **2** (or its activated form) is slowly reduced by the hydroperoxide (step 12), while the active metal catalyst derived from **1** is slowly oxidized by the hydroperoxide (step 13). The rate constants for peroxide decomposition by the active catalytic complexes derived from **1** ($k_{13} = 1.7 \text{ M}^{-1}\text{s}^{-1}$) and **2** ($k_{12} = 7.0 \text{ M}^{-1}\text{s}^{-1}$) were estimated by fitting cumyl hydroperoxide decomposition and cumene oxidation data to the proposed mechanism in Figure 2-9.

Figures 2-10 and 2-11 show the experimental data for cumene oxidation and peroxide decomposition catalyzed by **1** and kinetic fits calculated by using the proposed mechanism. The mechanistic scheme provides a reasonable model for predicting the

experimentally determined formation of ROOH, ROH and R'O. In the case of cumene oxidation and peroxide decomposition catalyzed by **2**, the agreement between the calculated values and those predicted by the model is also very good (Figures 2-12 and 2-13). Successful modeling of the differences in the induction period between **1** and **2** was achieved by using step 9 only in modeling reactions catalyzed by **1**, and steps 10 and 11 in modeling reactions catalyzed by **2**. Although **2** is activated by both ROOH and H₂O, the proposed rate constants of the two steps are much smaller than k_9 . The proposed mechanism also closely models the results of ROOH-initiated cumene oxidation catalyzed by **1** and **2**, as shown in Figures 2-14 and 2-5, respectively. The yields of the uncatalyzed reaction are also predicted closely by the proposed mechanism. Simulations done by using the steps and rate constants in Figure 2-9 and by setting the catalyst concentration to zero, predict the formation of only trace products. Uncatalyzed reaction simulation results are shown in Table 2-4. Product formation calculated by the model is consistent with experiment as is shown in the GC trace in Figure 2-17. After 5 hours of reaction under our conditions, in the absence of catalyst, only a trace amount of ROOH was detected with ROH and R'O at concentrations too low to be determined quantitatively (Table 2-4).

Although the proposed mechanism includes a fair amount of detail, a number of additional steps could be added in order to account for other pathways and the many possible trace products formed in autoxidation reactions. The complex, multi-step, free-radical chain mechanism of autoxidation, containing multiple initiation, propagation and chain termination pathways has been modeled in greater detail. For example,

Tolman et al.⁷⁴ proposed a cyclohexane autoxidation scheme comprising of 154 reactions.

The steps and rate constants in Figure 2-9 provide a reasonable model that fits all of the experimental data. The proposed mechanism provides a reasonable model that fits both catalyzed cumyl peroxide decomposition and cumene oxidation data using rate constants $\pm 10\%$ of the values reported in Figure 2-9. The 10% variation in the rate constants is within the experimental error for the oxidation experiments (Table 2-1). In addition, the values for the rate constants change with different media and we would expect a variation in the rate constants due to media effects in experiments where high concentrations of H_2O or ROOH were added in comparison to the autoxidation runs.

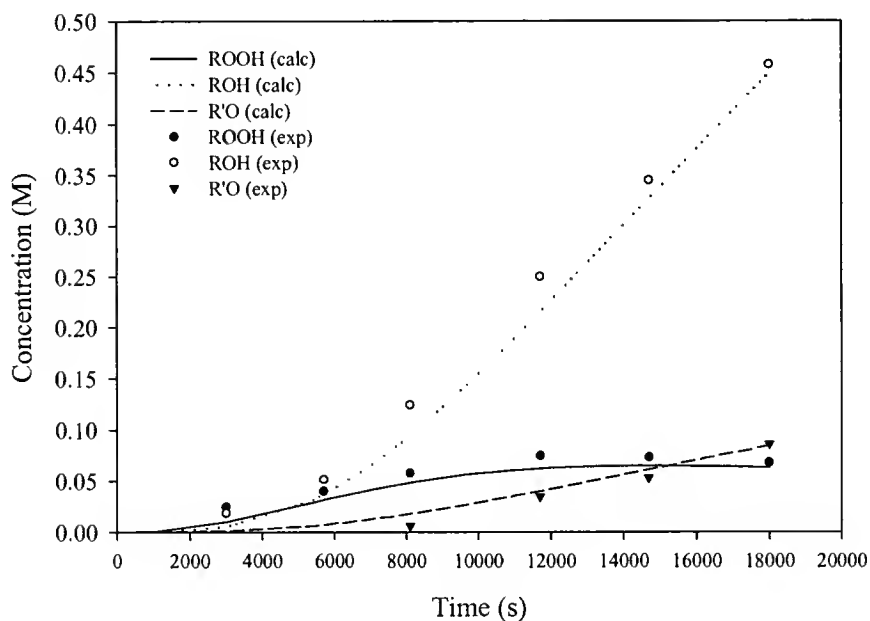


Figure 2-11. Simulation of cumene oxidation catalyzed by **1**; Data points correspond to experimental data while the lines are the calculated results

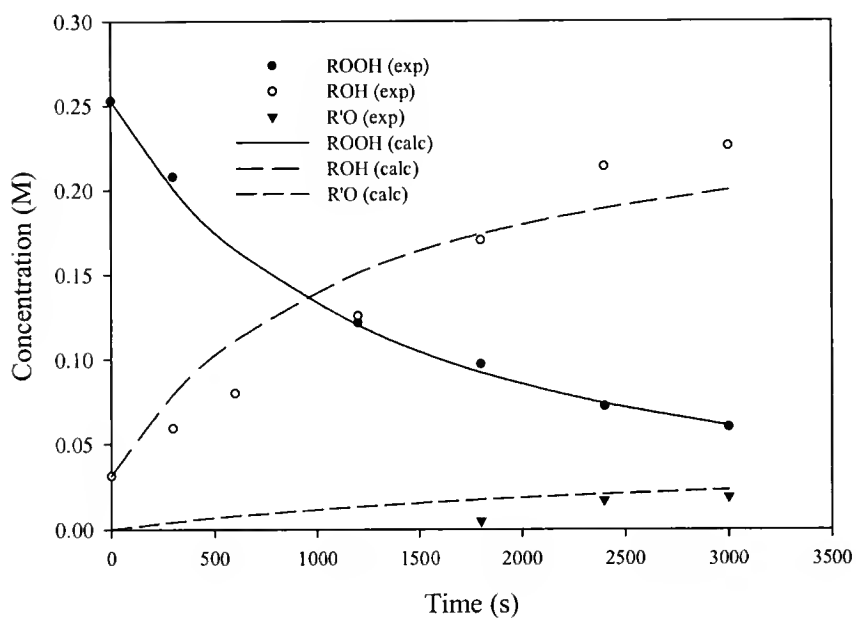


Figure 2-12. Simulation of cumyl peroxide decomposition catalyzed by 1

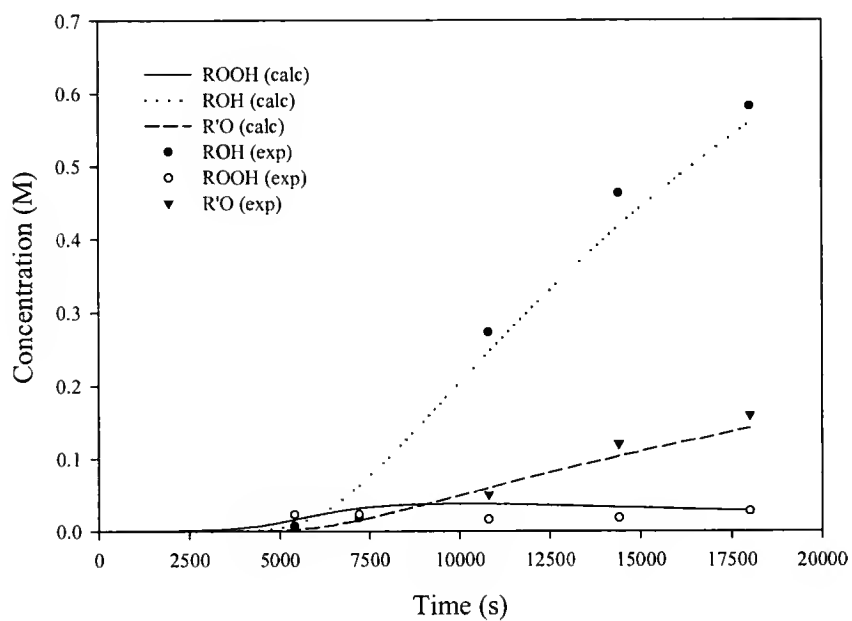


Figure 2-13. Simulation of cumene oxidation catalyzed by 2

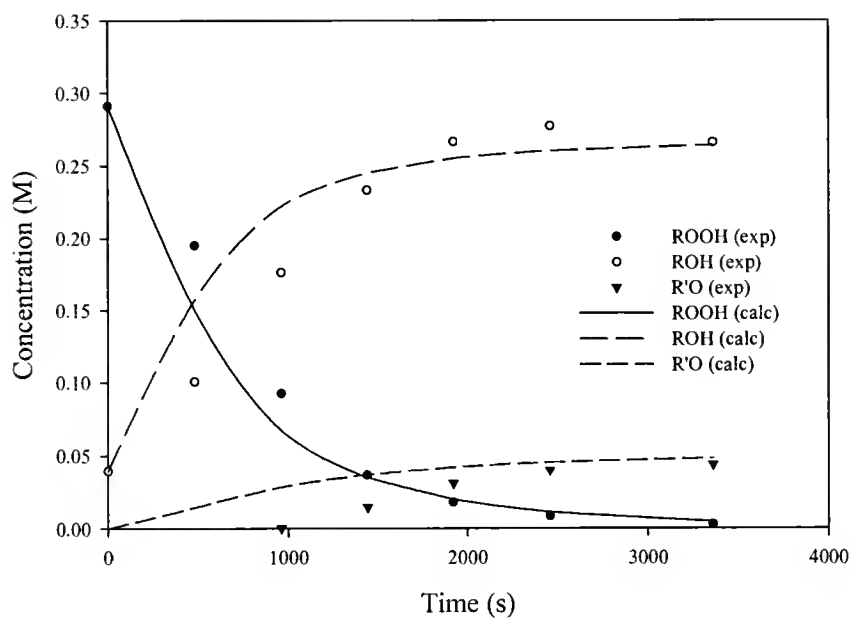


Figure 2-14. Simulation of cumyl peroxide decomposition catalyzed by 2

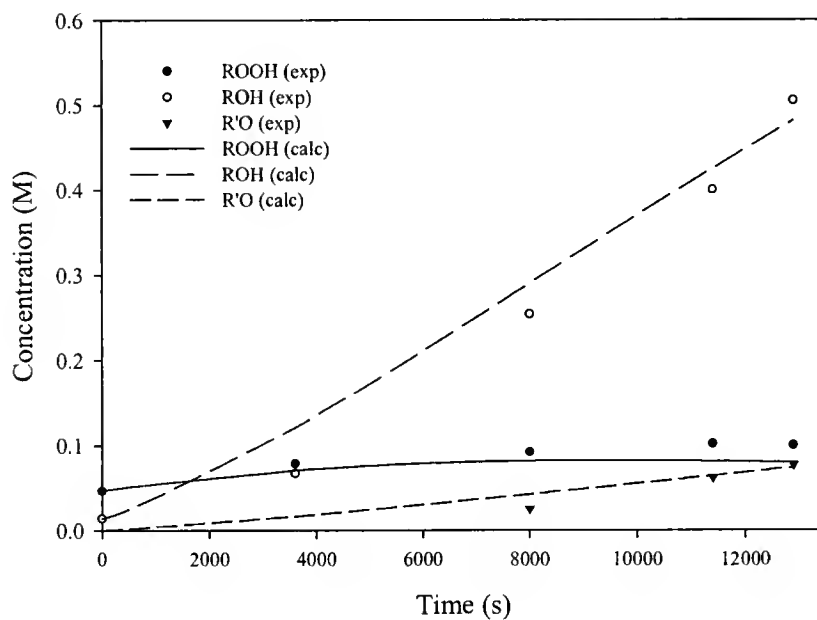


Figure 2-15. Simulation of ROOH initiated cumene oxidation catalyzed by 1

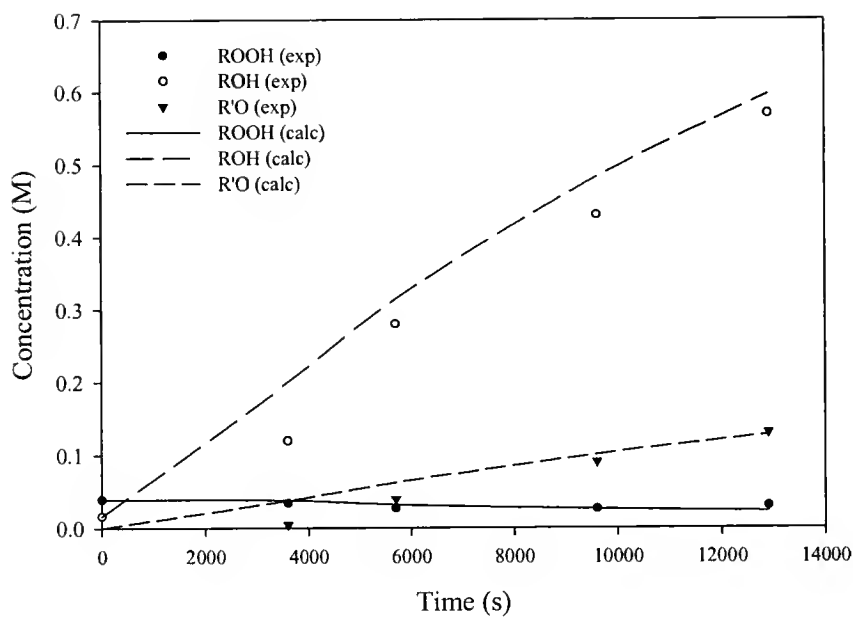


Figure 2-16. Simulation of ROOH initiated cumene oxidation catalyzed by 2

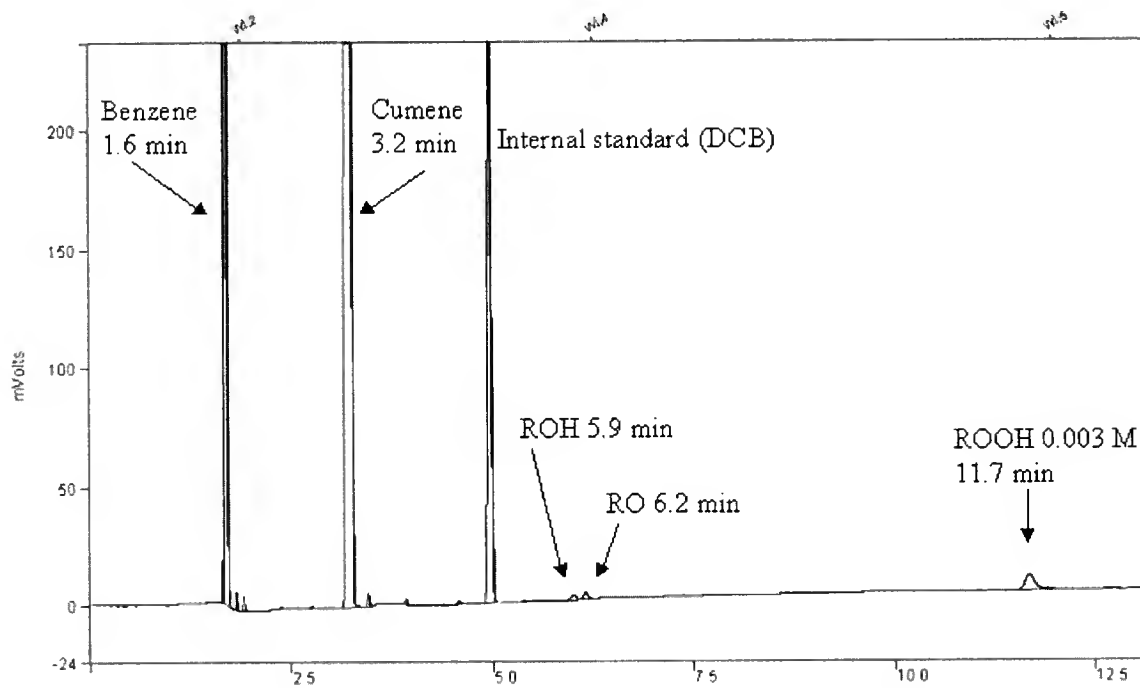


Figure 2-17. GC trace of sample after 5h of uncatalyzed reaction. Reaction conditions; 60 °C, 60 psi O₂, 50/50 cumene/benzene

Table 2-4. Simulated and experimental results for uncatalyzed cumene autoxidation

	ROOH (M)	ROH (M)	R'O (M)
Simulation results ^a	2.4×10^{-3}	1.4×10^{-5}	2.7×10^{-6}
Experimental results ^b	3×10^{-3}	Trace	Trace

Simulation and experimental results correspond to product concentrations after 5 h of reaction. ^a Steps and rate constants in Figure 2-9 used to calculate product concentrations, with the catalyst concentration set to zero. ^b Reaction conditions; 60 °C, 60 psi O₂, 50ml/50ml cumene/benzene.

Solvent Dependence

The effect of changing the solvent polarity was investigated for cumene autoxidation catalyzed by **1**. The reactions were carried out at a slightly higher reaction temperature of 80°C for a reaction time of 2 hours. The four solvents used, span a wide range of dielectric constants as shown in Table 2-5.

Table 2-5. Solvent effects on cumene oxidation catalyzed by **1**

Solvent (dielectric constant)	dO ₂ /dt ^a (M/s)	% Conv	% ROOH	% ROH	% R'O
Benzene (2.3)	1.0×10^{-4}	26±1	6±1	66±1	28±1
o-dichlorobenzene (9.9)	0.9×10^{-4}	17±1	15±2	62±1	23±1
t-butyl alcohol (12.5)	1.3×10^{-4}	25±1	9±2	52±2	39±1
acetonitrile (37)	1.4×10^{-4}	26±1	14±1	47±1	39±1

^a Rate of oxygen uptake obtained from slope of oxygen uptake curves. 50/50 cumene/co-solvent; 1.2×10^{-4} M **1**; run time=2h; 80 °C; 60 psi O₂

The results show a small dependence on solvent dielectric constant with o-dichlorobenzene resulting in the lowest activity of **1** out of the four solvents used. The reported dependence of the uncatalyzed free-radical steps of cumene autoxidation on solvent polarity is not significant.⁷⁵ For example, the reported rate dependence of cumene autoxidation in nitromethane (ϵ 36) versus chlorobenzene (ϵ 5.6) gives a ratio of only 1.26, a very modest increase in the rate when using nitromethane as a solvent while the difference between the dielectric constants is large.¹ Radical mechanisms involve

neutral reactants and products ; therefore, there is little charge separation in the transition state and the rate is expected to be relatively insensitive to the solvent.

The solvent does have an effect on product selectivity as well as the length of induction period as shown in Figure 2-18. For example, when using *t*-BuOH and CH₃CN as solvents the amount of oxygen uptake after 2 hours is ~0.08mol. However, when benzene is the co-solvent only 0.06mol of oxygen is consumed while the conversion to ROOH, ROH and R'O is comparable to reactions done in *t*-BuOH or CH₃CN (Table 2-5). The results suggest that in benzene, the catalysis is more selective toward the formation of ROOH, ROH and R'O than to over oxidation products such as CO and CO₂. The increased induction period in CH₃CN is also apparent when comparing the oxygen uptake curves in Figure 2-18.

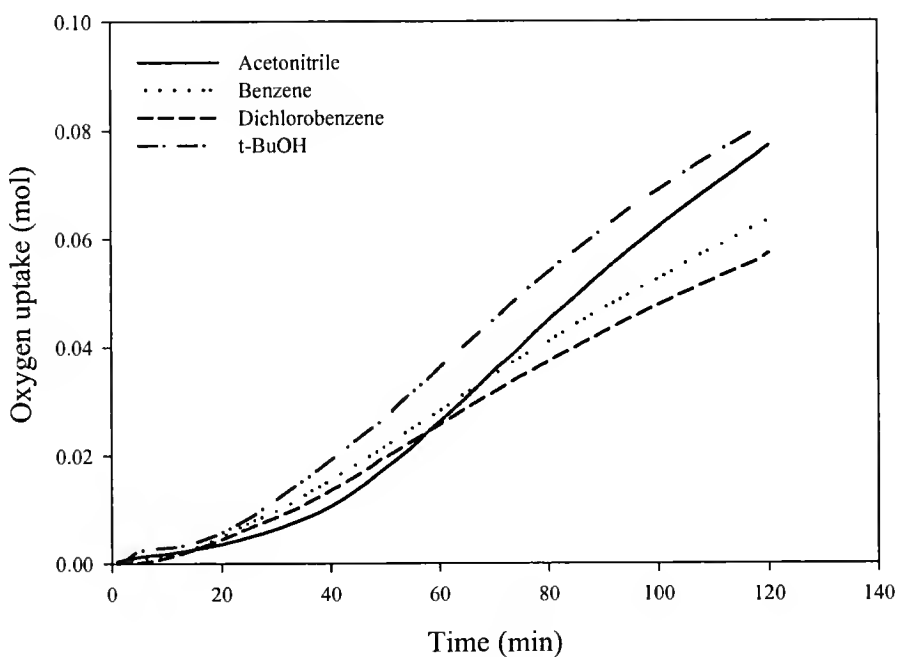


Figure 2-18. Oxygen uptake curves in cumene oxidation catalyzed by **1** in different solvents

Oxygen Pressure and Temperature Dependence

The dependence of autoxidation reactions on oxygen pressure is expected to be zero, even at atmospheric pressure. Considering the mechanism in Figure 2-9, the diffusion-controlled addition of molecular oxygen to R^\bullet is the only step where oxygen is a reactant. The oxygen pressure dependence in cumene oxidation catalyzed by **1** was investigated over a pressure range of 30-100 psi. The zero dependence of oxygen pressure is clearly seen in the oxygen uptake curves shown in Figure 2-19. The observed behavior provides further support for the radical autoxidation mechanism.

The expected effect of increasing the reaction temperature in autoxidation reactions is that of increased selectivity toward the secondary oxidation products, in our case ROH, $R'O$, etc. The ROOH concentration remains at a relative steady state over the range of temperatures while the conversion to ROH and $R'O$ increases as expected for an autoxidation mechanism (Figure 2-20).

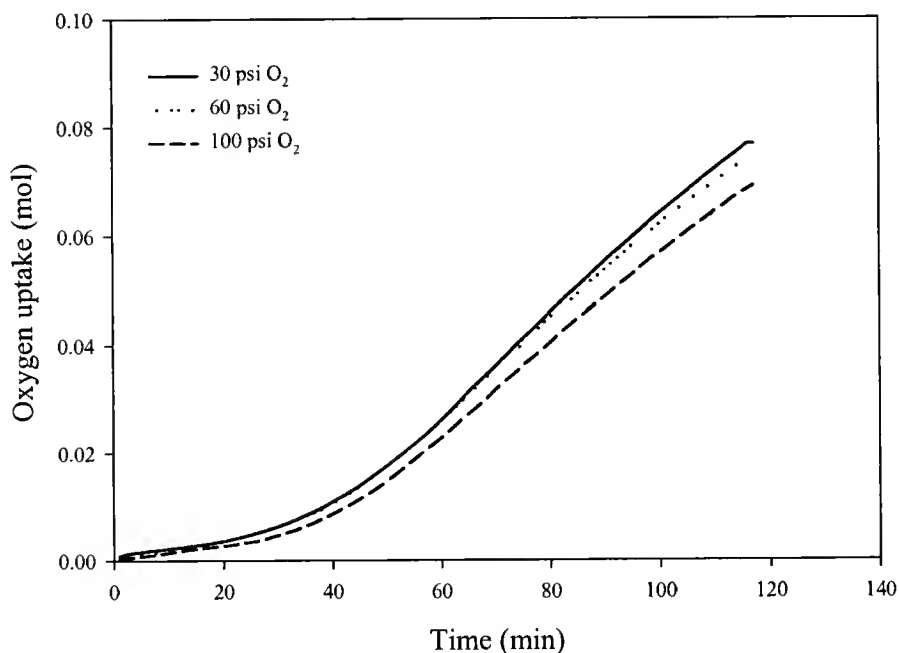


Figure 2-19. Dependence of rate of oxygen uptake on oxygen pressure

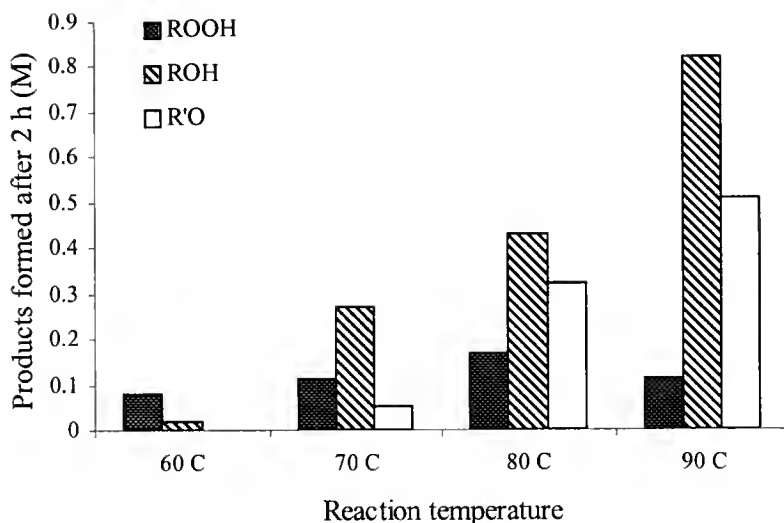


Figure 2-20. Temperature effects on product selectivity for cumene oxidation catalyzed by 1

Metal Concentration Dependence

An important feature of metal catalyzed autoxidation reactions is the maximum rate of oxidation.^{1,12} The maximum theoretical rate of oxidation is dependent on the substrate and is determined by the propagation and termination rate constants. The maximum rate equation derived from the general autoxidation mechanism (Figure 1-1) is shown in equation 2-2,

$$-dO_2/dt = \frac{k_p^2 [RH]^2}{2 k_t} \quad (2-2)$$

where k_p and k_t are the propagation and termination rate constants respectively.¹²

Equation 2-2 holds true in the presence of metal catalysts as long as they do not catalyze the propagation and termination steps. Hence the rate of oxygen uptake during metal catalyzed autoxidation can be increased only up to a limiting value. The theoretical limiting rate for cumene at 60 °C calculated from Eq. 2-2 is $3.1 \times 10^{-5} \text{ Ms}^{-1}$, and was

obtained using $k_p = 1.0 \text{ M}^{-1} \text{ s}^{-1}$ and $k_t = 2.1 \times 10^5 \text{ M}^{-1} \text{ s}^{-1}$. Constants k_p and k_t were calculated from literature activation energy values appropriate for a temperature of 60 °C.

The maximum rate was also calculated through simulations using our proposed mechanism and rate constants shown in Figure 2-9, and yielded a value of $3.8 \times 10^{-5} \text{ Ms}^{-1}$. The maximum rate was also determined experimentally by increasing the concentration of **1** until the rate of oxygen uptake leveled off. The experimental maximum rate is $4.4 \times 10^{-5} \text{ Ms}^{-1}$. Comparison of rates determined through experiment, our kinetic scheme and the theoretical rate calculated from Eq. 2-2 is shown in Figure 2-21. Our mechanism predicts a maximum rate more closely aligned with the theoretical maximum rate of $3.1 \times 10^{-5} \text{ Ms}^{-1}$ calculated from Eq. 2-2. The much larger maximum rate measured experimentally suggests that at high concentrations the metal may be involved in catalyzing more than just the peroxide decomposition steps. The metal may participate in reacting with the alkoxy or alkylperoxy radicals.

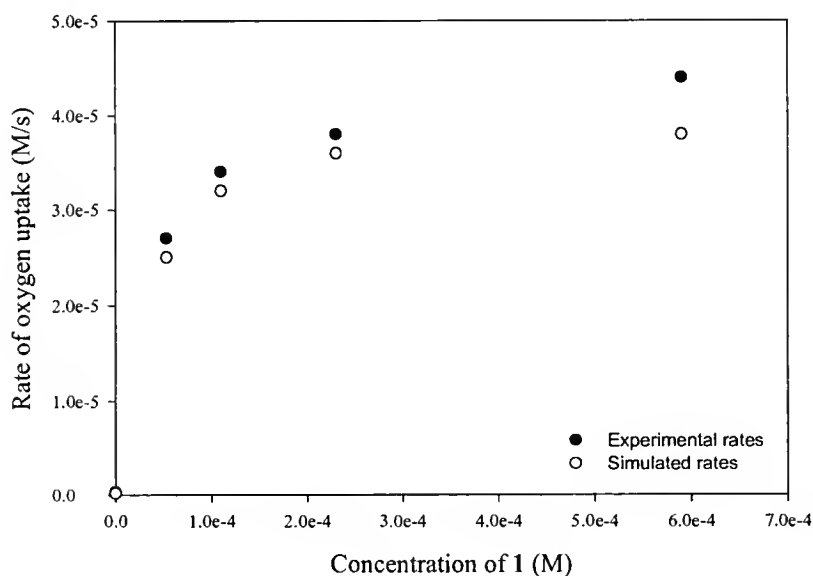


Figure 2-21. Experimental and calculated dependence of catalyst concentration on rate of oxygen uptake; 60 °C, 60 psi O₂, 50/50 benzene/cumene, Run time=5 h

Ligand Dissociation Studies

The possible involvement of ligand dissociation in the activation of precursor **1** was investigated. Complex **1** is formed in-situ (indicated by UV-visible spectrum characterization) when $\text{Fe}(\text{SO}_3\text{CF}_3)_2$ plus 1, 2, 3, or 6 equivalents of 4,7-diphenyl-1,10-phenanthroline (DPP) are used to catalyze the reaction. Product conversions increase from 1-3 equivalents along with a parallel increase of the in-situ concentration of **1** (Table 2-6). Using 6 equivalents of DPP results in a decrease in conversion (2%) although the in-situ concentration of **1** is high. The results confirm that **1** is not the catalytically active species, but a precursor to the active catalyst. Adding 3 equivalents of DPP to a precursor **1**-catalyzed oxidation also leads to inhibition. In order to ensure that the DPP ligand is not acting as a radical trap, 3 DPP equivalents were added to catalyst precursor **2**, in which case no inhibition of catalysis was observed. Therefore, adding excess ligand equivalents has no general inhibitory effect but only effects the formation of the active species in **1** catalyzed reactions (Table 2-6).

Table 2-6. Variation of ligand equivalents

Complex	Equiv DPP ^b	% Conv
1 ^a	0	15
	3	2
2 ^a	0	19
	3	23
$\text{Fe}(\text{Trf})_2$	1	4
	2	8
	3	10
	6	2
Reaction conditions 60 °C, 60psi O ₂ , reaction time=5 h, 100mL cumene. ^a 57 μM complex. ^b Number of equivalents based on moles of metal complex (57 μM). Trf = $(\text{SO}_3\text{CF}_3)^{-}$, DPP=4,7-diphenyl-1,10-phenanthroline.		

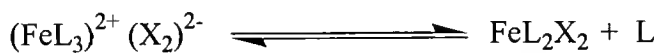
The results suggest that ligand dissociation, presumably to an FeL_2^{2+} species, could be an important step in the activation of **1** since equilibrium DPP dissociation would be

suppressed by the presence of free ligand. The ruthenium(II) analogue of **1** (RuDPP₃Cl₂), although soluble, has no catalytic activity in either autoxidation or peroxide decomposition, presumably because of its lower tendency to dissociate due to strong Ru-N bonds (Table 2-7).

Table 2-7. Cumene oxidation catalyzed by Ru analogue of **1**

Complex	% Conversion
FeDPP ₃ Cl ₂	10
RuDPP ₃ Cl ₂	Trace
Reaction conditions 60 °C, 60psi O ₂ , reaction time=5 h, ^b 50mL/50mL cumene/ o-dichlorobenzene, 57 μM complex.	

Ligand displacement in iron tris α,α'-diimine (L) complexes such as **1** has been reported to occur in the presence of a strong nucleophile in solvents having a low dielectric constant.⁷⁶



Although FeL₃²⁺ complexes are known to be substitution inert in an aqueous solvent, the interactions of charged species are expected to be very different in non-polar solvents.

The absence of strong ionic solvation leads to increased tendency for strong ion-pairing between the metal complex cation and the anion in non-polar solvents.

Fe(1,10-phenanthroline)₃(Cl)₂ was reported to form the FeL₂Cl₂ complex in dry dimethylsulfoxide (DMSO ε=4.7) due to the Cl⁻ trapping by the FeL₂²⁺ species.^{76,77} The formation of the bis complex from Fe(1,10-phenanthroline)₃(ClO₄)₂ was not observed, presumably because the ClO₄⁻ ion is not nucleophilic enough to trap the FeL₂²⁺ species.

Placing **1** in dry DMSO and adding LiCl results in the formation of a shoulder at λ~640 nm corresponding to the FeL₂Cl₂ species (Figure 2-22). Therefore, the expected

effect of a more nucleophilic X^- counterion is that it would push the equilibrium to the right by trapping the FeL_2^{2+} species.

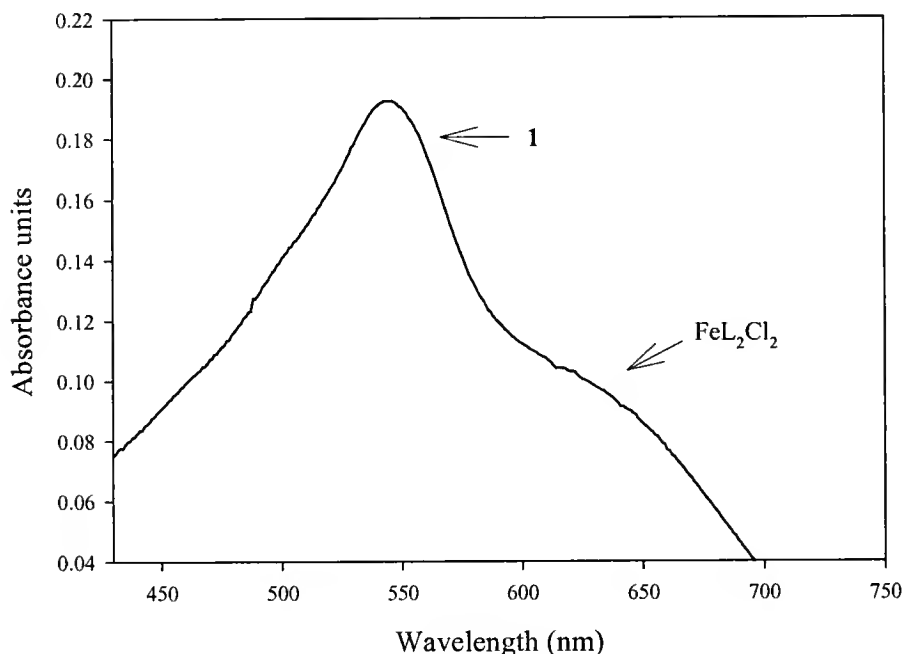


Figure 2-22. Formation of FeL_2X_2 from **1** in the presence of LiCl (Solvent DMSO)

We investigated the role of the counterion in the activation of the catalyst by comparing **1** to $Fe(4,7\text{-diphenyl-1,10-phenanthroline})_3Cl_2$ ($FeDPP_3Cl_2$). In our experiments both the $Fe(DPP)_3^{2+}$ chloride and triflate salts have comparable activities (Table 2-8). The results suggest that the difference in the coordination ability of the anion does not appear to have an effect on the formation of the active catalyst. It is likely that the counterion effect on the equilibrium is so small that under our reaction conditions it does not translate into a shorter induction period. Also the formation of water may interfere with the coordinating ability of the more nucleophilic counter-ion due to solvation effects. Alternatively, the ligand dissociation step may not be rate determining.

Table 2-8. Counter ion effects

Complex	% Conversion
1	12
Fe(DPP) ₃ Cl ₂	10
Reaction conditions 60 °C, 60psi O ₂ , reaction time=5 h, 50mL/50mL cumene/ o-dichlorobenzene, 57 μM complex. ^a DPP=4,7-diphenyl-1,10-phenanthroline.	

Precursor Degradation

Both precursors **1** and **2** exhibit a slow decrease in their signature UV-visible absorbance during the reaction. During 5 hour autoxidation reaction at 60°C the absorbance of **1** decreases by 38%. Direct monitoring of the Uv-visible absorbance of **1** in the presence of ROOH at 60°C was done in order to observe the spectral changes during reaction of **1** with ROOH. Shown in Figure 2-23 are the spectral changes over a period of 1 hour of a solution of **1** in benzene (1.5×10^{-6} M) in the presence of 1.5×10^{-4} M ROOH at 60°C. The large unresolved band between 430-540 nm corresponds to metal to ligand charge transfer (MLCT) transitions typical for Fe-tris diimine complexes. The large off-scale absorbance at ~315 nm is a result of ligand-centered π - π^* transitions. Over a time period of 1 hour, the spectrum shows a decrease in the MLCT band at $\lambda_{\text{max}} = 540$ nm. Concurrent formation of two shoulders at 380 nm and 650 nm is also observed. The shoulder at 650 nm may be a result of a FeL_3^{3+} species formed through the oxidation of **1** by ROOH. The formation of an $[\text{FeL}_3]^{3+}$ species from a $[\text{Fe}(1,10\text{-phenanthroline})_3]^{2+}$ complex in the presence of H_2O_2 has been reported in the literature, and absorbs in the 600-650 nm region.⁵⁹ The shoulder may also correspond to a FeL_2X_2 species shown to absorb in the same region (Figure 2-22). The identity of the shoulder formed at 380 nm is equally ambiguous. None of the expected products of ROOH decomposition (ROH, R'O) absorb in the 380 nm region. However, the absorbance of the free DPP ligand is slightly red shifted compared to the π - π^* transition

of the coordinated ligand; hence, the shoulder in the region may be the result of free DPP ligand. Alternatively the shoulder may be a result of a new iron species, likely an inactive iron complex.

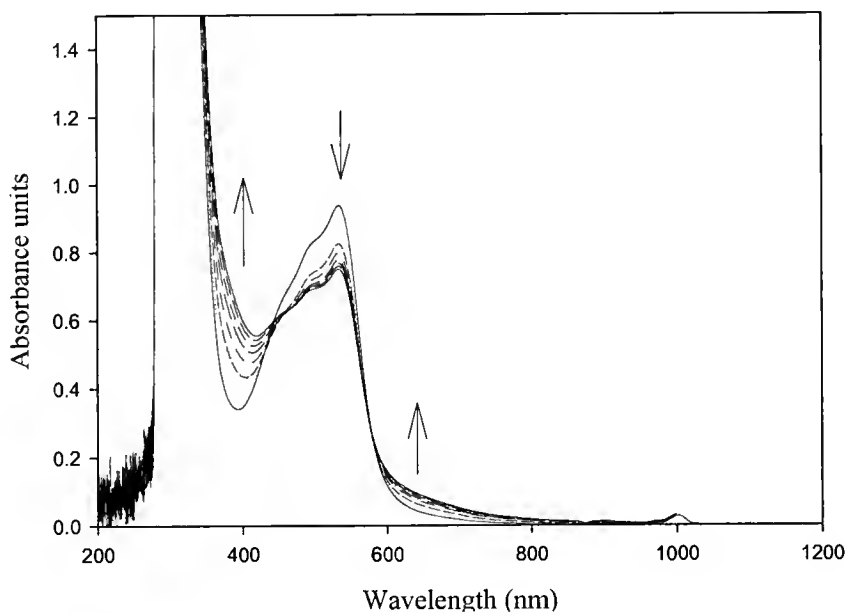


Figure 2-23. Spectral changes of **1** at 60 °C in the presence of ROOH

Attempts to isolate an iron-containing residue from the reaction solution following cumene oxidation catalyzed by **1** resulted in an oil that could not be characterized conclusively. Extraction of the reaction solution with NaCl saturated water and qualitative analysis of the aqueous layer using 1,10-phenanthroline and NCS^- as indicators, suggests the presence of both Fe(II) and Fe(III) in solution.

Co-oxidation by Reaction Products

In the absence of direct evidence of the active catalyst it is important to ensure the reaction products do not catalyze the reaction. Co-catalysis by oxidation products is referred to as ‘co-oxidation’ and has been reported in the literature.¹ Compounds such as alcohols and ketones are in general more reactive than the saturated hydrocarbon

substrate and in some cases form radicals easily. Cyclohexanone is susceptible to hydrogen atom abstraction because of the weak α C-H bond and the formation of a resonance stabilized radical. Therefore, in the autoxidation of cyclohexane (BDE 99 kcal mol⁻¹), the formation of cyclohexanone (BDE 94 kcal mol⁻¹) catalyzes the reaction. The co-oxidation phenomenon is commonly used to improve product yields, for example in the co-oxidation of alkenes and aldehydes.¹ The acylperoxy radicals formed from the aldehyde and the resulting peracid are utilized for the epoxidation of olefin and results in higher yield of epoxide than if aldehydes are not present.

Catalysis of cumene autoxidation by the reaction products was checked in order to ensure that ROOH, R'O and ROH were not catalyzing the reaction by forming radicals. Adding R'O in the presence of precursor 1 results in slight inhibition, where adding ROH results in a minor increase in conversion as shown in Table 2-9. The results of adding ROH and R'O are minor and their effect on the catalysis is considered relatively insignificant. Trace product ROOR (4×10^{-2} M) was also added to a 1 catalyzed reaction under identical conditions (Table 2-9). The concentration of ROOR did not change during the 5 hours of reaction. The presence of ROOR did not interfere with the expected formation of ROOH, ROH and R'O, and resulted in an oxygen uptake of 0.04 mol (compare to standard result of 0.039 mol in Table 2-1).

Table 2-9. Co-oxidation studies

	ROOH (M)	ROH (M)	R'O (M)
1	0.08±0.1	0.41±0.09	0.07±0.03
1 + R'O	0.14	0.36	0.10
1 + ROH	0.07	0.55	0.13
ROOH only	0.04	0.01	Nd
Reactions done at 60 °C, 60psi O ₂ , 56μM 1, 50/50 cumene/benzene; 4×10^{-2} M added R'O, ROH or ROOH, reaction time=5 h. Blank reaction under the same conditions yields trace ROOH only. Nd=none detected.			

The trace product α -methyl styrene was also checked for its ability to act as a co-oxidant. Cumene oxidation catalyzed by **1** in the presence of 0.7 M α -methyl styrene showed that the styrene is slowly converted to acetophenone ($R'O$). The observation explains the low concentrations of α -methyl styrene detected in solution. Figure 2-24 shows the oxygen uptake curve and product formation over time in the presence of added α -methyl styrene. The results show the absence of co-catalysis by α -methyl styrene, on the contrary the yield of ROH is slightly inhibited, due to the portion of the $ROO\cdot$ radicals being diverted to reacting with α -methyl styrene. Oxidation of α -methyl styrene in the presence of **1** under the same reaction conditions did not result in the formation of any products suggesting any radicals formed in the reaction must come from cumene. The proposed mechanism of the formation of acetophenone ($R'O$) from α -methyl styrene is shown in Figure 2-25.

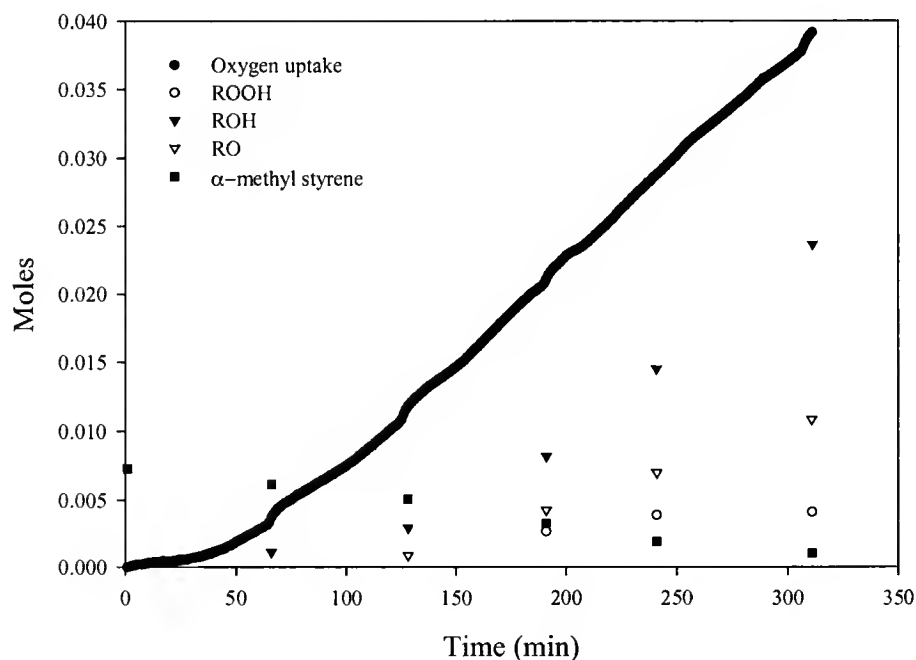


Figure 2-24. Product formation and oxygen uptake in cumene oxidation catalyzed by **1** in the presence of α -methyl styrene; Reaction conditions: 60 °C, 60psi O_2 , 56 μ M **1**, 50/50 cumene/benzene

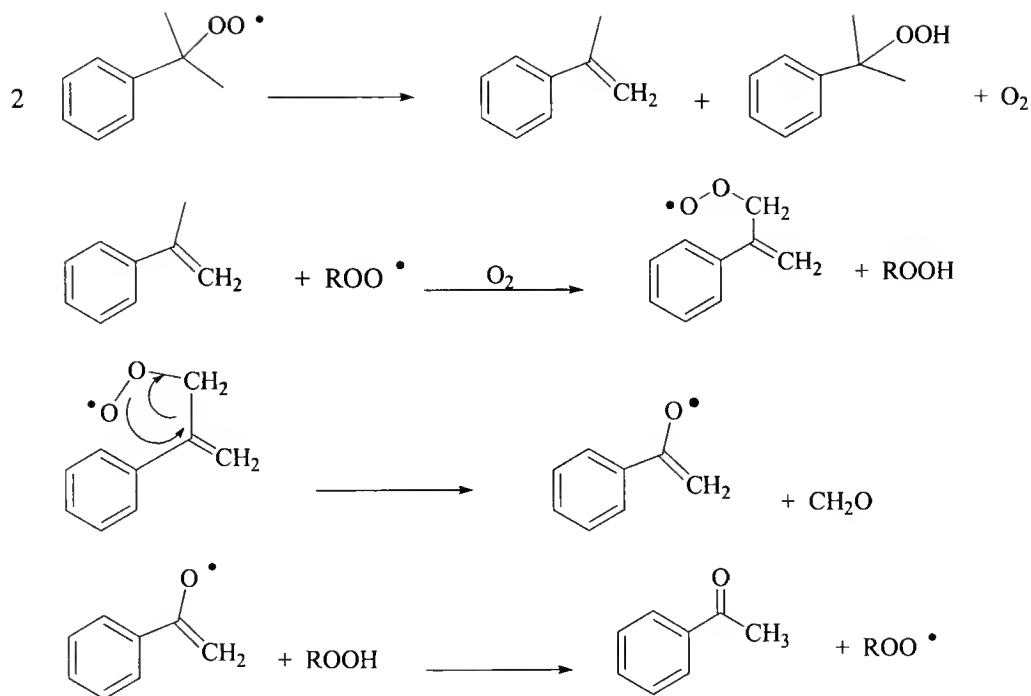


Figure 2-25. Proposed mechanism of α -methyl styrene formation

Uncatalyzed cumene oxidation in the presence of added ROOH produced only small amounts of additional ROOH (Table 2-9). Adding ROH or R'O also in the absence of catalyst did not yield any additional products even at an elevated reaction temperature of 80°C, as is evident by the moles of oxygen uptake compared to the blank reaction shown in Table 2-10.

The lack of co-oxidation in the presence of products is consistent with the bond energies of their abstractable C-H bonds as is shown in Table 2-11. The results support the assertion that the catalysis is being carried by an activated precursor species and not co-catalysis by the reaction products.

Table 2-10. Catalysis by products in the absence of 1

	Moles of O ₂ uptake
ROH only	0.015
R'O only	0.011
Blank	0.018
Reactions done at 80 °C, 60psi O ₂ , 4x10 ⁻² M ROH or R'O, 50/50 CH ₃ CN/cumene.	

Table 2-11. Bond dissociation energies

	Bond Dissociation Energy (kcal/mol) ^{78,79}
Cumene (D RCH ₃ C-H)	83.2-87.3
Acetophenone (D RCOCH ₂ -H)	90.7-93
2-phenyl-2-propanol (D RCH ₃ CO-H)	102-103

Active Catalyst Lifetime

Active catalyst lifetime can be assessed by comparing the experimental oxygen uptake curve over a long time period to the oxygen uptake curve predicted by the proposed mechanistic scheme (Figure 2-10).

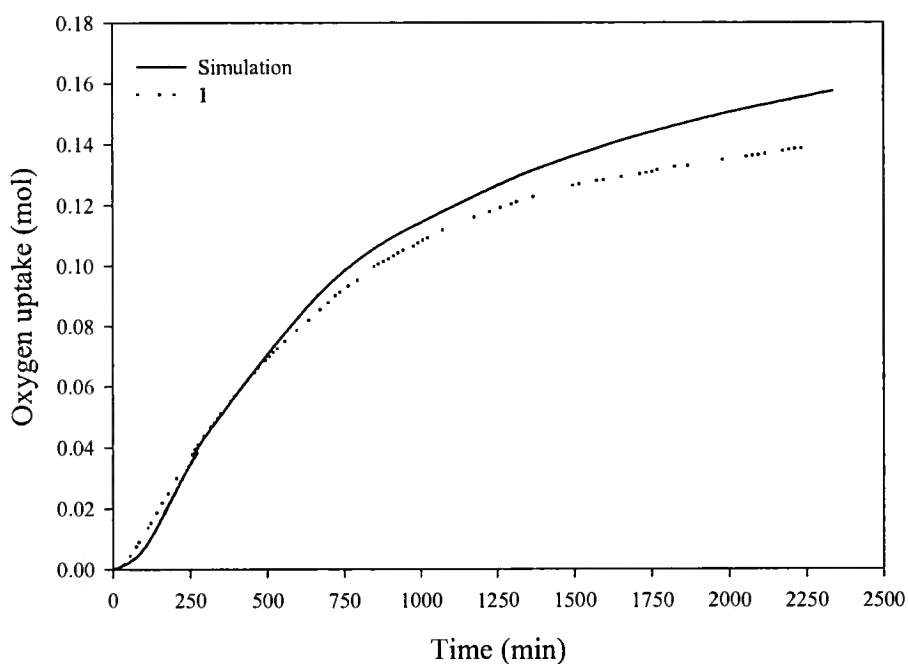


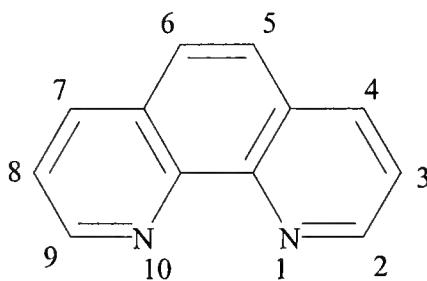
Figure 2-26. Comparison of oxygen uptake curve during cumene oxidation catalyzed by 1 and a curve predicted by simulation using proposed mechanism

The proposed mechanism does not include any steps leading to catalyst destruction so the predicted oxygen uptake curve does not take into consideration any decrease in the rate due to catalyst degradation. Comparison of the predicted oxygen uptake curve to that of the experimental curve shows that experimentally oxygen uptake levels off earlier than predicted suggesting some catalyst decomposition is occurring. The difference

becomes important at reaction times well beyond the 5 hour reaction time of the standard runs used in our experiments. Therefore, although active catalyst decomposition does occur during the reactions it occurs at a slow enough rate not to have a significant effect on the rate of oxygen uptake during the first 8 hours. The results indicate the active catalyst is robust and remains active for an extended period of time during the reaction.

Ligand variation studies

In order to investigate ligand effects, substituted 1,10-phenanthroline (phen) ligands were used to make a family of tris Fe(II) complexes. The phen ligand numbering scheme is shown in Figure 2-27 and the ligands used are listed in Table 2-12. All of the complexes are SO_3CF_3^- salts except for $[\text{Fe}(5\text{-NO}_2 \text{ phen})_3](\text{ClO}_4)_2$. In our previous discussion we established that counter-ions did not have a noticeable effect on reactivity and we will assume the same here. All of the complexes in Table 2-12 had low solubility in the benzene/cumene solvent system; therefore a 50/50 acetonitrile/cumene solvent system was used.



1,10-phenanthroline (phen)

Figure 2-27. Numbering scheme for the phen ligand

Electron donating substituents such as methyl groups are known to increase the ligand binding strength of the phen ligand resulting in a more stable complex and electron withdrawing substituents have the opposite effect. Considering that ligand dissociation

may be an important first step toward the formation of the active catalyst, we might expect stronger binding ligands to disfavor ligand dissociation leading to longer induction periods and lower product conversion during a specified time period. Binding strength also has an effect on the redox potentials of FeL_3X_2 complexes have been shown to parallel ligand binding strength where electron-withdrawing groups shift the potential to more positive values. A more positive potential results in a less favorable oxidation of Fe(II) to Fe(III) and presumably a slower peroxide decomposition step (k_{13} , Figure 2-10).

The results of cumene autoxidation catalyzed by a series of FeL_3X_2 complexes are shown in Table 2-12. Oxygen uptake curves during the first 100 minutes reveal a general trend correlating ligand binding strength with length of induction period (Figure 2-28). Therefore, shorter induction periods lead to higher oxygen uptake and conversion after a specified time period as expected.

While the induction period is affected by ligand binding strength, the maximum rate of oxygen uptake for all of the complexes is an average of $1.7 \pm 0.4 \times 10^{-4} \text{ Ms}^{-1}$. Therefore, the differences in redox potential do not result in significant variation of the active catalyst activity. The absence of substituent dependence differs from the reported redox potential influence on Fe(III) -halogenated porphyrin activity.^{51,53,80} For a redox range of -0.221 V to $+0.28 \text{ V}$ an approximately 3-fold increase in product formation was reported for a series of Fe(III) -halogenated porphyrin complexes.⁵¹ Although the series of complexes shown in Table 2-12 span a similar range of redox potentials ($\sim 0.4 \text{ V}$) we do not observe any dependence on the redox potential once the reaction reaches the maximum rate of oxygen uptake. The reason for the absence of substituent dependence on catalytic activity of FeL_3X_2 complexes may offer clues about the identity of the active

catalyst. The active catalyst may not contain the phenanthroline ligand, as it is present in the FeL_3X_2 complex. The formation of the active catalyst may include the destruction of the phenanthroline ligands leaving only portions of the ligands.

Table 2-12. Cumene oxidation and peroxide decomposition data of reactions catalyzed by FeL_3X_2 complexes

Complex ^a	E_0 (V) ⁸¹	Induction period (min) ^b	O_2 uptake (mol) ^c	$d\text{O}_2/dt$ (10^{-4} M s^{-1})
$\text{Fe}(5\text{-NO}_2 \text{ phen})_3^{2+}$	1.18	0	0.050	1.8
$\text{Fe}(\text{phen})_3^{2+}$	0.99	25	0.049	1.7
1	0.92	40	0.034	1.2
$\text{Fe}(4\text{-Me phen})_3^{2+}$	0.92	170	0.039	1.8
$\text{Fe}(4,7\text{-Me}_2\text{phen})_3^{2+}$	0.86	200	0.029	1.7
$\text{Fe}(3,4,7,8\text{Me}_4\text{phen})_3^{2+}$	0.81	180	0.046	1.9

^aAll of the complexes are SO_3CF_3^- salts except for $\text{Fe}(5\text{-NO}_2 \text{ phen})_3(\text{ClO}_4)_2$.

^bInduction period defined as the time when oxygen uptake curve becomes linear.

^cReactions done at 60°C and 60 psi of constant O_2 pressure; pre-catalyst = $57 \mu\text{M}$; 50 mL cumene; 50 mL CH_3CN ; reaction time=5 h. ^cReactions done in a Parr reactor at 60°C under argon; pre-catalyst = $57 \mu\text{M}$; Abbreviations: bpy=2,2'-bipyridine, phen=1,10-phenanthroline.

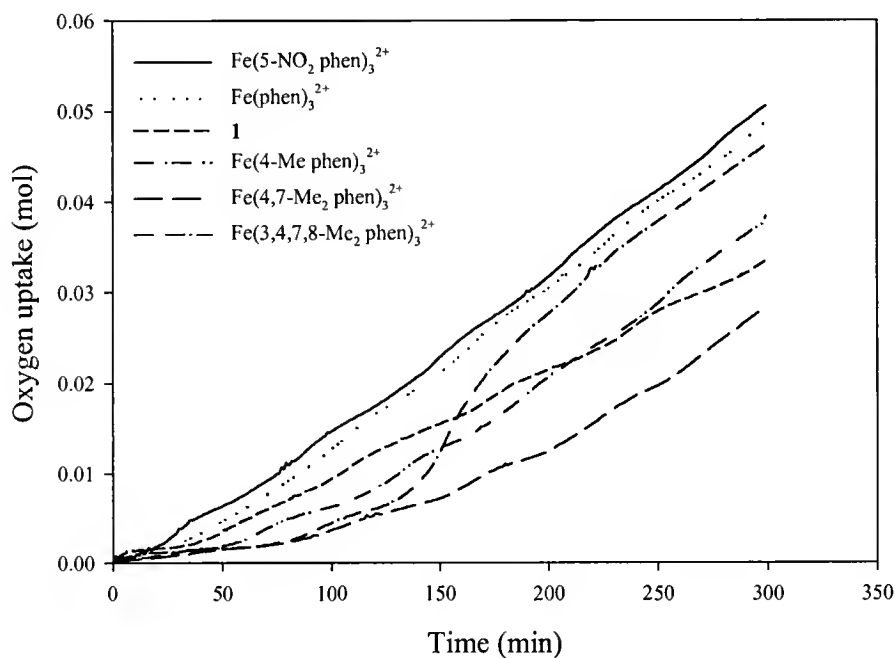


Figure 2-28. Oxygen uptake curves during cumene autoxidation catalyzed by FeL_3X_2 complexes

In such a case the redox potential of the active species would not be altered by substituents present on the phenanthroline ligand in the precursor complex.

$\text{Fe(3,4,7,8Me}_4\text{phen)}_3^{2+}$ deviates from the pattern of the other five complexes not only in induction period but the abrupt increase in the rate of oxygen uptake between 140-160 minutes (Figure 2-28). The peculiar behavior of $\text{Fe(3,4,7,8Me}_4\text{phen)}_3^{2+}$ could be related to the ligand being substituted in four positions instead on only one or two.

Conclusions

In summary, **1** is an active autoxidation catalyst precursor comparable in reactivity to the highly active halogenated iron porphyrins. Although the peroxide decomposition activity of precursor **2** ($k_{12} = 7.0 \text{ M}^{-1}\text{s}^{-1}$) is higher than that of **1** ($k_{13} = 1.7 \text{ M}^{-1}\text{s}^{-1}$), the later exhibits a shorter induction period resulting in comparable activities. The proposed mechanism suggests that the primary function of **1** is to provide an active catalyst that decomposes the intermediate hydroperoxide and generates chain-propagating radicals. The rate dependence on oxygen pressure, temperature, solvent polarity, and catalyst concentration was also investigated and is consistent with a free-radical mechanism.

Results imply **1** is not the active catalyst, and suggest that ligand dissociation is an important step toward catalyst precursor activation. Uv-visible investigations of spectral changes during the reaction of **1** with ROOH suggest the formation of new Fe species in-situ; however, the classification of any such species as the active catalyst is not certain. Co-oxidation by reaction products was ruled out and hence we conclude that catalysis through peroxide decomposition is indeed metal-mediated.

A series of FeL_3X_2 complexes with substituted 1,10-phenanthroline ligands were synthesized and a correlation between ligand binding strength with length of induction period was observed. The correlation supports the proposed ligand dissociation step

implicated in catalyst activation. Increasing the binding strength of the ligand results in a stronger metal ligand interaction and a complex less susceptible to ligand dissociation. The absence of substituent dependence on catalytic activity of FeL_3X_2 complexes suggests that the phenanthroline ligands may not remain intact in the active catalyst.

Simple iron-phenanthroline precursor **1** discussed here is comparable in activity to the halogenated iron porphyrins and is among the most active known hydrocarbon soluble, low temperature, autoxidation catalysts. Related FeL_3X_2 complexes with substituted 1,10-phenanthroline ligands are also highly active autoxidation precursors only when using a polar co-solvent such as acetonitrile to ensure solubility.

CHAPTER 3 HYDROCARBON OXIDATION CATALYZED BY FeL_2X_2 COMPLEXES

Introduction

The investigation of cumene autoxidation catalyzed by **1** presented in Chapter 2 brings up interesting questions about the identity of the active catalyst. The observed dependence of iron/ligand ratio on catalytic activity suggests that ligand dissociation is important in the formation of the active species. In an effort to explore this question, we investigated a series of Fe(II) bis α,α' -diimine (FeL_2X_2) complexes. In this chapter we will compare the catalytic activity and mechanism of catalysis by FeX_2L_2 complexes with the previously studied FeL_3X_2 precursors.

There have been prior reports of FeL_2X_2 ($\text{L}=2,2'$ -bipyridine) complexes used as catalysts for the air oxidation of hydrocarbons.^{61,82} In these studies, the proposed mechanism was that of metal-mediated activation of oxygen leading to a high oxidation state metal-oxo species followed by direct oxygen transfer to the substrate instead of the radical-based peroxide decomposition mechanism.^{60,61,82}

Sawyer et al. reported the catalytic activation of O_2 by iron(II) bis diimine complexes for the direct oxygenation of cyclohexene.^{60,82} $\text{Fe}(2,2'\text{-bipyridine})_2^{2+}$ was used as a catalyst. The suggested mechanism involves the formation of a high oxidation state iron complex and is shown in Figure 3-1. Radical pathways were ruled out since no cyclohexene hydroperoxide was detected.

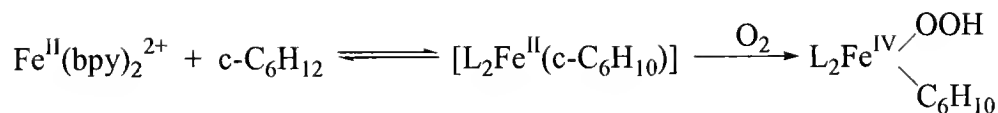
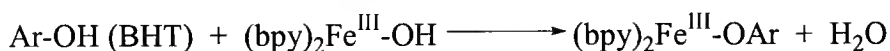


Figure 3-1. Proposed mechanism for the activation of O₂ by FeL₂X₂

The presence of 2,6-ditertbutyl-4-methylphenol (BHT), a known alkoxy-radical trap, was shown to completely inhibit the catalysis, which would suggest that radicals are present. The proposed function of BHT in this case was that of inhibition by coordination to the metal to form an inactive complex as shown below.⁶⁰



Other radical traps such as α -tocopherol and quercetin were also used and resulted in complete inhibition of oxidation. Although the structures of the radical traps are drastically different, reaction inhibition by all three radical traps was proposed to occur by the same mechanism shown above. The structures of the radical traps are shown in Figure 3-2.

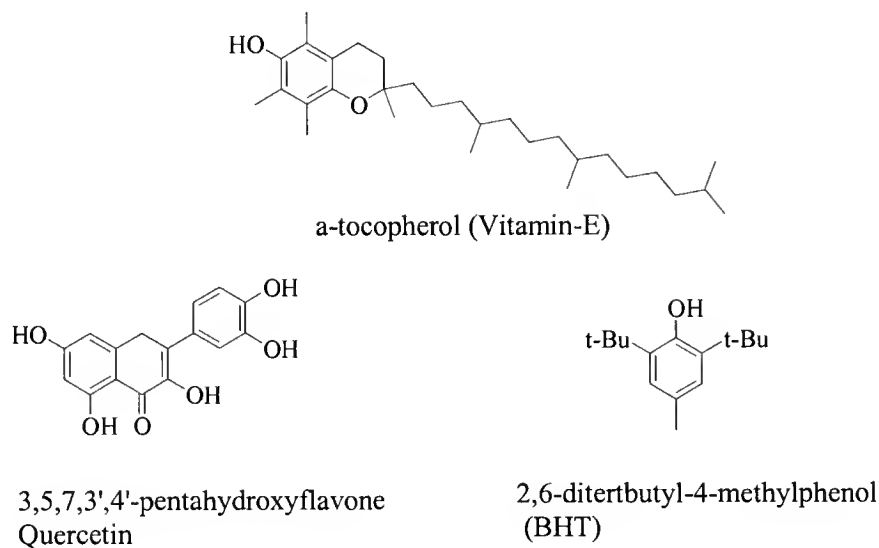


Figure 3-2. Examples of radical traps.

A related iron(II) complex was reported as an active catalyst for the air oxidation of cyclohexane. The complex [*cis*-Fe(2,9-dimethyl-1,10-phenanthroline)₂(H₂O)₂](SO₃CF₃)₂

(Fedmp) (Figure 3-3) was suggested to activate molecular oxygen through the same mechanism as was proposed by Sawyer et al.⁶¹ for $\text{Fe}(\text{2,2' bipyridine})_2^{2+}$.

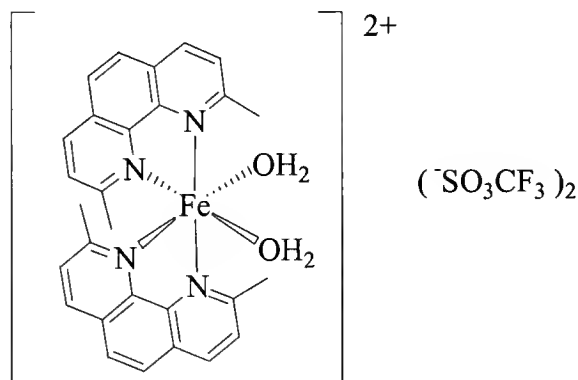


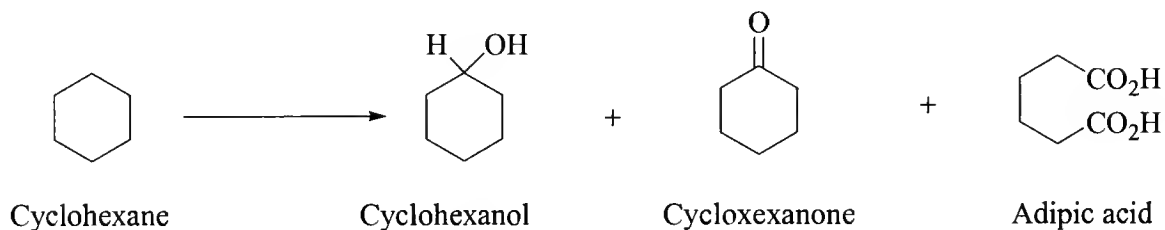
Figure 3-3. $[\text{cis-Fe}(\text{2,9-dimethylphenanthroline})_2(\text{H}_2\text{O})_2](\text{SO}_3\text{CF}_3)_2$ (Fedmp)

The high temperature (125°C) and pressure (550 psi air) at which the oxidation was done, as well as the formation of typical autoxidation products such as cyclohexanol, cyclohexanone, adipic acid etc., suggests the possibility that Fedmp catalyzes the reaction through the free-radical peroxide decomposition mechanism. Our investigation of the air oxidation of cyclohexane and cumene catalyzed by Fedmp and related complexes will be discussed and compared to the mechanism and activity of **1**.

Results and Discussion

cis- $[\text{Fe}(\text{2,9-dimethyl-1,10-phenanthroline})_2(\text{H}_2\text{O})_2](\text{SO}_3\text{CF}_3)$ (Fedmp) was reported to catalyze the air oxidation of cyclohexane in the presence of small amounts of cyclohexanone as initiator. The expected yield is 20% conversion to cyclohexanol, cyclohexanone, adipic acid and small amounts of short chain acids. The reported products and reaction conditions are shown in Figure 3-4. Because of the limitations of our high-pressure reactor we were forced to modify the total pressure of the reaction. The total pressure was dropped to 100psi, this provided an oxygen partial pressure of ~60

psi compared to the 110psi partial pressure of oxygen when 550 psi air is used as reported.



Reaction conditions: 125 °C, 550 psi air, 1.5×10^{-5} mol Fedmp, 125ml CH₃CN, 5ml cyclohexane, 8.2 mL cyclohexanone, reaction time 4 h.

Figure 3-4. Products of the air oxidation of cyclohexane

After 4 h of reaction under 100 psi total pressure (~ 60 psi O₂) and otherwise identical conditions as described in Figure 3-4, only traces of cyclohexanol and cyclohexanone were detected by GC/FID (Figure 3-5, Table 3-1). Increasing the Fedmp concentration to 10x the reported value results in slightly higher conversion, as shown by the oxygen uptake curves in Figure 3-6. Even at higher Fedmp concentration, the yield is only $\sim 1\%$ and does not compare well with the reported 20% conversion. Running the reaction in neat cyclohexane also gave a low product yield of only 3%; however, this may be because of the insolubility of Fedmp in the neat substrate.

Eventually, we were able to run the oxidation under 550 psi air; however, the resulting product yields were almost identical to reactions run at a lower pressure (Table 3-1). The apparent lack of dependence on oxygen pressure is an indicator of a free-radical autoxidation mechanism as discussed in Chapter 2. Furthermore, the blank reaction yields approximately the same amount of product as the catalyzed reaction (Table 3-1). All of the detected products are likely a result of the co-oxidation by the

added cyclohexanone and not metal catalysis. As discussed in Chapter 2, cyclohexanone (BDE 94 kcal mol⁻¹) has a weak α C-H bond and forms radicals more easily than cyclohexane (BDE 99 kcal mol⁻¹).

The poor agreement of our results and the reported observations led us to question the accuracy of the GC analysis. Upon closer inspection we observed poor reproducibility of the GC analysis and poor mass balance between the amount of substrate consumed and products detected. The low reproducibility of the GC analysis was possibly because of the low miscibility of cyclohexane in CH₃CN, resulting in a non-homogeneous solution. An attempt to solve the miscibility problem by diluting the sample in a solvent that was miscible with both components has not improved the reproducibility to a great extent or changed the results.

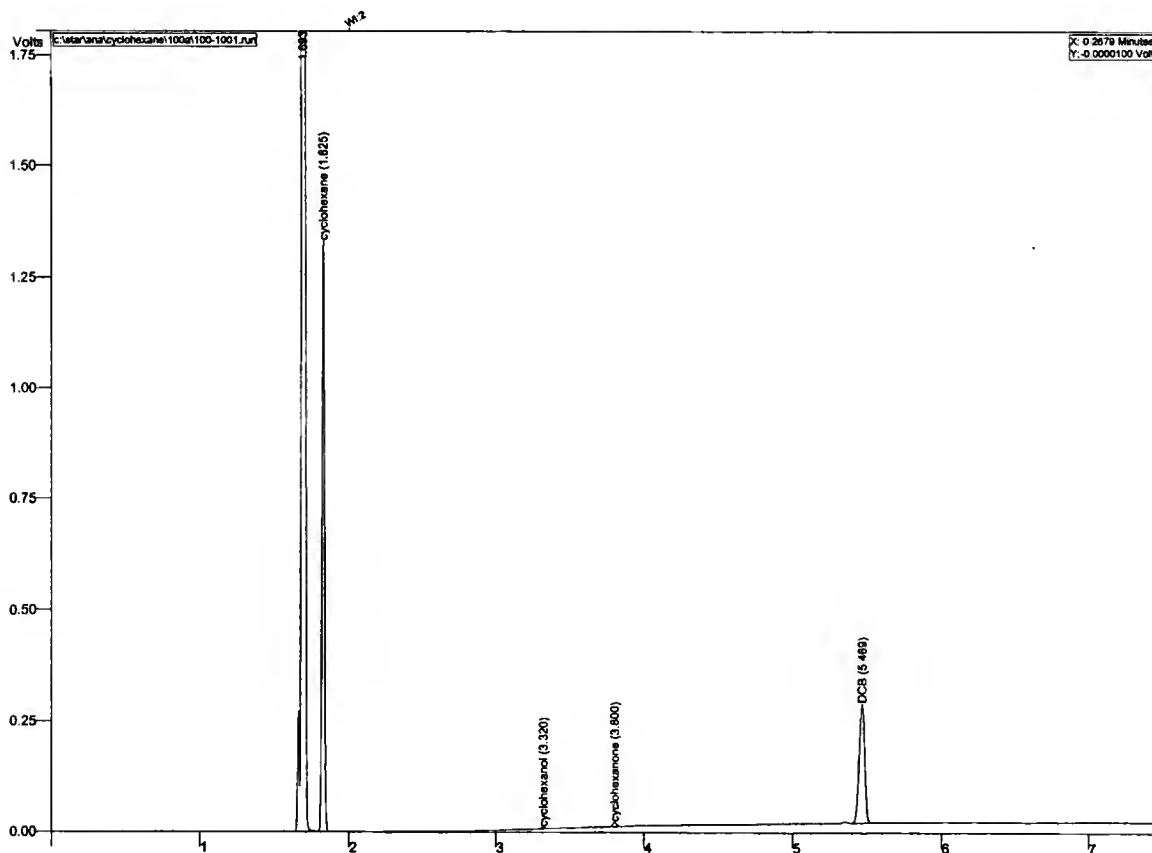


Figure 3-5. GC trace after 4h of cyclohexane oxidation catalyzed by Fedmp

Table 3-1. Cyclohexane oxidation catalyzed by Fedmp

	Cyclohexanone (M)	Cyclohexanol (M)	Run time
100 psi O ₂	0.01	0.005	4 h
100 psi O ₂	0.03	0.007	24 h
550 psi air	0.01	0.003	4 h
Blank 100 psi O ₂	0.01	0.004	4 h
125 °C, 1.5x10 ⁻⁵ mol Fedmp, 125ml CH ₃ CN, 5ml Cyclohexane 5ml, Cyclohexanone 0.008 ml.			

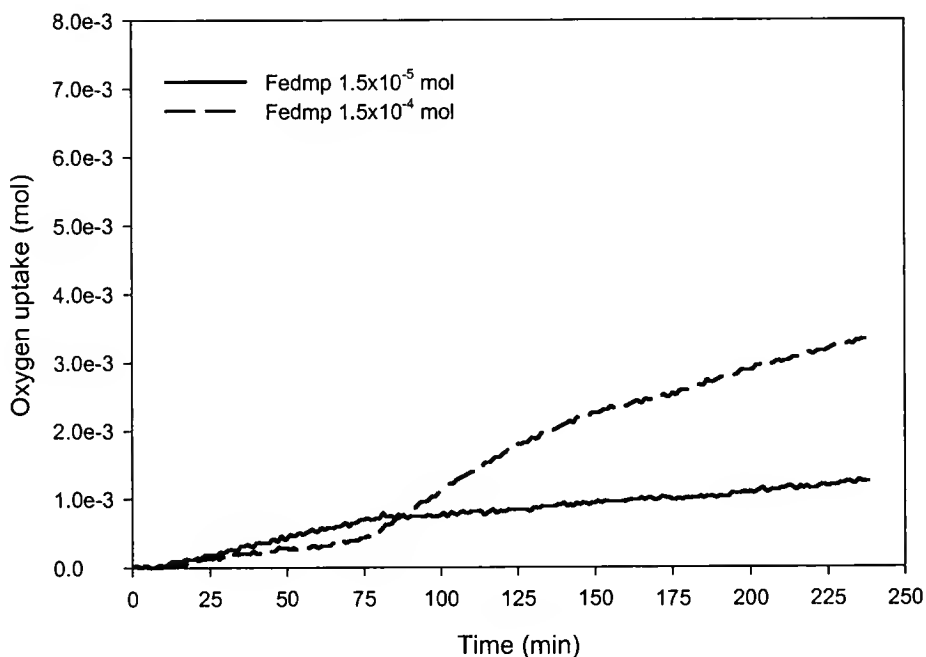


Figure 3-6. Oxygen uptake curves for Fedmp catalyzed cyclohexane oxidation

In view of the apparent low activity and the miscibility problem we chose to investigate alternative reaction conditions. In our previous studies of cyclohexane autoxidation catalyzed by **1**, we employed a 50/50 o-dichlorobenzene (DCB)/cyclohexane solvent system.⁵⁸ Although Fedmp was not fully soluble in the solvent system at room temperature, the solution was homogeneous at the end of the reaction suggesting full solubility at the reaction temperature. Products of Fedmp catalyzed reaction are cyclohexanone, cyclohexanol, adipic acid and three

uncharacterized minor products Figure 3-7. The same major products were observed in our studies of cyclohexane oxidation catalyzed by **1**. Comparison of the product yields using the two complexes is shown in Table 3-2. Complex **1** is clearly more active and yields more products at lower complex concentrations and shorter reaction time. The drastic difference in the catalytic activity between **1** and Fedmp can be appreciated by examining the oxygen uptake curves during cyclohexane oxidation. Fedmp exhibits a long induction period and slow oxygen uptake while **1** has practically no induction and consumes almost double the oxygen in only 30 minutes Figure 3-8. Following the 30-minute time period the oxygen uptake curve of **1** levels off. Prior research in the Richardson labs has shown that oxygen uptake ceases because of buildup of CO and CO₂ in the reactor headspace causing the internal pressure to exceed the set regulator pressure of the incoming O₂.⁵⁸

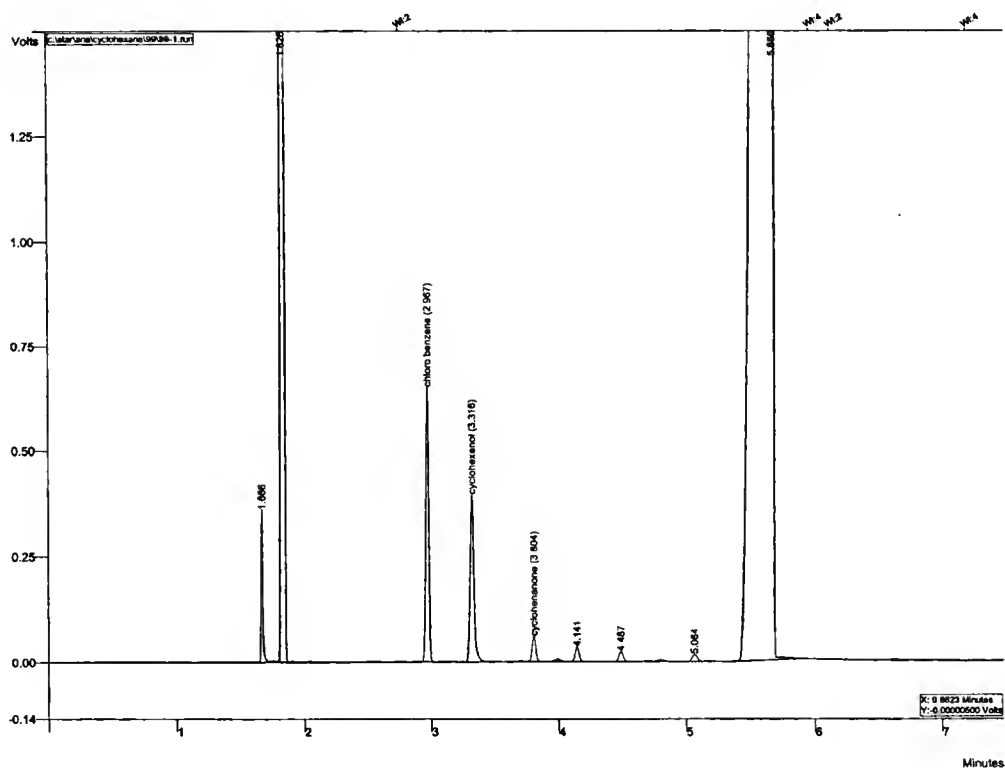


Figure 3-7. GC trace of cyclohexane oxidation in 50/50 cyclohexane/DCB

Table 3-2. Products from cyclohexane oxidation catalyzed by **1** and Fedmp

	Amt. Cat. (mol)	Cy-one (mol)	Cy-ol (mol)	Adipic acid (mol)	Run time
Fedmp	6.2×10^{-5}	1.3×10^{-3}	1.0×10^{-2}	1.8×10^{-4}	4 h
1	3.5×10^{-5}	1.0×10^{-2}	1.2×10^{-2}	1.6×10^{-3}	2 h

Reaction done in 50/50 DCB/cyclohexane by volume, 135 °C, and 50psi oxygen

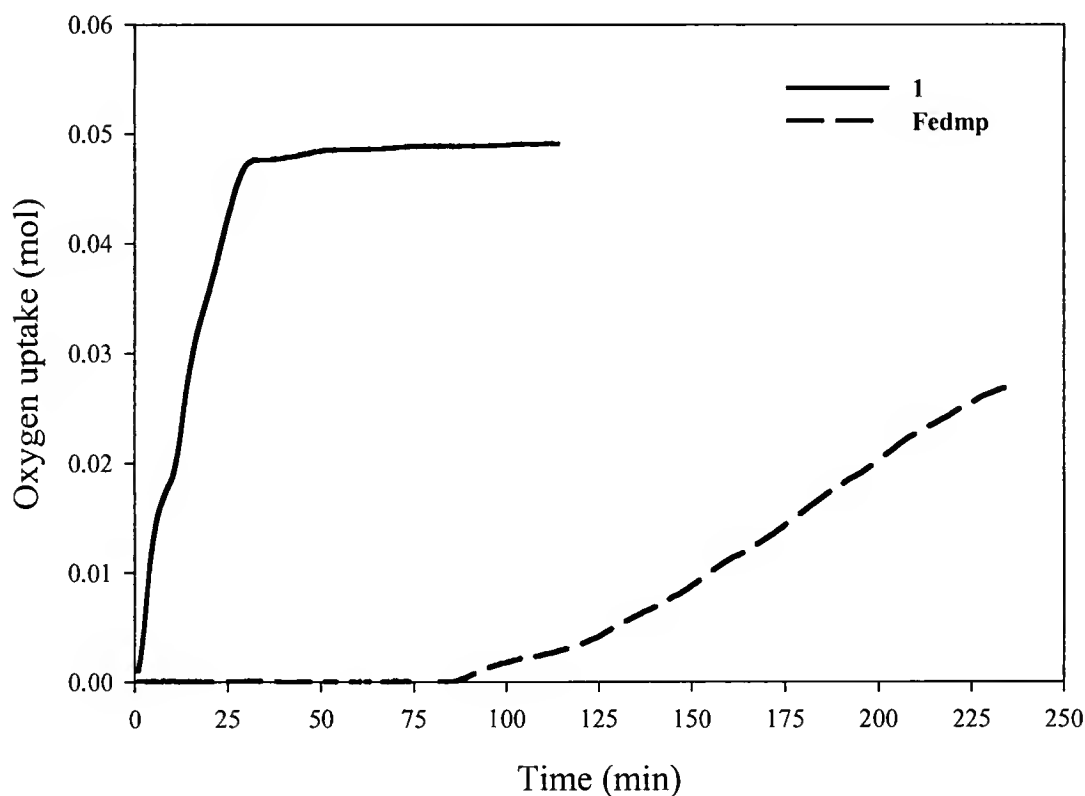


Figure 3-8. Oxygen uptake curves for cyclohexane oxidation catalyzed by **1** and Fedmp. Reaction conditions same as in Table 3-2

Considering the lack of dependence on oxygen pressure and the presence of an induction period, the most likely mechanism of catalysis is that of metal catalyzed peroxide decomposition and not metal mediated activation of oxygen leading to a high oxidation state metal-oxo species followed by direct oxygen transfer to the substrate.

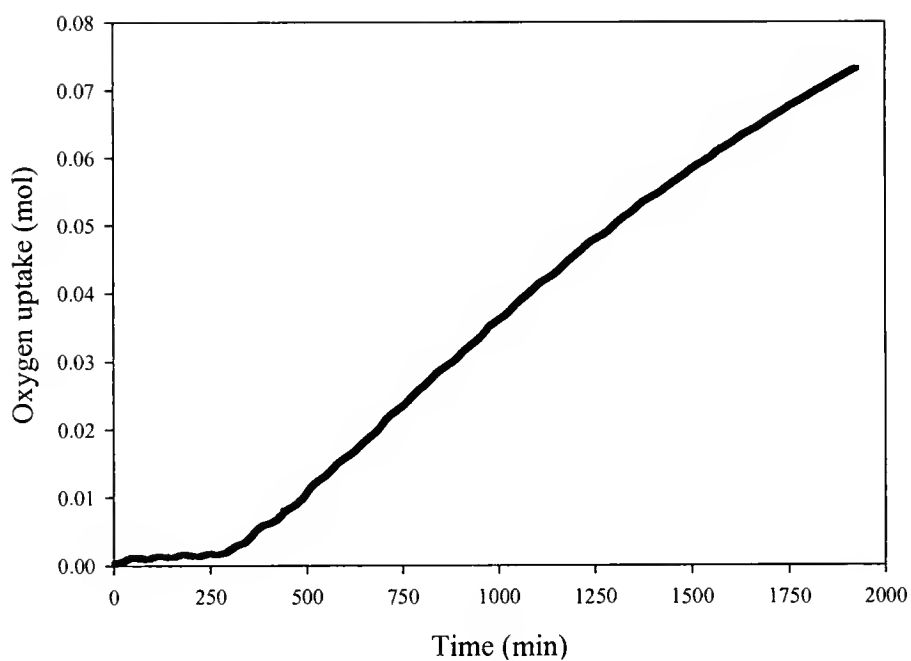


Figure 3-9. Oxygen uptake curve during cumene oxidation catalyzed by Fedmp at 60°C

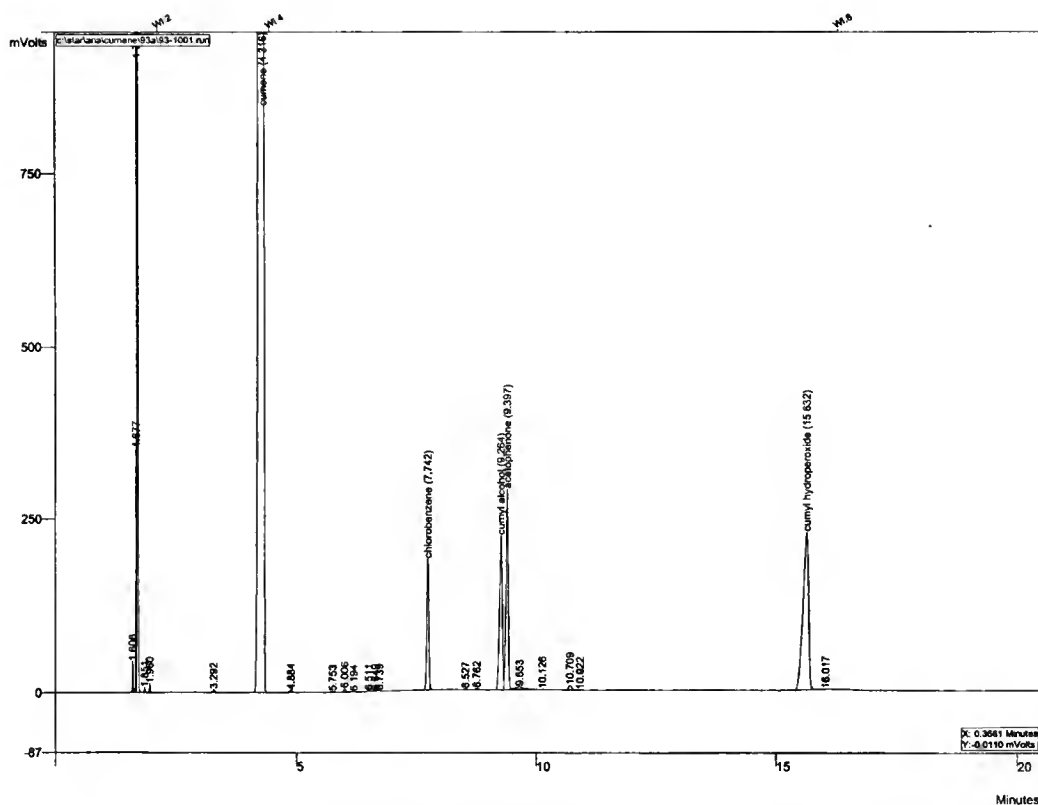


Figure 3-10. GC trace of sample taken after 2 h of cumene oxidation catalyzed by Fedmp

Solution-state studies of Fedmp

The low activity of Fedmp in cumene oxidation and cumyl peroxide decomposition prompted us to investigate the solution-state structure of the complex. Upon closer solution-state analysis of Fedmp it became clear that the *cis* configuration might not be retained in solution. Although CHN analysis supports a 2:1 ligand metal ratio, the ^1H -NMR analysis does not support the presence of the *cis* configuration in solution. An ^1H -NMR spectrum of the dmp ligand and Fedmp complex in d_6 -acetone is shown in Figure 3-11. If the solution geometry was indeed *cis* we would expect the dmp ligand to lose its C_2 symmetry axis and result in 2 methyl peaks and 6 aromatic hydrogen peaks. If we compare the Fedmp spectrum to that of the symmetrical free dmp ligand we see very little difference between the two except for the downfield shift of the Fedmp peaks.

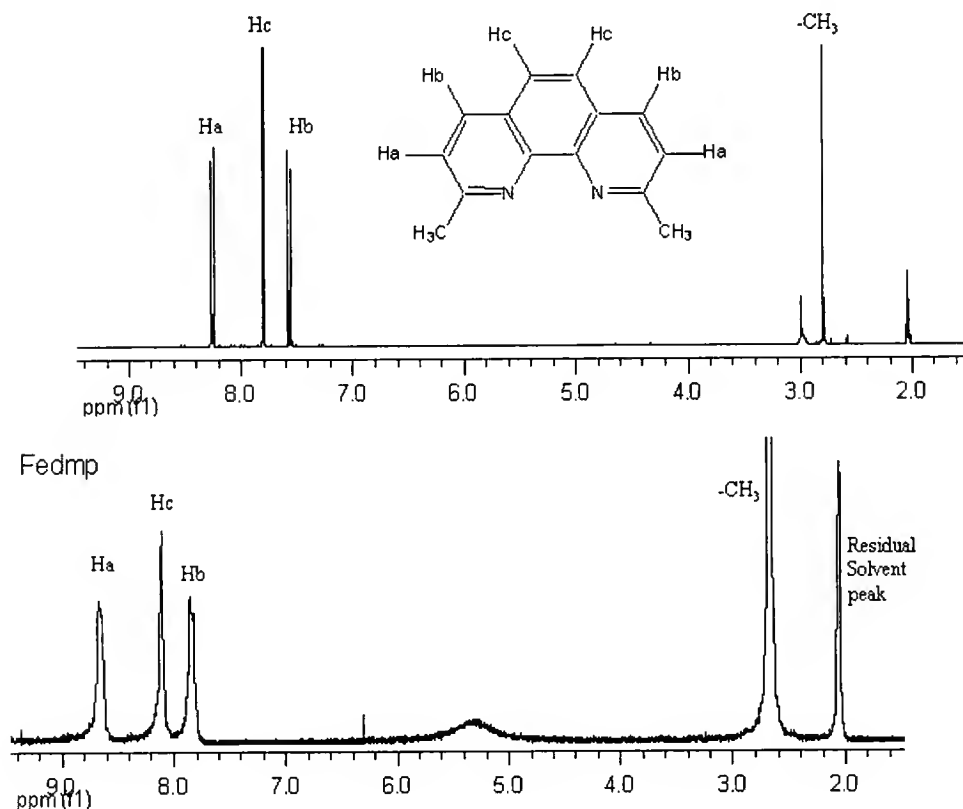


Figure 3-11. Top; 2,9-dimethylphenanthroline (dmp), Bottom; Fedmp in d_6 -acetone

Variable temperature studies were done to rule out fast exchange between the two ligands, which would make them appear symmetrical. Spectra down to -60°C do not reveal any splitting of the aromatic or methyl peaks suggesting that there is no fast ligand exchange occurring in solution (Figure 3-12). On the contrary all of the peaks are sharpened as the temperature is lowered. The probability that the complex adopts a *trans* geometry is low because of the steric interactions of the methyl groups. In fact there is no reported *trans* complex of the FeL_2X_2 (L=diimine) type, even in the absence of substituents in the 2 and 9 positions. The only known example of a related *trans* complex is that of $\text{Ru}(\text{bipy})_2(\text{OH}_2)_2^{2+}$, which is formed through photoisomerization of the *cis* complex.⁸³ We conclude that although in the solid state Fedmp exists as the *cis* complex, once it is dissolved the complex loses this geometry and has a symmetrical structure with respect to the dmp ligand. Disproportionation of $\text{Fephen}_2\text{X}_2$ complexes has been previously reported in the literature, where the more stable tri-substituted complex is formed.⁸⁴



Although a Fedmp_3X_2 complex has never been isolated, presumably because of the inability of three 2,9-dimethyl-1,10-phenanthroline ligands to approach the metal closely for good overlap, it is possible that in solution the three ligands aggregate around one Fe^{2+} to stabilize the ion. Instability of Fedmp_2X_2 complexes in solution has been previously reported, and most of the literature characterization was done in the solid state.^{85,86} We rationalized based on ligand field strength of the X^- ligands that a more stable analogue of Fedmp would be $\text{Fedmp}_2\text{NCS}_2$; however, once synthesized it too had a symmetrical ^1H -NMR spectrum.

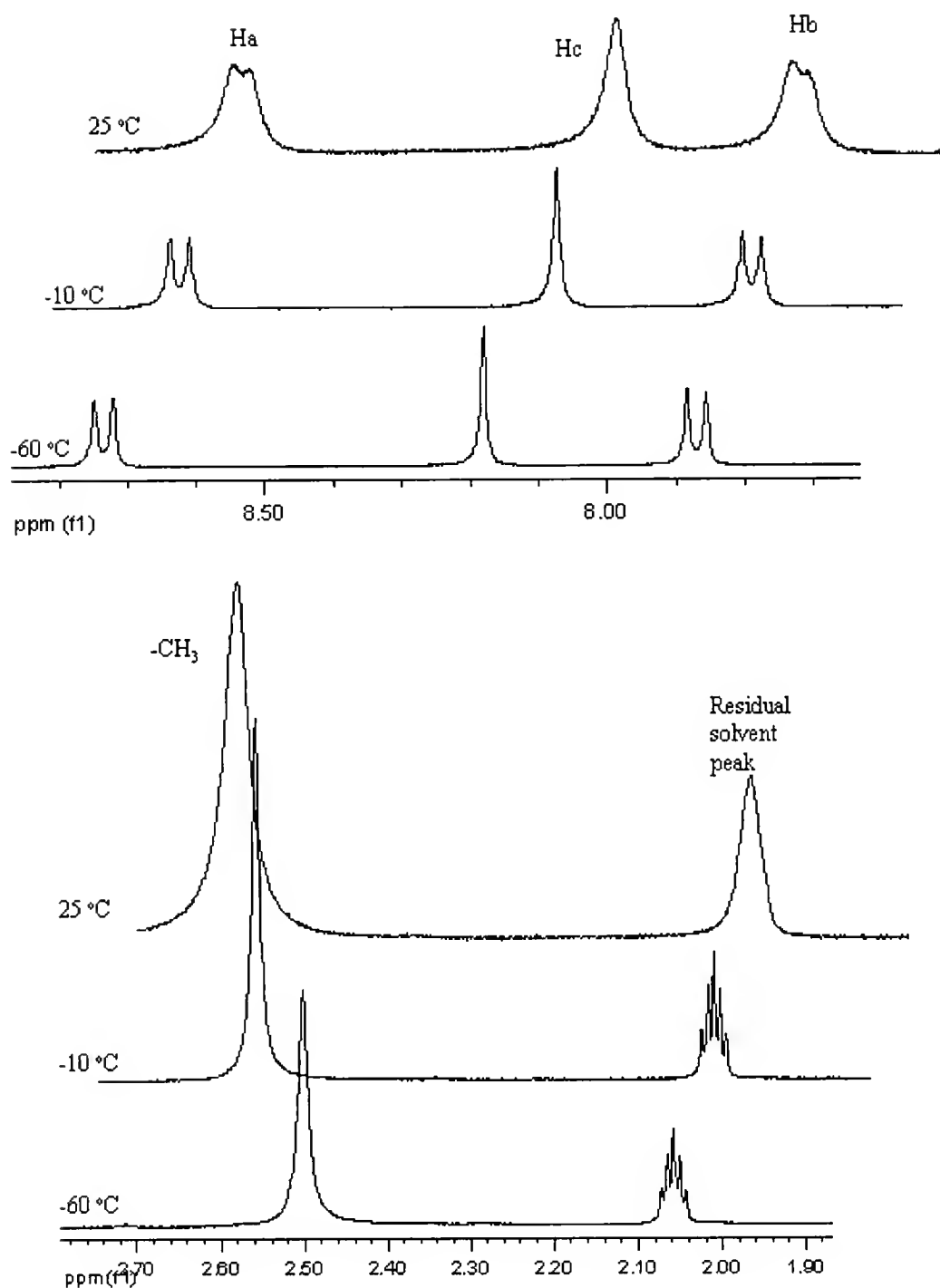


Figure 3-12. Variable temperature ^1H -NMR spectrum of Fedmp in d_6 -acetone. Top; aromatic region, Bottom; methyl protons and residual solvent peaks

The dmp ligand does not provide as strong a ligand field as other α,α' -diimines that are not substituted in the 2 and 9 positions. On the basis of electron-donating character of the methyl substituents, the dmp ligand is expected to be a stronger field ligand compared to 1,10-phenanthroline (phen). Comparison of x-ray structures of $\text{Fedmp}_2\text{NCS}_2$ and $\text{Fephen}_2\text{NCS}_2$ reveal the reasons for the weaker binding of the dmp ligand to iron. The $\text{Fe-N}_{\text{diimine}}$ distances were shown to be on average longer in the case of dmp (2.27 Å) compared to average bond lengths of 2.205 Å for $\text{Fephen}_2\text{NCS}_2$.^{87,88} The longer bond length suggests a weaker interaction between the metal and dmp ligand. The reason for the longer bonds can be attributed to steric crowding of two methyl groups. Each of the methyl groups experiences intramolecular contacts with the neighboring dmp ligand. In order to avoid the close contacts with the neighboring ligand the methyl groups are forced to twist away from the interaction. The distortions caused by the crowding are evident from the planarity of the ligand, where the largest deviation from the plane of the ligand is 0.162 for $\text{Fedmp}_2\text{NCS}_2$ compared to only 0.039 Å in $\text{Fephen}_2\text{NCS}_2$. The result of the ligands bending away from each other is that the iron atom deviates 1.004 Å from the plane of the dmp ligands. This compares to an approximate planar configuration of the metal in $\text{Fephen}_2\text{NCS}_2$ where the deviation is only 0.077 Å.⁸⁸

In view of the poor dmp ligand orbital overlap with the metal we chose to explore FeL_2X_2 complexes where L= 1,10-phenanthroline (phen), in hopes of retaining the *cis* configuration in solution.

We prepared a series of *cis*- $\text{Fephen}_2\text{X}_2$ ($\text{X}=\text{CN}^-$, NCS^- , Cl^-) complexes in order to compare them to the activity of **1** and evaluate the effect of changing the X^- ligand.

The complexes in the series were characterized by CHN and IR the results of which support the assignment of a *cis* geometry. The complexes maintain the *cis* configuration in solution as is clearly demonstrated by the ^1H -NMR spectrum of $\text{Fephen}_2\text{CN}_2$ (Figure 3-13). The *cis* configuration is expected to lead to loss of phen ligand symmetry resulting in 8 different aromatic proton resonances instead of only 4 present in the uncoordinated ligand.

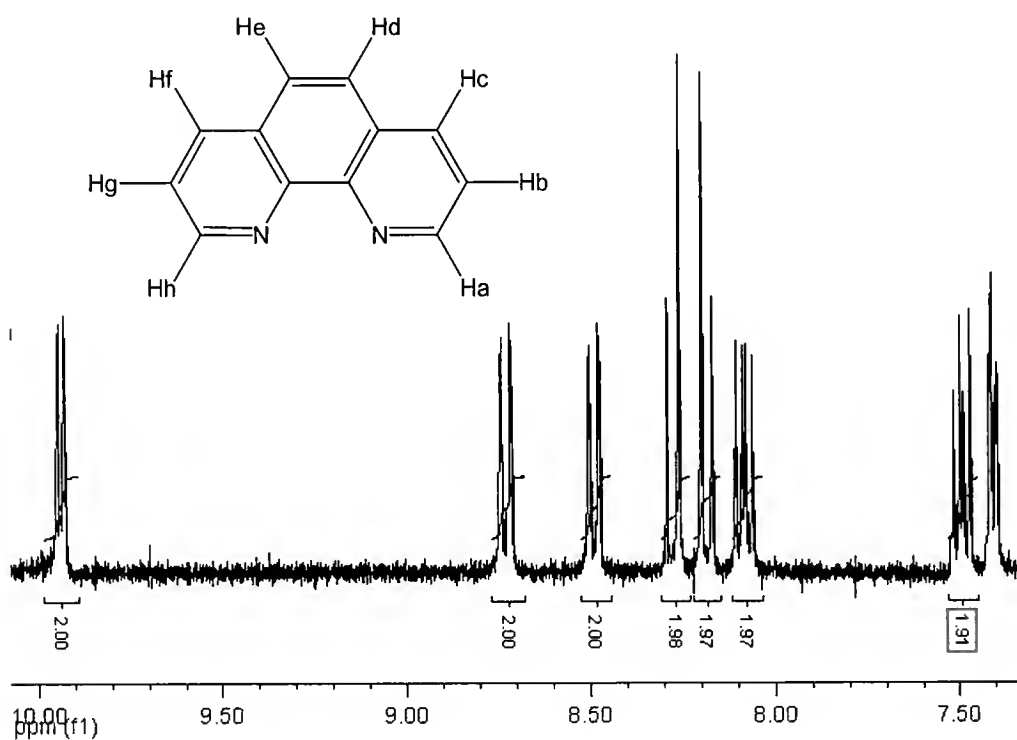


Figure 3-13. ^1H -NMR spectrum of $\text{Fephen}_2\text{CN}_2$

^1H -NMR spectra of $\text{Fephen}_2\text{Cl}_2$ and $\text{Fephen}_2\text{NCS}_2$ were not obtained because of poor solubility in standard NMR solvents. The *cis* arrangement in solution was verified by Uv-visible spectroscopy (Chapter 6).

In previous studies of cumene autoxidation catalyzed by **1**, results suggest that ligand dissociation is an important step in catalyst activation. In the case of $\text{Fephen}_2\text{X}_2$

complexes one of the diimine ligands is replaced by two X^- ligands. Such a change in the ligand environment should have a notable effect on the formation of the active catalyst as well as the robustness of the complex. Presumably the weaker X^- ligand will favor dissociation and the formation of the active species.

The relative reactivities of the three $\text{Fephen}_2\text{X}_2$ complexes are in agreement with the ligand field strength of the X^- ligands, $\text{CN}^- < \text{NCS}^- < \text{Cl}^-$ (Table 3-4). The complex bearing CN^- ligands is by far the least active and has the longest induction period (Figure 3-14). The observation is not entirely surprising since CN^- is a stronger field ligand than even 1,10-phenanthroline.

Table 3-4. Cumene oxidation catalyzed by $\text{Fephen}_2\text{X}_2$ complexes

Complex	%Conv	%ROOH	%ROH	%RO
$\text{Fephen}_2\text{CN}_2$ ^a	7±1	45±1	39±2	16±1
$\text{Fephen}_2\text{NCS}_2$ ^a	15±1	48±5	32±3	21±3
$\text{Fephen}_2\text{Cl}_2$ ^b	18±1	20±4	59±2	22±3
Fedmp ^a	5±1	79±1	18±1	1±1
1 ^a	26±2	14±1	47±1	39±1
50/50 cosolvent/cumene, 1.2×10^{-5} mol complex, 80 °C, 60psi O_2 , run time=2 h; Product yields and errors calculated from 2 or more experiments; ^a cosolvent CH_3CN ; ^b cosolvent o-dichlorobenzene				

The difference in product conversion between $\text{Fephen}_2\text{NCS}_2$ and $\text{Fephen}_2\text{Cl}_2$ is small, but the difference in moles of oxygen consumed is much larger as shown in Figure 3-14. The reason for the apparent discrepancy is that $\text{Fephen}_2\text{Cl}_2$ is much less selective and produces more secondary reaction products such as CO and CO_2 .

The activity differences between $\text{Fephen}_2\text{NCS}_2$ and $\text{Fephen}_2\text{Cl}_2$ cannot be interpreted entirely based on ligand field strength since the autoxidation reactions were done in different solvents. Unlike the NCS^- and CN^- complexes the $\text{Fephen}_2\text{Cl}_2$ complex disproportionates to the FeL_3Cl_2 complex in CH_3CN and the reactions had to be done in o-dichlorobenzene.

We might have expected that $\text{Fephen}_2\text{NCS}_2$ and $\text{Fephen}_2\text{Cl}_2$ would be more active than **1** based on the ligand field strength order of $\text{phen} > \text{NCS}^- > \text{Cl}^-$; however, this is not the case. Although bleaching of the FeL_2X_2 complexes is observed to occur within the first 30 minutes, the rate of oxygen uptake does not show evidence of slowing down because of degradation of the active catalyst (Figure 3-14). The low activity is likely a direct result of replacing one phenanthroline ligand with two X^- ligands. Presumably the X^- ligands are not able to provide the appropriate environment for the formation of a highly active catalyst.

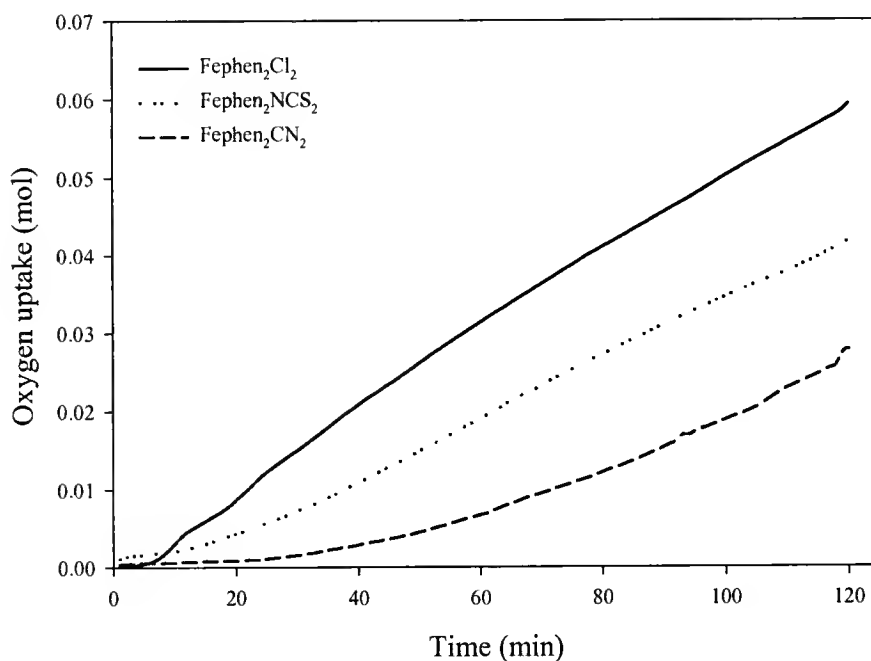


Figure 3-14. Oxygen uptake curves during cumene oxidation catalyzed by $\text{Fephen}_2\text{X}_2$ complexes

Conclusions

The Fedpm catalyst was shown to be a poor catalyst for the oxidation of both cumene and cyclohexane under autoxidizing conditions. Solution state studies suggest that the *cis* configuration of Fedmp is not retained in solution. Further evidence suggests

that the dmp ligand does not bind to the metal as strongly as other diimine ligands not substituted in the 2,9 positions. The weak ligand strength of the dmp ligand may be the reason for the poor catalytic activity. Product profiles, the presence of an induction period and zero dependence on oxygen pressure all suggest that Fe^{dmp} catalyzes the reaction by decomposition of the intermediate peroxide and not through molecular oxygen activation and direct transfer of the oxygen to the substrate as previously suggested.

$\text{Fe}^{\text{phen}_2\text{X}_2}$ complexes are less catalytically active in cumene autoxidation compared to the previously studied complex **1**. The low activity does not appear to be a result of active catalyst decomposition since the rate of oxygen uptake does not slow down during the reaction. Presumably the X^- ligands are not as good as 1,10-phenanthroline ligands at providing the needed ligand environment for the formation of the active catalyst.

CHAPTER 4 COMPARISON OF FeL_3X_2 TO KNOWN AUTOXIDATION CATALYSTS

Introduction

The uniquely high activity of **1** as an autoxidation catalyst in hydrocarbon media is a direct result of the lipophilic nature of the ligand, which solubilizes the metal in the non-polar reaction medium thereby facilitating catalysis. We were interested in comparing the activity of **1** to well-known autoxidation and peroxide decomposition catalysts not soluble in hydrophobic solvents such as benzene. In order to assess the relative activity of **1** compared to other autoxidation catalysts the following discussion focuses on reactions done in acetonitrile as a co-solvent.

Results and Discussion

Fe and Co Acetylacetonates

Many of the early studies of autoxidation were with Co, Cu and Fe acetates, decanoates and acetylacetonates (acac =2,4-pentanedionate). One of the more active autoxidation catalysts is Co(II)acac_2 .⁸ Under our conditions the activity of the Co(II) complex is approximately half that of **1** (Table 4-1). In the case of Co(III)acac_3 the reaction yields only trace ROOH and we observe no color change of the reaction solution indicating the Co(III)acac_3 remains unaltered throughout the reaction. When using the analogous Fe(II)acac_2 or Fe(III)acac_3 the conversion to products is very low in both cases.

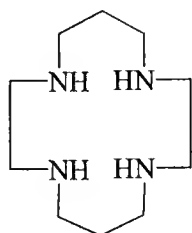
Table 4-1. Cumene oxidation catalyzed by Fe and Co acetyl acetonates

Complex	% Conv	% ROOH	% ROH	% R'O
Fe(II)acac ₂	1	94	6	0
Fe(III)acac ₃	trace	trace	0	0
Co(II)acac ₂	12	63	25	12
Co(III)acac ₃	trace	trace	0	0
1	24	15	47	38
Blank	0.5	>99	trace	trace

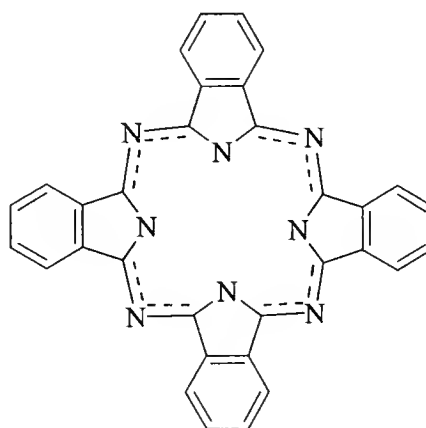
50/50 cumene/CH₃CN; 1.2x10⁻⁴ M metal complex; run time=2h; 80 °C; 60 psi O₂

Fe Complexed by Macrocyclic Ligands

Fe(II)phthalocyanine (Fe(II)Pc) is considered analogous to iron porphyrin complexes because of the similarity of the phthalocyanine ligand (Figure 4-1) to porphyrin.⁸⁹ The interest in using Fe(II)Pc complexes in the presence of oxygen atom donors such as iodosyl benzene and alkyl peroxides stems from the desire to obtain synthetic mimics of the enzyme P-450 as discussed in Chapter 1. Reports of using Fe(II)Pc supported on zeolite or carbon black as a catalyst in cyclohexane oxidation in the presence of t-BuOOH suggest a non free-radical mechanism.^{90,91} Fe(II)Pc is also reported to have high peroxide decomposition activity, and has been used as an autoxidation catalyst.⁸



1,4,8,11-tetraazacyclotetradecane (cyclam)



phthalocyanine (Pc)

Figure 4-1. Structures of macrocyclic ligands

Under our reaction conditions, Fe(II)Pc catalyzed oxidation of cumene resulted in moderate activity (14 % conv.); however, still considerably lower than **1** (Table 4-2).

Fe(II) 1,4,8,11-tetraazacyclotetradecane (Fe(II)cyclam) complexes have been used in the catalytic epoxidation of olefins both in the presence of iodosyl benzene and H₂O₂. The observed high selectivity to the epoxide suggests the absence of radical species.⁹²

However, when using alkyl peroxides the high selectivity to the epoxide is lost because of homolytic cleavage of the peroxide leading to the formation of free radicals.

Cumene oxidation catalyzed by Fe(II)cyclam was observed to give very low product yields as shown in Table 4-2. Oxidative attack on the methylinic carbons of the ligand may contribute to active catalyst destruction and the low activity.

Table 4-2. Cumene oxidation catalyzed by Fe(II)Pc and Fe(II)cyclam

Complex	% Conv	% ROOH	% ROH	% R' O
Fe(II)Pc	14	49	28	23
Fe(II)cyclam	3	56	25	19
1	24	15	47	38
blank	0.5	>99	Trace	trace

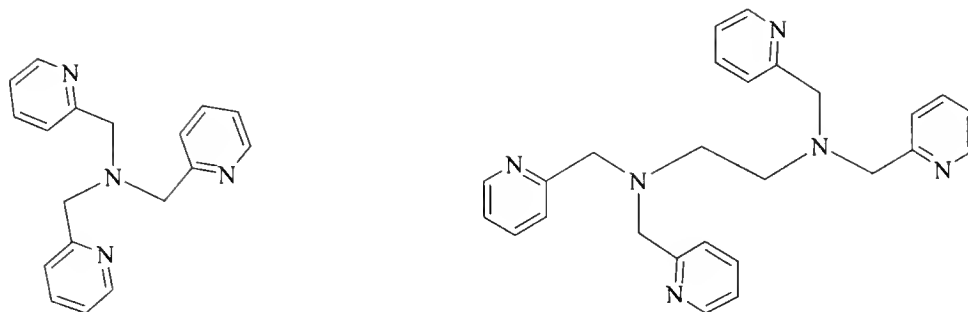
50/50 cumene/CH₃CN; 1.2x10⁻⁴ M metal complex; run time=2h; 80 °C; 60 psi O₂

Fe Complexed by Hexa and Tetra Coordinating Pyridyl Ligands

In view of the high activity of pyridyl ligands such as 1,10-phenanthroline we investigated other examples of pyridyl-based ligands. Some of the more common examples are 2-pyridylmethyl ligands such as tris(2-pyridylmethyl) amine (tpa) and N,N,N',N'-tetrakis(2-pyridylmethyl)-aminopyridyl (tpen) both of which were chosen for our study and are shown in Figure 4-2. Iron tpen and tpa complexes have been used extensively as mimics of non-heme iron oxygen activating enzymes.^{93,94} The formation of iron (III) peroxo species from both Fetpen and Fetpa complexes in the presence of H₂O₂ or t-BuOOH has recently been reported.^{93,95,96} Peroxoiron(III) complexes are

increasingly being considered as potential intermediates in oxidations catalyzed by non-heme iron centers in biology. Numerous claims of selective oxygen transfer to alkanes and alkenes particularly by mono and di-nuclear Fetpa complexes in the presence of alkyl peroxides have been reported.⁹⁷ Such claims have been challenged by the view that the peroxoiron(III) species slowly undergoes homolytic scission to form free radicals responsible for the observed products.^{98,99} We chose two complexes of the type discussed above and investigated the peroxide decomposition activity of Fe(III)tpen(ClO₄) and (Fe(II)tpa(CH₃CN)₂](SO₃CF₃)₂ as well as their activity in cumene autoxidation. The catalytic activity in the air oxidation of ethylbenzene of a large group of iron complexes bearing penta, hexa and tetradentate pyridyl type ligands has recently been reported.¹⁰⁰ (Fe(II)tpa(CH₃CN)₂](SO₃CF₃)₂ and an iron complex bearing a ligand closely related to tpen were included in the report.

Cumene oxidation catalyzed by Fe(tpen)(ClO₄)₃ resulted in high conversions especially in the early minutes of the reaction. The initial rate of the reaction was approximately twice that seen for the **1** catalyzed reaction. The rate of oxygen uptake was $1.4 \times 10^{-3} \text{ Ms}^{-1}$ for Fe(tpen)(ClO₄)₃ (Fetpen) compared to the maximum rate of $8.0 \times 10^{-4} \text{ Ms}^{-1}$ for the **1** catalyzed autoxidation. Although no induction period was observed for Fe(tpen), the oxygen uptake slowed down after ~40 min indicating catalyst destruction. A comparison of the oxygen uptake curves is shown in Figure 4-3. The absence of induction period suggests that Fetpen is an extremely efficient peroxide decomposition catalyst.



tris(2-pyridylmethyl)amine (TPA)

N,N,N',N'-tetrakis(2-pyridylmethyl)-aminopyridyl (TPEN)

Figure 4-2. Structures of tpa and tpen ligands

Table 4-3. Cumene autoxidation catalyzed by Co and Fe complexes

Complex	% Conv	% ROOH	% ROH	% R'O
Fe(III)tpen(ClO ₄)	19	20	31	49
[Fe(II)tpa(CH ₃ CN) ₂] (SO ₃ CF ₃) ₂	34	4	45	51
[Fe(II)tpa(CH ₃ CN) ₂] (SO ₃ CF ₃) ₂ at 30 °C (5 h)	10	14	67	19
Fe(SO ₃ CF ₃) ₂	2	64	9	26
Fe(Pyridine) ₄ (Cl) ₂	0.7	>99	trace	trace
1	24	15	47	38
Fe(phen) ₃ (SO ₃ CF ₃) ₂	36	10	46	44
blank	0.5	>99	trace	trace

50/50 cumene/CH₃CN; 1.2x10⁻⁴ M metal complex; run time=2h; 80 °C; 60 psi O₂

Cumene oxidation catalyzed by [Fe(II)tpa(CH₃CN)₂](SO₃CF₃)₂ (Fetpa) results in the highest activity seen for any of the complexes investigated in this study. In addition to the three major products listed in Table 4-3, a considerable amount of α,α -dimethyl benzyl methyl ether is also formed. The formation of the ether likely occurs through the reaction of the RO \cdot radical with MeOO \cdot as shown in Figure 4-4. The proposed pathway is reasonable since the β -cleavage of RO \cdot results in the formation of R'O and MeOO \cdot (Figure 2-10, Step 7). Assuming most of the R'O formed occurs though

step 7, the high selectivity toward R'O dictates the formation of large concentration of the MeOO• radical as well.

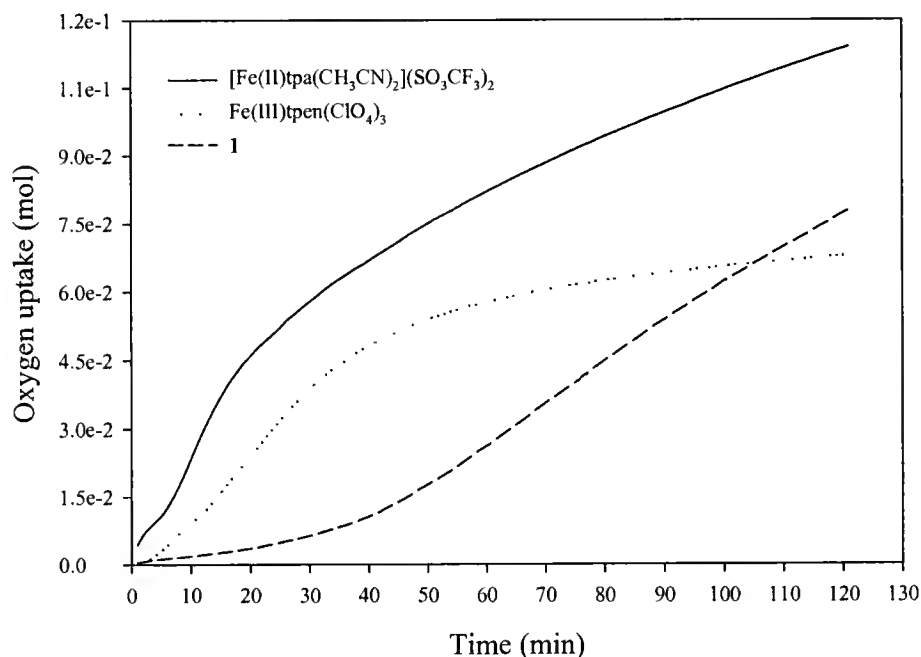


Figure 4-3. Comparison of oxygen uptake curves during cumene oxidation

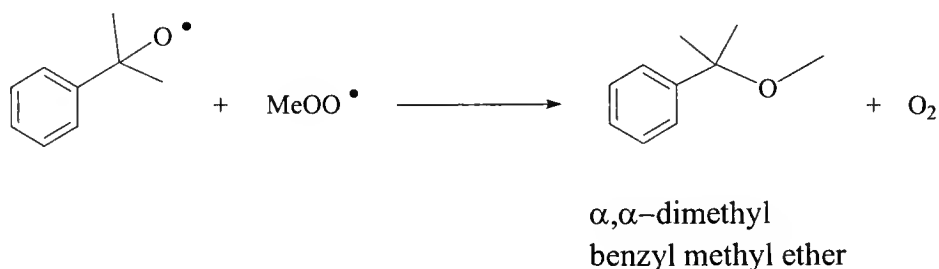


Figure 4-4. Proposed mechanism of α,α -dimethyl benzyl methyl ether formation

Unlike Fetpen, Fetpa does not suffer from loss of activity and continues catalyzing the oxidation although at a somewhat slower rate after ~25 minutes (Figure 4-3). Fetpa is an active catalyst even at 30 °C, where **1** has no activity at all (Table 4-3). Cumyl peroxide decomposition catalyzed by Fetpa is extremely rapid even at room temperature.

Approximately half of the ROOH is decomposed during the first minute, followed by a considerably slower rate of decomposition. The observed decrease in ROOH concentration over time is shown in Figure 4-5. Upon the addition of the complex to a solution of 0.1M ROOH a short-lived blue species is observed.

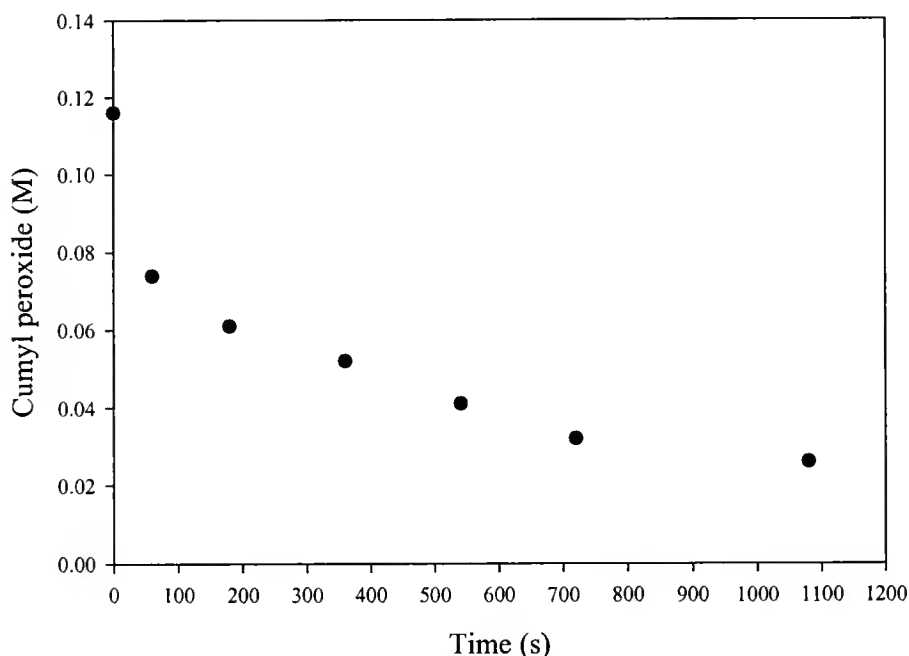


Figure 4-5. Cumyl peroxide (ROOH) decomposition catalyzed by Fetpa

The blue color is consistent with a previously reported blue Fe(III)peroxo species ($\lambda_{\text{max}} \sim 600 \text{ nm}$) formed when reacting Fetpa and t-BuOOH.⁹³ Following the rapid disappearance of the blue intermediate, a reddish brown solution remained. The blue Fe(III)peroxo species likely decomposes through the homolytic decomposition of the FeO-OR bond. The formation of alkoxy radicals from alkyl hydroperoxides exposed to Fetpa complexes has been reported.^{98,99}

In order to determine whether the species formed after decomposition of the blue Fe(III)peroxo complex is catalytically active, we added one equivalent of cumyl peroxide to a solution of Fetpa and used that solution as the catalyst in cumene oxidation. To our

surprise the oxygen uptake curve and product yields were practically identical as when Fetpa itself was used. ^1H -NMR analysis of Fetpa solutions with one equivalent of added ROOH was inconclusive because of the interference of the cumene and ligand peaks in the aromatic region. The same experiment was done using $t\text{-BuOOH}$ in place of cumyl peroxide in order to decrease the number of peaks in the aromatic region. The ^1H -NMR of the resulting solution shows the absence of peaks in the aromatic region suggesting that not only is the Fetpa complex itself decomposed, so are all of the peaks belonging to the free ligand (Figure 4-6). The NMR analysis suggests that the peroxide destroys the ligand completely leaving some other uncharacterized iron species.

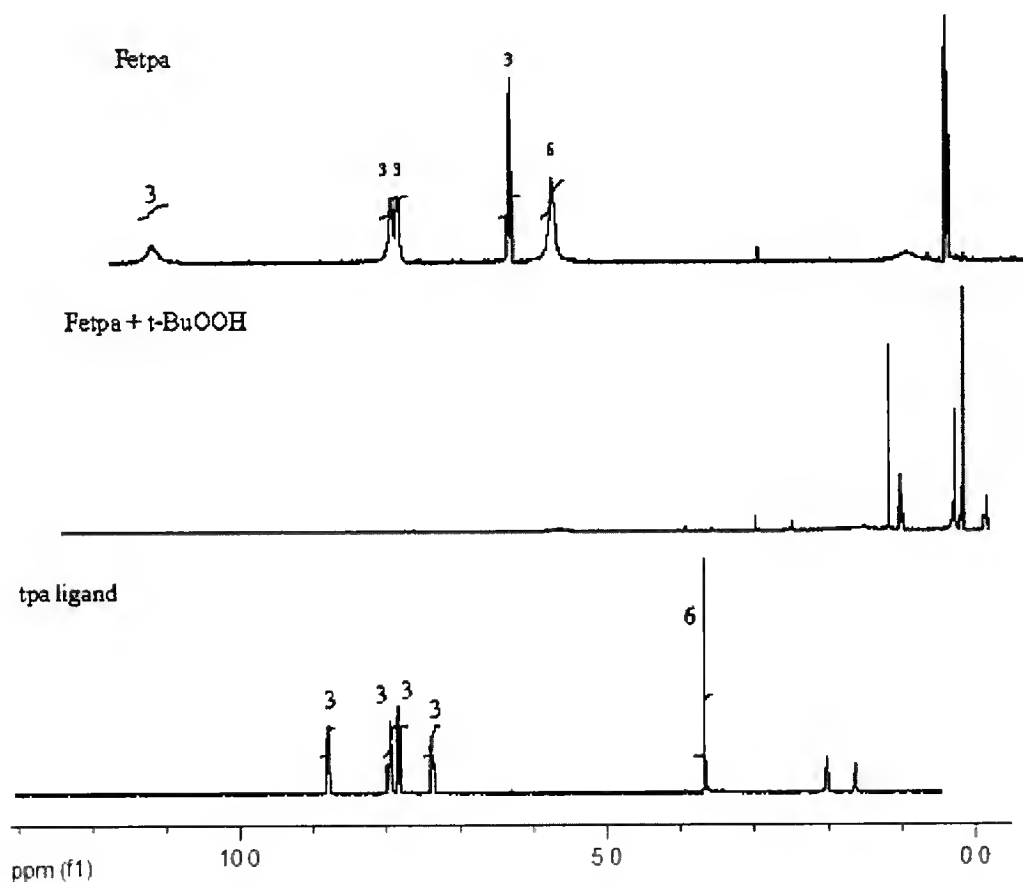


Figure 4-6. ^1H -NMR spectra in acetonitrile- d_3

If, in the absence of detectable ligand the catalysis is high, a simple Fe salt should also result in a highly active catalyst. This possibility was explored by using $\text{Fe}(\text{SO}_3\text{CF}_3)_2$ as a catalyst; however, the yield was low at 2%. The unusual feature of the $\text{Fe}(\text{SO}_3\text{CF}_3)_2$ catalyzed reaction was the relatively fast oxygen uptake at the very beginning of the reaction where most of the oxygen was consumed during the first 15 minutes as shown in Figure 4-7. In addition, the high selectivity to $\text{R}'\text{O}$ is unusual at such a low product conversion (Table 4-3). Clearly an active catalyst is formed at the very beginning of the reaction but presumably because of the inability of the SO_3CF_3^- ligand to provide stability the active catalyst is quickly decomposed resulting in loss of reactivity.

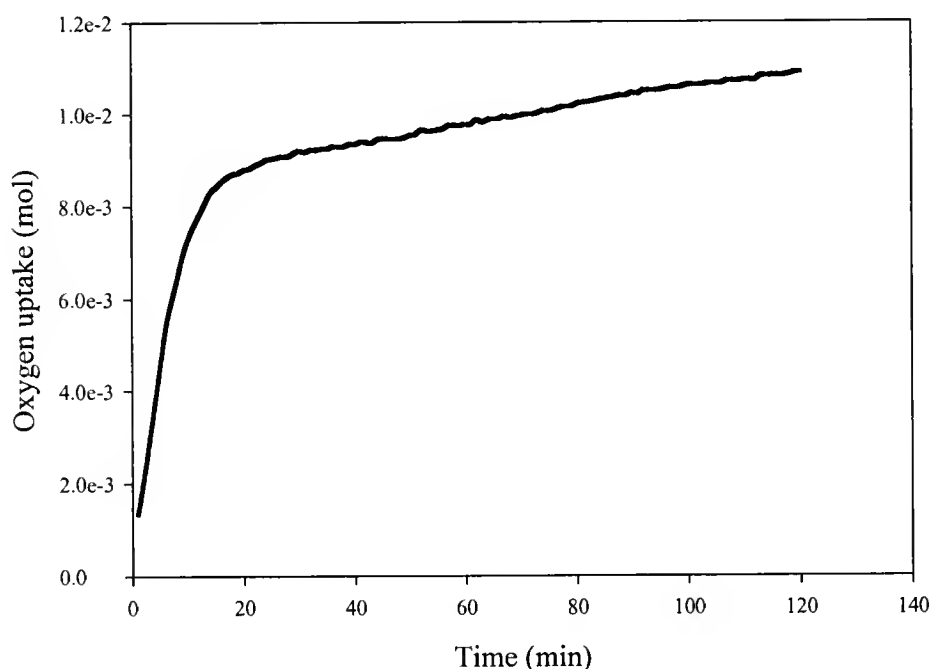


Figure 4-7. Oxygen uptake curve in cumene oxidation catalyzed by $\text{Fe}(\text{SO}_3\text{CF}_3)_2$

$\text{Fe}(\text{pyridine})_4(\text{Cl})_2$ was also used as a catalyst under the same conditions. The reactivity was just slightly higher than that of the blank reaction. Therefore, a nitrogen donor ligand such as pyridine did not favor the formation of a highly active catalyst.

Pyridine is a weak base and a mono-dentate ligand, which may contribute to the low activity.

Poly-Nuclear Iron Complexes

In view of the reported high activity of oxo centered tri-nuclear iron mixed valence complexes in the oxidation of alkanes in Gif systems^{19,20} (Chapter 1) we investigated the catalytic activities of two such complexes (Figure 4-8) in cumene oxidation. Complex **3** has been previously reported and **4** is our own modification using a fluorinated ligand in order to improve solubility and possibly the catalytic activity of the complex. Although soluble, both complexes **3** and **4** gave low product yields compared to **1** (Table 4-4). However, we do see increased activity when using complex **4**, possibly a result of ligand fluorination. Once again, complex **1** exhibits much higher activity in catalyzing the autoxidation of cyclohexane.

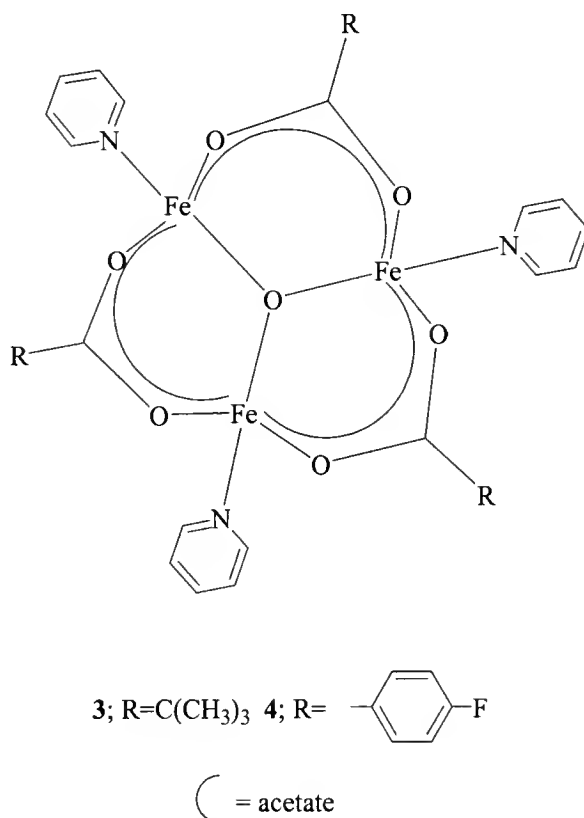


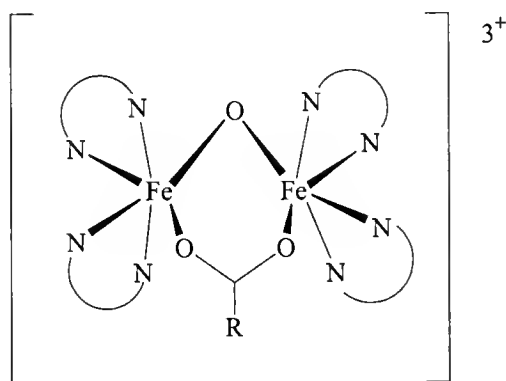
Figure 4-8. Structure of complex **3** and **4**

Table 4-4. Cumene oxidation catalyzed by μ -oxo Fe complexes

Complex	% Conv.	% ROH	% ROOH	% R'O	Run time
3	8.3	8.3	91.7	0	6h
4	9.4	7.8	92.2	0	4h 20min
1	19	62	6.5	31.5	40min

Reactions done in a Parr reactor at 80 C° and 60 psi of constant O₂ pressure in 100ml of neat cumene; complex = 65 μ M

In an effort to further explore the identity of the active species, a number of di-nuclear iron complexes were investigated. Complexes **5** and **6** have been previously published and **7** is a modification replacing acetate with pivalate as the bridging acetate ligand as shown in Figure 4-9. Many similar complexes have been implicated in selective oxidation of alkanes and alkenes in the presence of peroxidic oxygen donors.^{101,102} Table 4-5 shows the catalytic activities of the three di-nuclear iron complexes in cyclohexane autoxidation. Complexes **5-7** all exhibit induction periods as long as 4 hours followed by slow oxygen uptake. Compared to the high activity of **1**, all three of the complexes investigated are markedly inferior.



5; R=CH₃, L=2,2'-bipyridine

6; R=CH₃, L=1,10-phenanthroline

7; R=C(CH₃)₃, L=2,2'-bipyridine

Figure 4-9. Structures of di-nuclear iron complexes

Table 4-5. Catalytic activity of di-nuclear Fe complexes in cyclohexane oxidation

	Oxygen uptake (mol)	Induction period (min)	Run time (min)
5	0.06	165	470
6	0.1	235	570
7	0.1	210	570
1	0.05	None	30
130 °C, 50/50 ml o-dichlorobenzene/cyclohexane, 80 psi O ₂ , 3x10 ⁻⁵ mol complex.			

Conclusions

The survey of ten complexes has revealed the relative activity of **1** among complexes known for autoxidation and peroxide decomposition activity in a polar solvent. The results show **1** to be a highly active catalyst precursor among those studied. We might conclude that the stability of 1,10-phenanthroline ligand lends itself to the formation of a stable active catalyst. For example Fe(II)cyclam has a much lower activity than Fe(II)Pc, presumably because of the attack on the methylinic carbons of the cyclam ligand. On the other hand, the tpa and tpen ligands both have methylinic carbons but still result in complexes having very high activity. In addition, ¹H-NMR evidence suggests that once alkyl peroxide is added to Fetpa the ligand is completely decomposed; however, high activity is still observed. Observations suggest that the ligand is unimportant; however, simple Fe salts are not active.

Presumably, the ligand is partially or fully degraded by the radicals present in solution. Results suggest that iron coordinated by pyridyl multi dentate ligands is especially effective at forming a highly active autoxidation catalyst as illustrated by the high activities of **1**, Fetpa and Fetpen.

CHAPTER 5
ALKENE EPOXIDATION CATALYZED BY TRANSITION METAL COMPLEXES
USING BICARBONATE ACTIVATED PEROXIDE (BAP)

Sulfonated Styrene Epoxidation with Mn(III)porphyrin/BAP

Introduction

Previous reports and work in our labs have shown that Mn^{2+} catalyzes the epoxidation of alkenes in the presence of H_2O_2 and HCO_3^- or Bicarbonate Activated Peroxide (BAP).⁴⁷ More than 30 d and f-block metals were screened only to find two other metal ions, Cr^{2+} and Fe^{3+} , with moderate activity in the BAP system.^{47,103} In addition, no other anionic salt was shown to catalyze the epoxidation reaction. Using alkyl peroxides instead of H_2O_2 also did not result in epoxidation of alkenes.

Previous studies by Drago et al. and Richardson et al.⁴⁸ have shown the equilibrium formation of the peroxycarbonate ion in solutions containing H_2O_2 and HCO_3^- (Figure 4-1). Other anionic salts such as NaOAc do not form peroxy acid species in equilibrium with H_2O_2 , and alkyl peroxides form peroxy esters that are not active epoxidation agents in the presence of Mn^{2+} . These observations suggest the active epoxidizing agent can only be formed in the presence of the peroxycarbonate ion. Kinetic and EPR studies carried out by Richardson et al.¹⁰³ and Burgess et al.⁴⁷ suggest the peroxycarbonate and/or bicarbonate act as ligands and transfer an oxygen atom to form a high oxidation state Mn-oxo complex as an active epoxidation agent.

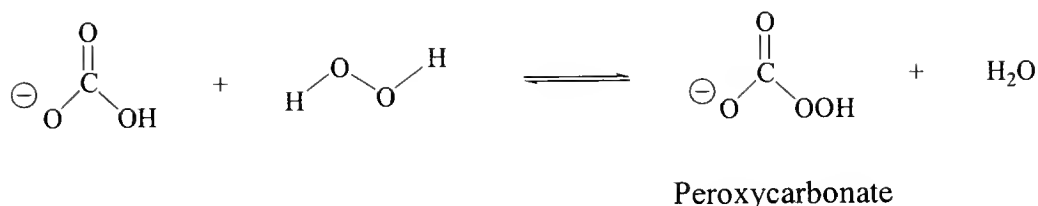


Figure 5-1. Equilibrium formation of peroxycarbonate

The high yield and selectivity of epoxidation catalyzed by the Mn^{2+} /BAP system prompted us to investigate the application of the BAP system in the presence of known epoxidation catalysts. The literature contains many examples of epoxidation catalysts, which reportedly form a high oxidation state metal-oxo complex in the presence of active oxygen donors such as hydrogen peroxide, t-butyl peroxide, hypochlorite and iodosyl benzene. Although H_2O_2 is not the oxidant of choice because of possible radical production and catalyst degradation, the possibility that the BAP system would offer an advantage to using H_2O_2 alone was an attractive proposition. Styrene epoxidation was investigated using the BAP system in the presence of a water soluble Mn porphyrin complex.

Results and Discussion

Epoxidation of sulfonated styrene (SS) was investigated using Mn(III) meso-tetrakis(4N-methylpyridinium)porphyrin (MnTMPyP) in the presence of BAP. The Mn-porphyrin is a water soluble complex with the structure shown in Figure 5-2. Under the reaction conditions (Figure 5-3) sulfonated styrene was converted completely to epoxide without the formation of detectable side products within 60 min, as shown in the ^1H -NMR spectrum in Figure 5-4. Blank reactions were carried out in the absence of HCO_3^- , in which case no products were detected. We were also interested in how MnTMPyP compared to the Mn^{2+} catalyzed reaction. The reaction using MnSO_4 as the

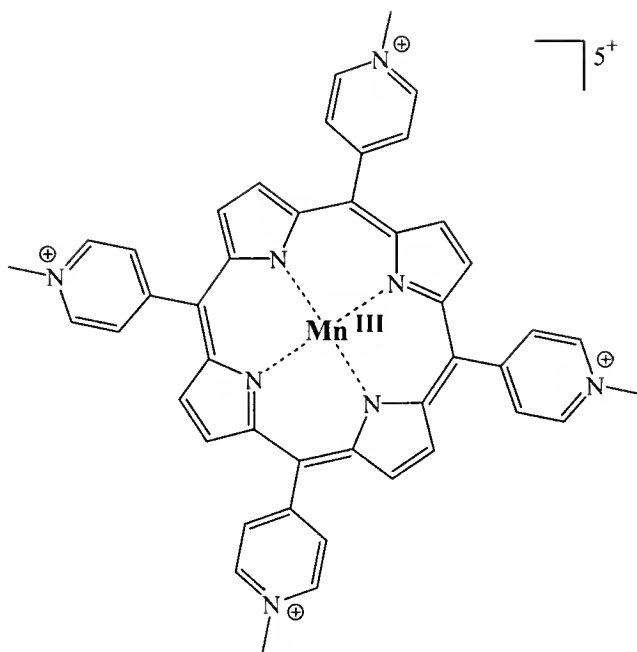


Figure 5-2. Mn(III) meso-tetrakis(4N-methylpyridinium)porphyrin (MnTMPyP)

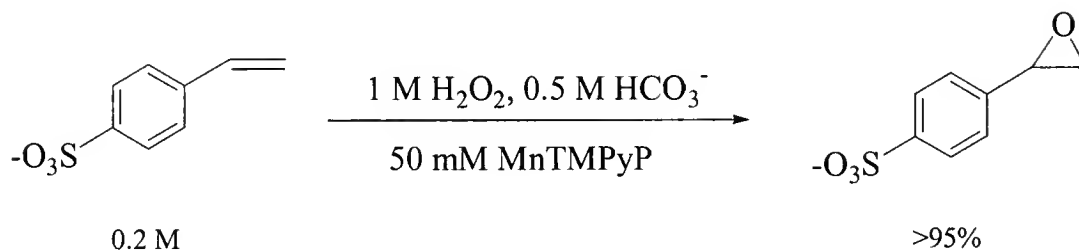


Figure 5-3. MnTMPyP/BAP catalyzed room temperature epoxidation of sulfonated styrene

free manganese source also resulted in complete conversion within approximately the same amount of time.

The effect of added imidazole was also investigated because of previous reports of improved yields when using metal porphyrins and H_2O_2 as an oxidant. The reactions with added imidazole also gave complete conversion to products in approximately 60 min.

In order to measure the observed rate constants and compare between Mn^{2+} and MnTMPyP catalyzed reactions, further experiments were done under pseudo first order conditions and analyzed using the HPLC. Sulfonated styrene (SS) and the epoxide (SSO) resolved well on the C18 column (Figure 5-5). The disappearance of SS was monitored over time and the first order plots of the disappearance of SS shown in Figure 5-6. The observation of slow product formation in the background reaction is likely because of trace metals present in the bicarbonate salt. Both the reactions catalyzed by MnTMPyP and MnSO_4 have k_{obs} values within experimental error. MnTMPyP degradation was suspected resulting in the release of free Mn^{2+} into the solution. Uv-visible analysis of an MnTMPyP solution after the addition of H_2O_2 revealed rapid bleaching of the catalyst,

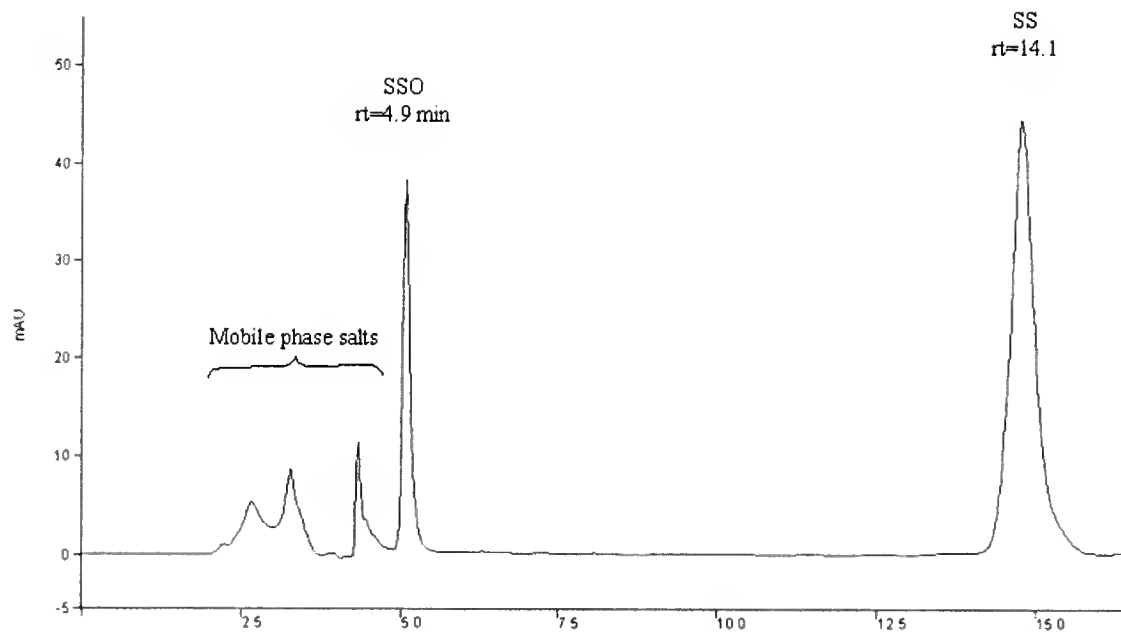


Figure 5-5. HPLC trace of reaction solution after 6 min. 1 M H_2O_2 , 0.5 M HCO_3^- , 5 μM MnTMPyP, 1 mM SS, Na_2HPO_4 and NaH_2PO_4 buffer for IS=1

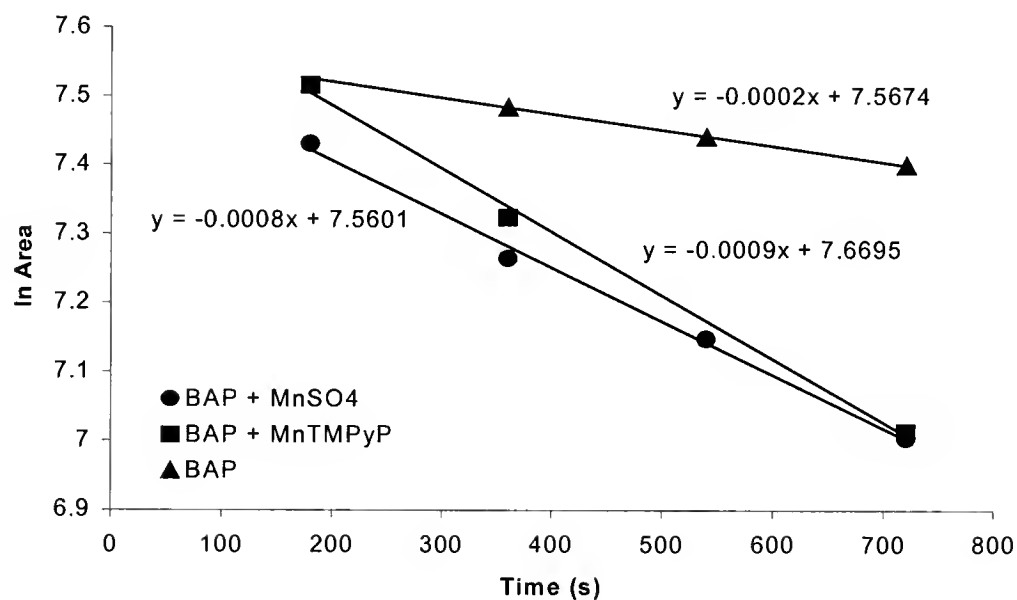


Figure 5-6. $\ln[\text{SS}]$ vs. time plots

presumably leaving free Mn^{2+} in solution (Figure 5-7). The conclusion based on the experimental results is that MnTMPyP is not resistant to attack by the reactive intermediate and experiences rapid degradation of the ligand leaving free Mn^{2+} in solution to carry out the catalysis. In view of these results we were forced to search out a more robust catalyst.

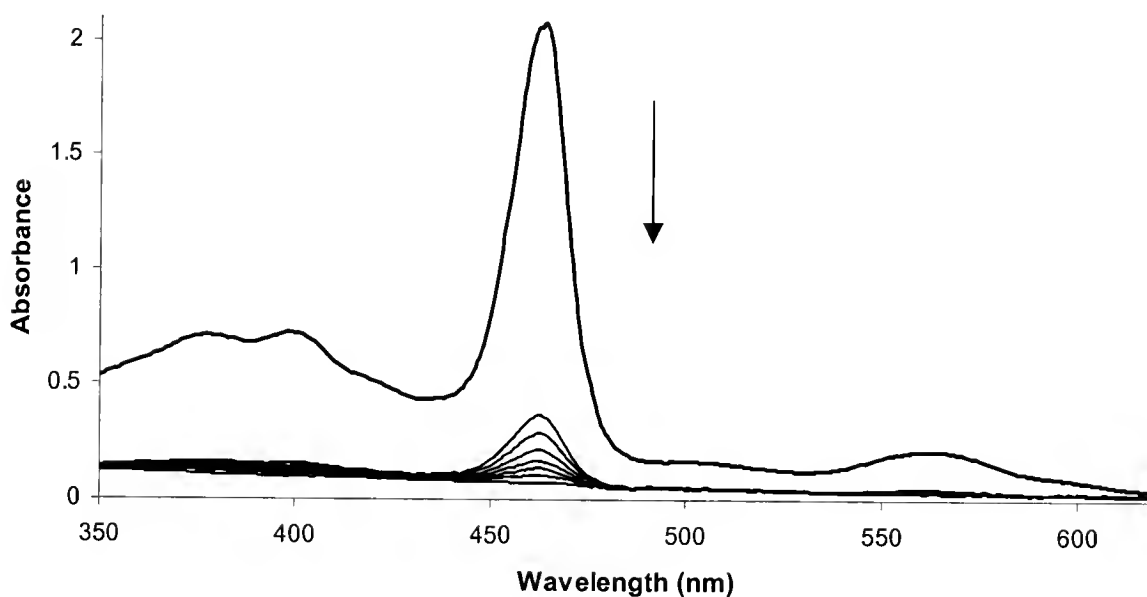


Figure 5-7. Fast decomposition of MnTMPyP in the presence of BAP; $t=30s$

Styrene Epoxidation with Jacobson's Catalyst/BAP

Introduction

Chiral Mn(III)-salen (N,N'-bis(salicylideneamino)ethane) complexes are effective catalysts for the asymmetric epoxidation of virtually every class of unfunctionalized conjugated olefins.^{42,44,104,105} Introduced by Jacobson et al.⁴² in 1990, the Mn(III)-salen family of asymmetric catalysts provides high enantiomeric excess, facile catalyst preparation, and the use of cheap oxidants such as aqueous hypochlorite. The chiral salen

ligand provides for the facial selectivity in the first C-O bond-forming step; however, the details of the remaining steps are still a topic of debate. Most proposed schemes involve a Mn(V)=O species, although the existence of such an intermediate has not been proven.¹⁰⁶ The mechanism favored by experimental evidence and DFT calculations is that of direct attack of the olefin at the oxo ligand of the Mn(V)=O species and involves a short lived radical intermediate which leads to cis/trans isomerization (Figure 5-8).^{107,108}

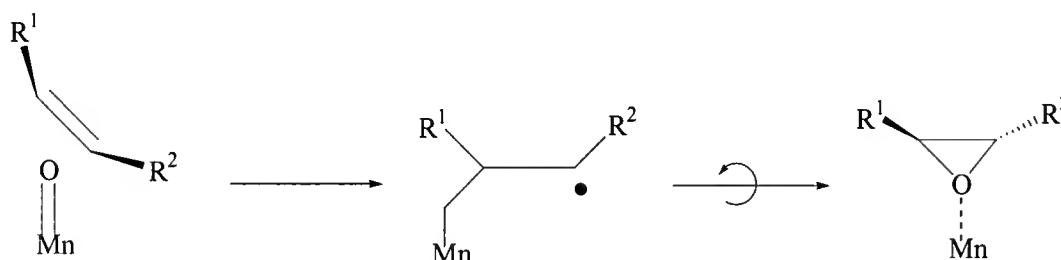


Figure 5-8. Proposed mechanism of Mn(III)-salen catalyzed epoxidation

There are only a limited number of reports where H_2O_2 was used as the oxidant in the Mn(III)-salen system. The common problems with using H_2O_2 are catalyst degradation, homolytic cleavage of the HO-OH bond and the relative ease of H_2O_2 dismutation by the catalyst. Increased enantioselectivity was achieved in the presence of nitrogen heterocycles such as imidazoles, pyridines and tertiary amine N-oxides, as well as carboxylate anions. Because of the limited effectiveness of utilizing H_2O_2 as an oxidant in asymmetric catalysis we saw this as an opportunity to test the BAP system in hopes of improving the stereoselectivity when using H_2O_2 as an oxidant. We investigated asymmetric styrene epoxidation catalyzed by Jacobson's catalyst (S,S)-(+)-N,N'-bis(3,5-di-tert-butylsalicylidene)-1,2cyclohexanediamoniomanganese(III) chloride (Figure 5-9) utilizing $\text{H}_2\text{O}_2/\text{HCO}_3^-$ as an oxidant.

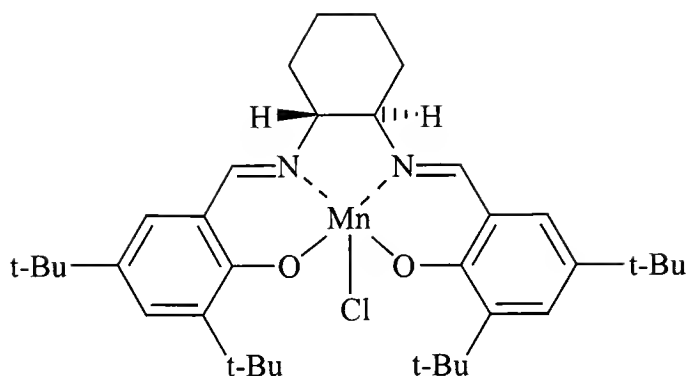


Figure 5-9. Jacobson's catalyst

Results and Discussion

Our initial studies focused on determining the appropriate solvent system to carry out the epoxidation reaction. A single-phase solvent system was preferred in which the bicarbonate salt was soluble. The co-solvents shown in Table 5-1 were screened and from the results DMF was chosen as the best solvent based on product formation and solubility of reactants. Higher product yields were obtained when the aqueous layer containing $\text{H}_2\text{O}_2/\text{HCO}_3^-$ was added slowly over 30-45 min. The reactions were highly exothermic and resulted in the formation of a brown oily residue layer.

Table 5-1. Styrene oxide yields using different solvent systems

	THF	DMF	Dioxane	t-BuOH	i-PrOH	EtOH
SO/S ratio ^a	No epoxide	1.1	0.34	0.35	0.32	0.31

57 μl styrene; 95 μl H_2O_2 ; 6mg Mn-salen; 0.02g NH_4HCO_3 ; 600 μl H_2O + 900 μl co-solvent; ^a ratio calculated from peak areas as determined by GC/FID

Table 5-2. Experimental expoxide conversion

	% Conversion to epoxide
Mn(III)-salen + HCO_3^-	74
Mn(III)-salen (no HCO_3^-)	3
H_2O_2 + HCO_3^- only	4

6mg Mn-salen and 100 μl styrene in DMF; 0.02g NH_4HCO_3 + 200 μl H_2O_2 in H_2O ; 100 μl DMF solution was added to the aqueous solution every 5min. Products analyzed after 35min. Organic layer extracted with CH_2Cl_2 , most of solvent evaporated for GC analysis.

Table 5-2 shows that the conversion to epoxide is high only when Mn-salen, H₂O₂ and HCO₃⁻ are all present. The enantiomeric selectivity of the reaction was investigated using an NMR shift reagent. Eu tris[3-(heptafluoropropylhydroxymethylene)-(+)-camphorate] was chosen because of its good solubility in organic solvents and because it results in large enantiomeric shift differences. The resolution of a mixture of enantiomers is achieved when the optically active shift reagent interacts with a pair of optical isomers resulting in the formation of two diastereomers. The separation of the resonances results from the differences in the geometric term of the pseudocontact shift equation shown in Figure 5-10. Therefore the chemical shift difference will change depending on the values of r and θ . The shifts in the proton resonances of H₁, H₂ and H₃ in Figure 5-10 will be different based on the orientation of the molecule with respect to the shift reagent.

$$\Delta\delta = k(3\cos^2\theta - 1) (r^{-3})$$

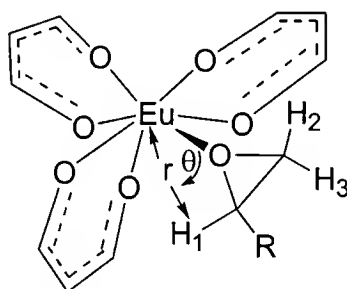


Figure 5-10. Pseudocontact shift equation

Below are the standard ¹H NMR spectra of styrene in CDCl₃ and in the presence of shift reagent (Figure 5-11). The ¹H NMR spectrum of styrene in the presence of the shift reagent results in the full resolution of both the Ha and Hb protons and a shift of all the peaks downfield. As expected a standard sample of styrene oxide is racemic where the %EE can be calculated using the peak integration values by equation 5-1.

$$\%EE = \frac{0.5 - 0.56}{0.5 + 0.56} \times 100 = 6\% \quad (5-1)$$

^1H NMR analysis of styrene oxide synthesized under the reaction conditions shown in Table 5-2 reveals that the epoxide is racemic. Therefore, in a DMF/ H_2O solvent system the Mn-salen/BAP system does not lead to enantiomeric selectivity. Reactions carried out in the same solvent system using MnSO_4 instead of Jacobson's catalyst resulted in similar product yields. The results show that catalyst degradation is a key problem in these systems. As long as the free Mn^{2+} reaction is occurring enantioselectivity is impossible to achieve.

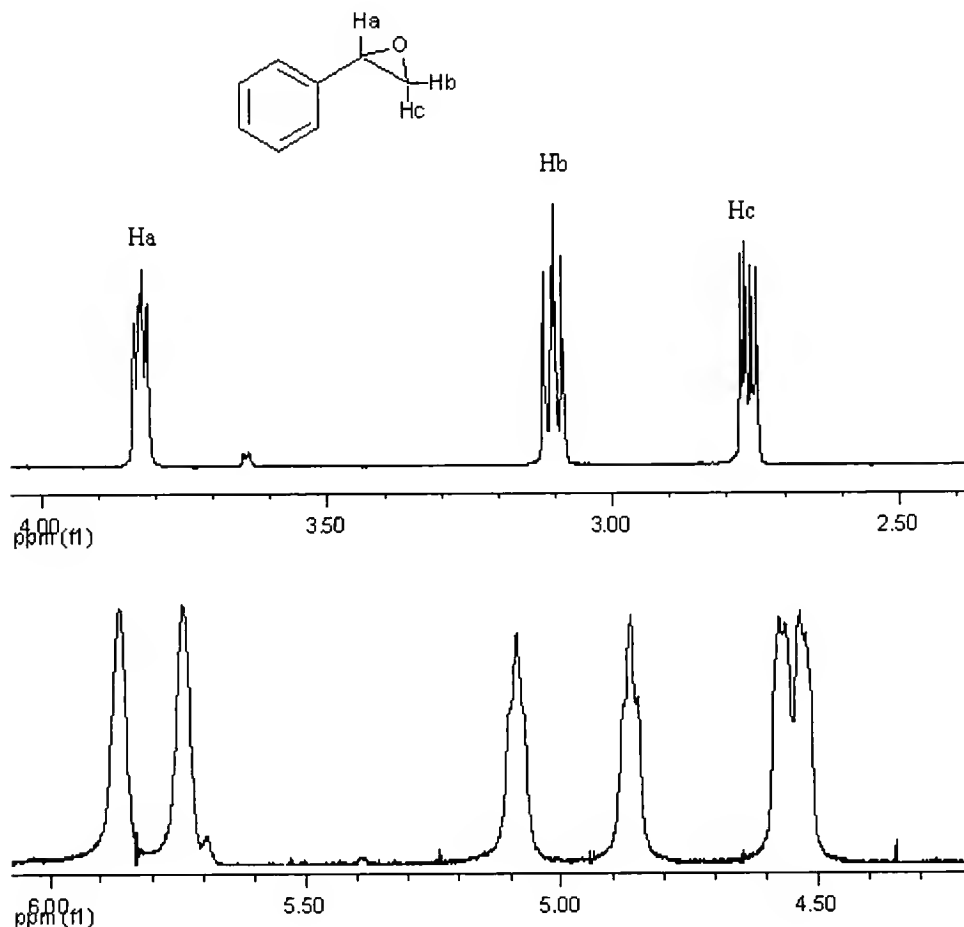


Figure. 5-11. ^1H -NMR spectrum of a standard styrene sample (top) and styrene in the presence of a shift reagent (bottom)

Since catalyst degradation is inevitable in any catalytic system, the method of preventing the non-selective free Mn^{2+} reaction is to choose a solvent system where the free Mn^{2+} pathway is no longer effective.

Published methods of epoxidation using Jacobsen's catalyst report the use of a biphasic solvent system. Since catalyst degradation is a major problem the biphasic solvent system may protect the catalyst from peroxide attack and prevent the free Mn^{2+} based catalyst from diffusing into the organic layer. The following reactions were carried out at room temperature in $\text{MeOH}/\text{CH}_2\text{Cl}_2$ as organic solvent by the slow addition of the aqueous phase containing $\text{H}_2\text{O}_2/\text{HCO}_3^-$. Analysis of %EE in the biphasic solvent yielded only racemic products; however, running the same reaction at 0 °C did result in a 32% enantiomeric excess (Table 5-3). Although the %EE is low, such a value is not uncommon when styrene is used as a substrate. High %EE in styrene epoxidation requires not only high facial selectivity, but also high diastereoselectivity in the ring closure step since the cis/trans products of styrene are enantiomeric.

Table 5-3. Determination of enantiomeric selectivity

Temperature	% Yield	% EE
25 °C	29	Racemic
0 °C	32	38
0.33 M styrene; 4×10^{-3} M Mn-salen; 1 M H_2O_2 ; 0.07 M NH_4HCO_3 ; 10ml $\text{CH}_2\text{Cl}_2/\text{MeOH}$; Aqueous solution added 250 μl every 10min.		

Since modest %EE was achieved using the Mn-salen/BAP system, further experiments were carried out to determine the effect of bicarbonate concentration on enantiomeric selectivity. Doubling the bicarbonate concentration does lead to higher epoxide yield but at the expense of selectivity. Since increasing the bicarbonate concentration results in an increase in the equilibrium concentration of peroxy carbonate, it is possible that HCO_4^- opens up alternate pathways, which lead to loss of enantioselectivity.

The use of additives in Mn(III)-salen catalyzed epoxidation reactions is reported to facilitate faster reaction rates, higher yields and improved enantioselectivity.^{45,106,109} The most common additives are nitrogen heterocycles such as imidazoles, pyridines and tertiary amine N-oxides, as well as carboxylate anions.⁴⁵ The additive is thought to function as an axial ligand stabilizing the high oxidation state Mn(V)=O species. Also the binding of the ligand may help to dissociate any multiple nuclearity Mn centers ensuring that only the mononuclear species is present.¹⁰⁶ In the case of lipophilic N-oxides the phase transfer ability of the additive has also been noted.¹¹⁰ The effect of carboxylate salts was of particular interest since HCO_3^- was a part of our system. The addition of NH_4OAc when using H_2O_2 as an oxidant lead to increased yields and improved %EE.⁴⁵ Our own experiments using sodium acetate in place of bicarbonate lead to %EE comparable to those obtained using the BAP system (Table 5-4). This argues against the idea that peroxycarbonate acts as the oxygen transfer agent since there is no evidence of a peroxy acid species forming in equilibrium with H_2O_2 and ^-OAc . Our experiments suggest the oxygen transfer is carried out by the hydrogen peroxide only, and the function of the bicarbonate ion is no different than of other additives. This result is not consistent with what was observed for the free Mn^{2+} /BAP system where other anionic salts did not result in the epoxidation of alkenes.

Although bicarbonate has no advantage over other carboxylate salts we were interested in using additives in the presence of BAP in hopes of improving the enantiomeric selectivity. N-methyl morpholine (NMO) and $(t\text{-Bu})_4\text{N}^+\text{Cl}^-$ (TBACl) have been used as both phase transfer agents and axial ligands stabilizing the active species. Neither NMO or TBACl result in an improvement of %EE, conversely the resultant

enantioselectivity was decreased. Results obtained using the Mn(III)-salen/BAP system are shown in Table 5-4.

Table 5-4. Epoxidation data

H ₂ O ₂ (M)	HCO ₃ ⁻ (M)	Styrene (M)	Additive	% Yield	% EE
1	0.07	0.33	None	15	40
1	0.25	0.33	None	24	22
1	None	0.33	None	3	-
1	None	0.33	NaOAc	22	33
2.5	0.25	0.9	NMO	15	20
2.5	0.25	0.9	TBACl	16	22
Reactions done in CH ₂ Cl ₂ /MeOH 1:1 solvent at 0 °C; Mn-salen 4x10 ⁻³ M					

Conclusions

The H₂O₂/HCO₃⁻ system proved unsuitable as an oxygen transfer agent when used with water soluble MnTMPyP. Upon addition of BAP to a solution of MnTMPyP, the characteristic absorbance associated with the complex bleached immediately as was observed by Uv-visible spectrophotometry. Presumably, this leads to the release of the free Mn²⁺ into the solution giving way to the well-known Mn²⁺/BAP catalyzed pathway.

Asymmetric epoxidation using Jacobson's catalyst was shown to be successful in a biphasic solvent where the free Mn²⁺ pathway is shut down. However, unlike the free Mn²⁺/BAP system, the HCO₃⁻ ion did not prove to be a unique ingredient in catalyzing alkene epoxidation by Jacobson's catalyst and H₂O₂. Here we find that other anionic salts such as AcO⁻ also result in similar product yield and enantiomeric excess as when HCO₃⁻ is used. These results suggest that the presence of the peroxycarbonate ion is not necessary to carry out the oxygen transfer to the catalyst.

CHAPTER 6

SUMMARY

The proposed autoxidation mechanism suggests that the primary function of **1** and **2** is to provide an active catalyst that decomposes the intermediate hydroperoxide and generates chain-propagating radicals. Our detailed kinetic simulations show that metal catalysis of the peroxide decomposition steps is sufficient to account for the high catalytic activities of both complexes **1** and **2**. Good fits to both metal catalyzed cumene oxidation and peroxide decomposition data was achieved using the proposed mechanism and rate constants. The rate dependence on oxygen pressure, temperature, solvent polarity, and catalyst concentration is also consistent with a free-radical mechanism.

The high catalytic activity of **1** in hydrocarbon solvent is ascribed to the solubilizing properties of the phenyl substituents on the phenanthroline ligand. Analysis of the catalytic activity of substituted FeL_3X_2 complexes in a polar solvent reveal that less electron donating ligands such as the unsubstituted 1,10-phenanthroline and 5- NO_2 -phenanthroline ligands result in more active catalyst precursors. The effect is largely due to a decrease in the induction period rather than an intrinsic increase in the activity of the active catalyst. The result supports the idea that ligand dissociation is important in the formation of the active catalyst; however, it puts into question the importance of the ligand on the activity of the active species.

However, the identity of the ligand does carry some importance as was shown in experiments comparing the catalytic activity of FeL_3X_2 complexes to other known autoxidation and peroxide decomposition catalysts. For example, Fe(II)cyclam ,

$\text{Fe}(\text{pyridine})_4\text{Cl}_2$, and $\text{Fe}(\text{SO}_3\text{CF}_3)_2$ all have very low catalytic activity. Other metal complexes such as $\text{Co}(\text{II})\text{acac}$ and $\text{Fe}(\text{II})\text{Pc}$ do have moderate activity but still significantly lower than the highly active FeL_3X_2 complexes. Even replacing one of the diimine ligands with two X^- ligands as in the FeL_2X_2 complexes, resulted in a significant decrease in reactivity of the catalyst precursor.

Early investigations of simple metal salts as autoxidation catalysts proposed a variety of possible active catalyst formulations depending on the metal, substrate and solvent used. Metal dimers, metal peroxy adducts and coordinatively unsaturated species have been proposed based on kinetic data.¹¹ In general, ligand destruction was associated with catalyst deactivation. Our own investigations of the identity of the active catalyst possibly offer an alternative interpretation. The absence of substituent dependence in FeL_3X_2 complexes on the maximum rate of oxygen uptake suggests that the active catalyst may not contain the ligand in its original form. The $[\text{Fe}(\text{II})\text{tpa}(\text{CH}_3\text{CN})_2](\text{SO}_3\text{CF}_3)_2$ complex and the tpa ligand were observed to decompose completely in the presence of alkyl peroxide; however, the solution remains highly active in catalyzing cumene autoxidation.

All of these observations suggest that the catalyst precursors may form active species following radical attack of the ligands. Results also suggest that not every ligand type degrades to form an active catalyst. Presumably, some unique feature of pyridyl ligands such as diimines, tpa and tpen result in the formation of highly active catalytic species following ligand degradation.

The hypothesis that ligand degradation actually leads to the formation of an active catalyst is contrary to most ideas about catalytic species. However, the idea might offer a

way to understand the seemingly contradictory evidence collected in this and other studies.

Simple iron-phenanthroline precursor **1** discussed here is comparable in activity to the halogenated iron porphyrins and is among the most active known hydrocarbon soluble, low temperature, autoxidation catalysts. Related FeL_3X_2 complexes with substituted 1,10-phenanthroline ligands are also highly active autoxidation catalyst precursors compared to other known autoxidation and peroxide decomposition catalysts when using a polar co-solvent such as acetonitrile.

CHAPTER 7 EXPERIMENTAL

General

Product analysis was done using the following instruments: Varian CP-3800 GC/FID with a DB-35MS column, Varian 300Mz NMR, Finnigan MAT95 Q GC/MS, Varian HPLC. Oxidation and peroxide decomposition reactions were done in a glass lined stainless steel Parr 4560 300ml Mini Bench Top Reactor. Constant O₂ pressure was achieved by using a gas burette. O₂ gas uptake (oxidation) and O₂ production (peroxide decomposition) was monitored by a pressure transducer, connected to a Cole-Parmer Solid State Paperless Data Recorder.

Materials

Cumene and benzene of the highest purity were purchased from Aldrich, distilled over Na and stored under an inert atmosphere. Cyclohexane was distilled over CaH₂. Acetonitrile was distilled over P₂O₅ and CaH₂. Fe(III)-tetra-(pentafluorophenyl)-porphyrin chloride (FeTPPF) and Mn(III) meso-tetrakis(4N-methylpyridinium)porphyrin (MnTMPyP) were purchased from Mid-Century and used as received. Co-naphthanate solution in mineral oil (6.8% Co metal) was purchased from Aldrich and used as received. Fe(SO₃CF₃)₂·6H₂O, Fe(4,7-diphenyl-1,10-phenanthroline)₃Cl₂ and Ru(4,7-diphenyl-1,10-phenanthroline)₃Cl₂ were synthesized using published procedures.^{111,112} All other materials were purchased from Aldrich and used without further purification.

Kinetic Modeling

Numerical kinetic simulations were done with Kinetica99, a program based on the Gear integration method (D. E. Richardson, University of Florida, 1999).

Oxidation Experiments

Cumene oxidation was done by charging the reactor with a specified amount of catalyst and cumene, cumene/co-solvent. The reactor was heated to the specified temperature (60-90 C°). Once the temperature was reached a constant O₂ feed was maintained at 60 psi during the entire reaction time. Liquid samples were periodically removed from the reactor through a sampling tube. Samples were analyzed by GC/FID (ROH, RO, ROOH) and ¹H NMR (ROOR). Head space gas samples were also collected and analyzed by GC/TCD. All products were characterized by GC/MS and by comparison to standards.

Cyclohexane oxidation was done by charging the reactor with a specified amount of catalyst and cyclohexane/co-solvent. The reactor was pressurized to 50psi and heated to 135 C°. Once heated, a constant O₂ feed was maintained at the specified pressure. The reaction solution was sampled periodically and analyzed by GC/FID. Due to potential explosion hazard the reactor was cooled in ice prior to venting the gases.

Peroxide Decomposition Experiments

The reactor was charged with solvent solution under and inert atmosphere. The reactor was heated to 60 C° and 5ml ROOH added by syringe, immediately followed by the addition of a 5ml solution of the catalyst. The reaction solution was sampled periodically and analyzed by GC/FID. Oxygen release was monitored by a pressure transducer.

Sulfonated Styrene Epoxidation

Kinetic studies were done at room temperature in DI water as solvent. The peroxide and bicarbonate were mixed separately and allowed to equilibrate for 5 min. The reaction was started by adding a solution of the metal source to the BAP/substrate solution. Aliquots of the reaction solution were taken periodically and added to a solution of the enzyme catalase in order to stop the reaction by dismutating all of the remaining H_2O_2 . The aliquots were analyzed by HPLC. The NMR reactions were done in DOH and allowed to react until all evolution of bubbles ceased (~1 h).

HPLC Analysis

The separation of sulfonated styrene and sulfonated styrene oxide was achieved by isocratic elution using a C18 reverse phase column using an ion-pairing reagent $(\text{t-Bu})_4\text{N}^+\text{Cl}^-$ (TBACl) in the mobile phase. The mobile phase was composed of A: 75% 0.2 mM TBACl, 2.0 mM NaH_2PO_4 and B: 25% 20/20 $\text{CH}_3\text{CN}/\text{H}_2\text{O}$.

Styrene Epoxidation

Reactions were carried out by dissolving the Mn-salen, substrate and additive in the organic solvent and adding aliquots (100 μl /5 min) of the aqueous phase containing the H_2O_2 and HCO_3^- . The product was extracted using CH_2Cl_2 and the solvent evaporated. The unpurified solution was used to determine yield using GC/FID. The epoxide was separated from the substrate and Mn-salen by passing through a silica gel column by slowly increasing the polarity of the hexanes/ethyl acetate mobile phase. The eluent was concentrated by evaporating the solvent and the enantiomeric purity of the epoxide determined by ^1H NMR with the help of the shift reagent Europium tris[3-(heptafluoropropylhydroxymethylene)-(+)-camphorate]. Enantiomeric excess was calculated from the peak integrals.

Synthesis

(1) [Fe(4,7-diphenyl-1,10-phenanthroline)₃](SO₃CF₃)₂ · H₂O

10 ml of 1 M AgCF₃SO₃ aqueous solution was added to 10 ml of 0.5 M FeCl₂ aqueous solution. A white precipitate (AgCl) formed immediately upon mixing. The solution was allowed to stir for three hours before filtering. The filtrate containing an aqueous solution of Fe(CF₃SO₃)₂ was added to 30 ml of an ethanolic solution of 0.5 M DPP. The solution immediately turned dark red. The dark red solution was allowed to stir for 3 hours uncovered allowing the solution volume to reduce to ~ 10 ml. The resulting solution contained a dark red precipitate, which was isolated and washed with small amounts of ethanol. Dark red solid was dried in a vacuum oven at 65 °C for 6 hours resulting in dark red powder (yield 87 %). ¹H NMR (300MHz, DMSO): δ8.3 (6H, s, phen H5,6), δ8.0 (6H, d, J=5.7, phen H2,9), δ7.8 (6H, d, J=5.7, phen H3,8), δ7.7-7.6 (30H, m, phenyl groups). ¹³C NMR (75MHz CDCl₃): δ156.5, δ150.0, δ149.4, δ135.3, δ129.9, δ129.7, δ129.1, δ128.1, δ127.0, δ125.9. Anal. Calcd. for; Fe₁C₇₄H₅₀N₆O₇F₆S₂ (%): C, 64.91; H,3.68; N, 6.14. Found (%): C, 64.72; H, 3.51; N, 6.07. Electron spray ionization spectroscopy (ESI-MS): MW=1053 [Fe(DPP)₃²⁺]; MW=869 [Fe(DPP)₂(SO₃CF₃)⁺]; MW=720 [Fe(DPP)₂²⁺]; MW=333 [HDPP⁺].

[Fe(L)₃] X₂ complexes

All of the CF₃SO₃⁻ complexes were made by the method described above for 1. The ClO₄⁻ salt was made by mixing an ethanolic solution of Fe(ClO₄)₂ with an ethanolic solution of three equivalents of ligand. The resulting solution was concentrated and the

solid filtered. Solid was recrystallized from CH₃CN. CHN analysis of complexes is shown below.

[Fe(2,2'-bipyridine)₃](CF₃SO₃)₂

Anal. Calcd. for; C₃₂H₂₄F₆FeN₆O₆S₂ (%): C, 46.73; H, 2.94; N, 10.22; Found (%): C, 46.86; H, 2.75; N, 9.93;

[Fe(4-methyl-1,10-phenanthroline)₃](CF₃SO₃)₂ · 2H₂O

Anal. Calcd. for; C₄₁H₃₄F₆FeN₆O₈S₂ (%): C, 50.63; H, 3.52; N, 8.64; Found (%): C, 50.91; H, 3.09; N, 8.34;

[Fe(4,7-dimethyl-1,10-phenanthroline)₃](CF₃SO₃)₂ · H₂O

Anal. Calcd. for; C₄₄H₃₈F₆FeN₆O₇S₂ (%): C, 53.02; H, 3.84; N, 8.43; Found (%): C, 53.42; H, 3.83; N, 8.27;

[Fe(3,4,7,8-tetramethyl-1,10-phenanthroline)₃](CF₃SO₃)₂ · H₂O

Anal. Calcd. for; C₅₀H₅₀F₆FeN₆O₇S₂ (%): C, 55.56; H, 4.66; N, 7.77; Found (%): C, 55.71; H, 4.58; N, 7.64;

[Fe(5-NO₂-1,10-phenanthroline)₃](ClO₄)₂

Anal. Calcd. for; C₃₆H₂₁Cl₂FeN₉O₁₄ (%): C, 46.48; H, 2.28; N, 13.55; Found (%): C, 46.16; H, 1.99; N, 13.18

[Fe(2,9-dimethyl-1,10-phenanthroline)₂(H₂O)₂](SO₃CF₃)₂

Synthesized according to published procedure.⁶¹ Anal. Calcd. for; C₃₀H₃₂F₆FeN₄O₁₀S₂ (%): C, 42.76; H, 3.83; N, 6.65. Found (%): C, 42.36; H, 3.50; N, 5.95.

Fe(1,10-phenanthroline)₂Cl₂

Synthesized according to published procedure.¹¹³ Anal. Calcd. for; C₂₄H₁₆Cl₂FeN₄ (%): C, 59.17; H, 3.31; N, 11.50. Found (%): C, 59.93; H, 3.65; N, 11.78.

Fe(1,10-phenanthroline)₂(CN)₂

Synthesized according to published procedure.¹¹³ Anal. Calcd. for: C₂₆H₁₆FeN₆ (%): C, 66.68; H, 3.44; N, 17.95. Found (%): C, 66.23; H, 3.38; N, 17.68. IR bands; ν C \equiv N 2067 cm⁻¹, 2063 cm⁻¹, ν C=N diimine 1628 cm⁻¹

Fe(1,10-phenanthroline)₂(NCS)₂

Synthesized according to published procedure.¹¹⁴ Anal. Calcd. for: C₂₆H₁₆FeN₆S₂ (%): C, 58.6; H, 3.03; N, 15.78. Found (%): C, 58.83; H, 3.09; N, 15.52. IR bands; ν N \equiv CS str. 2071 cm⁻¹, 2060 cm⁻¹; NC-S str. 789cm⁻¹; N-C-S bend 473 cm⁻¹, 482 cm⁻¹.

[Fe(N,N,N',N'-tetrakis(2-pyridylmethyl)-aminopyridyl)](ClO₄)₃

Synthesized according to published procedure.⁹⁴ Anal. Calcd. for: C₂₆H₂₈Cl₃FeN₆O₁₂ (%): C, 40.10; H, 3.62; N, 10.79. Found (%): C, 40.44; H, 3.64; N, 10.61

Fe(tris(2-pyridylmethyl)amine)(SO₃CF₃)₂ · CH₃CN

Synthesized according to published procedure.⁹³ Anal. Calcd. for: C₂₂H₂₁F₆FeN₅O₆S₂(%): C, 38.55; H, 3.09; N, 10.22. Found (%): C, 38.10; H, 3.09; N, 10.03

[Fe₂O(2,2'-bipyridine)₄(CH₃CO₂)](ClO₄)₃

Synthesized according to published procedure.¹⁰¹ Anal. Calcd. for: C₄₂H₃₉Cl₃Fe₂N₈O₁₇(%): C, 44.03; H, 3.40; N, 9.78. Found (%): C, 44.79; H, 3.36; N, 10.45

[Fe₂O(2,2'-bipyridine)₄((CH₃)₃CO₂)](ClO₄)₃

Fe(ClO₄)₃ (1 mmol) was added to a solution of (CH₃)₃COOH (pivalic acid) (1 mmol) and KOH (1 mmol) in EtOH. Solution color changed from yellow to dark green. Solution of 2,2'-bipyridine (2 mmol) in CH₃CN was added to the previous solution and a white

precipitate immediately appeared. White precipitate was filtered off and the solution volume reduced to isolate a green powder. Anal. Calcd. for: $C_{45}H_{41}Cl_3Fe_2N_8O_{15}$ (%): C, 46.65; H, 3.54; N, 9.68. Found (%): C, 45.68; H, 3.67; N, 9.39

$Fe_3O((CH_3)CCOO)_6(Pyridine)_3$

Synthesized according to published procedure.¹¹⁵ Anal. Calcd. for: $C_{45}H_{69}Fe_3N_3O_{13}$ (%): C, 52.6; H, 6.72; N, 4.09. Found (%): C, 52.39; H, 6.93; N, 3.98

$Fe_3O(4\text{-fluorobenzoate})_6(Pyridine)_3$

$FeCl_2 \cdot H_2O$ (2.6g), 4-fluorobenzoic acid (3.3 g), were added to dimethoxy ethylene glycol (20 ml) and H_2O (20 ml). The biphasic solution was refluxed for 24 h. EtOH and pyridine (5 ml) were added to the cooled solution turning the solution black. Solvent was reduced and black micro crystals formed. Product was isolated by filtration and vacuum dried. Anal. Calcd. for: $C_{57}H_{39}Fe_3N_3O_{13}$ (%): C, 54.53; H, 3.13; N, 3.35. Found (%): C, 54.42; H, 3.02; N, 3.81

APPENDIX-A VARIATIONS IN RATE CONSTANTS

The following figures were generated by keeping all rate constants of Figure 2-10 constant except the indicated rate constant.

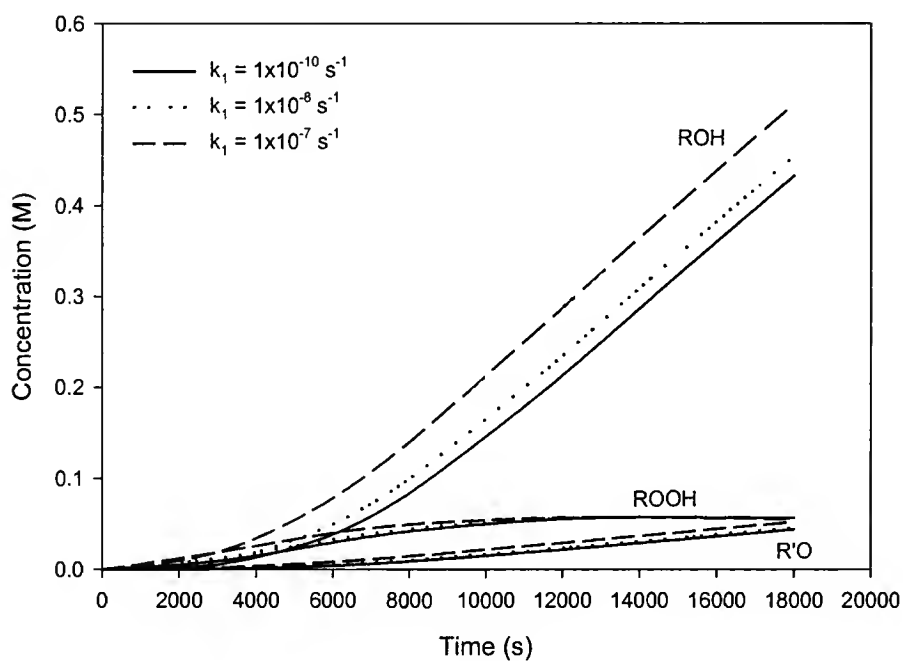


Figure A-1. Variation in k_1 ($\text{RH} \rightarrow \text{R}\cdot$)

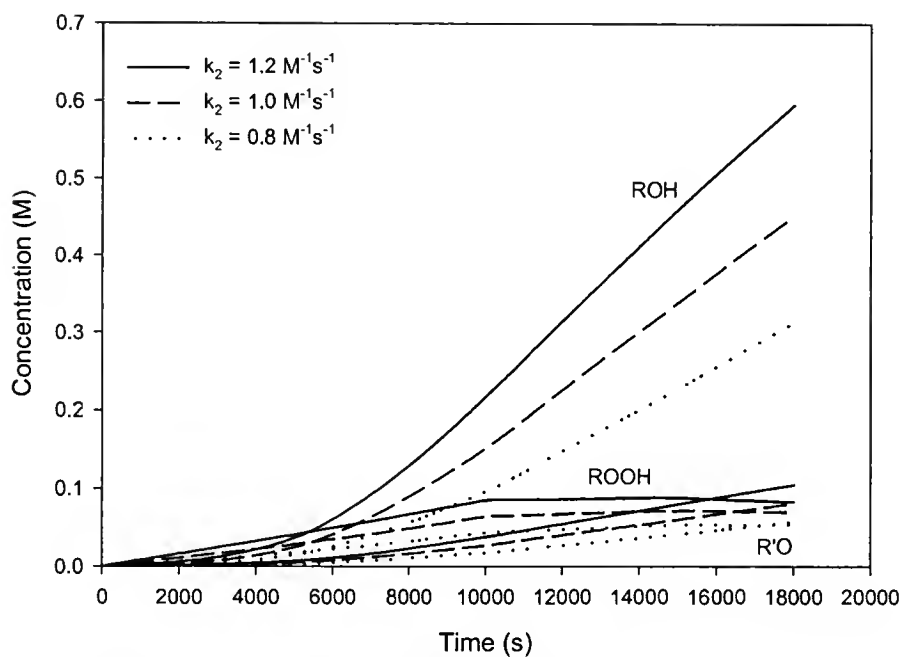


Figure A-2. Variation in k_2 ($\text{ROO}\cdot + \text{RH} \rightarrow \text{ROOH} + \text{R}\cdot$)

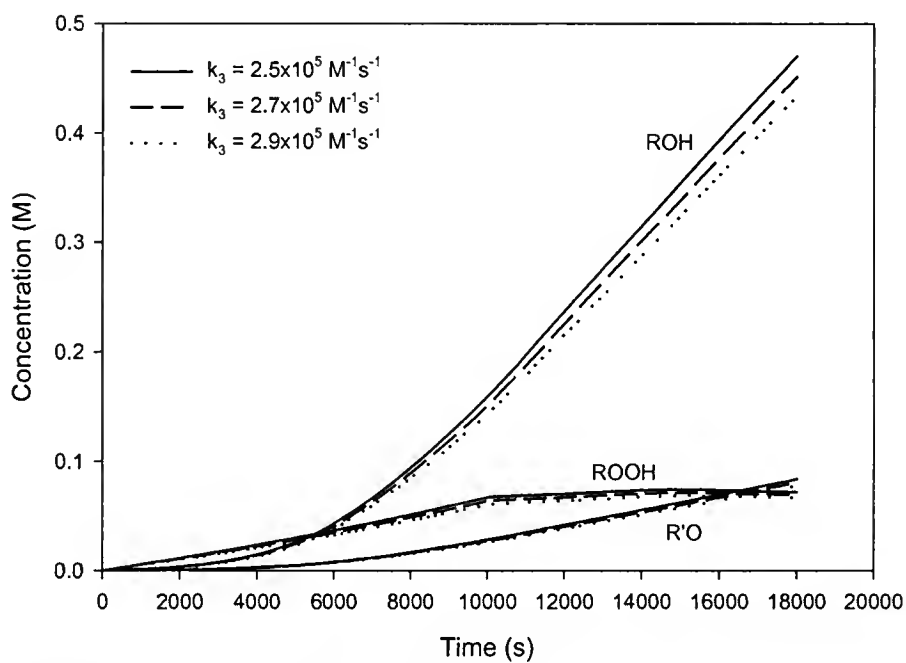


Figure A-3. Variation in k_3 ($2 \text{ROO}\cdot \rightarrow 2 \text{RO} + \text{O}_2$)

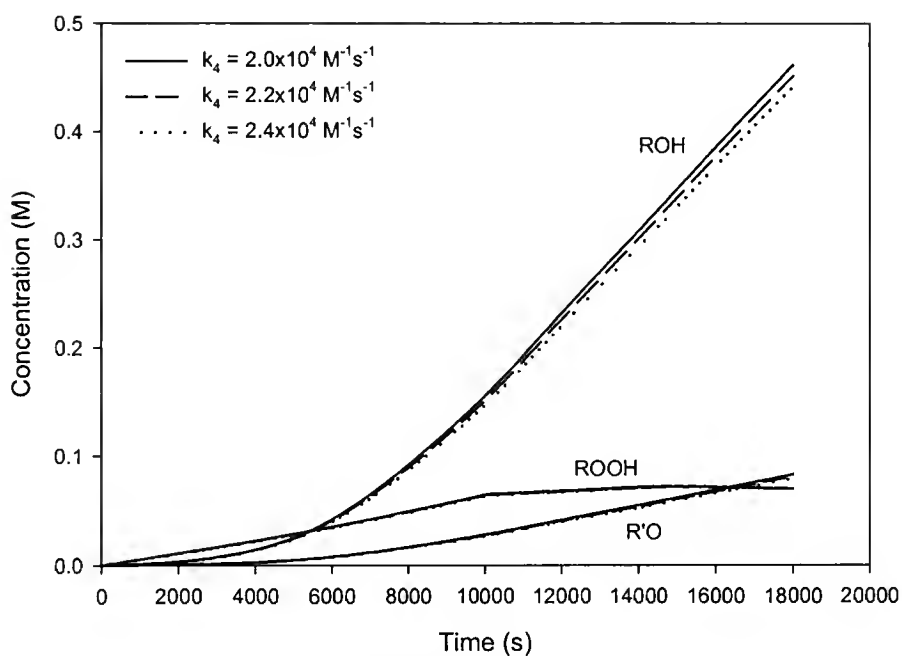


Figure A-4. Variation k_4 ($2 \text{ROO}\cdot \rightarrow \text{ROOR} + \text{O}_2$)

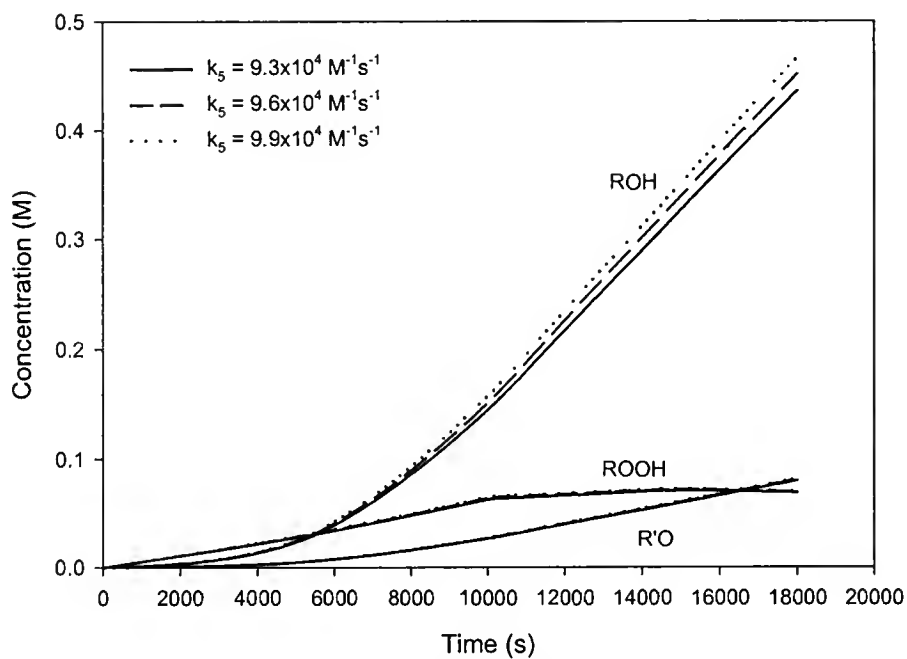


Figure A-5. Variation in k_5 ($\text{RO}\cdot + \text{RH} \rightarrow \text{ROH} + \text{R}\cdot$)

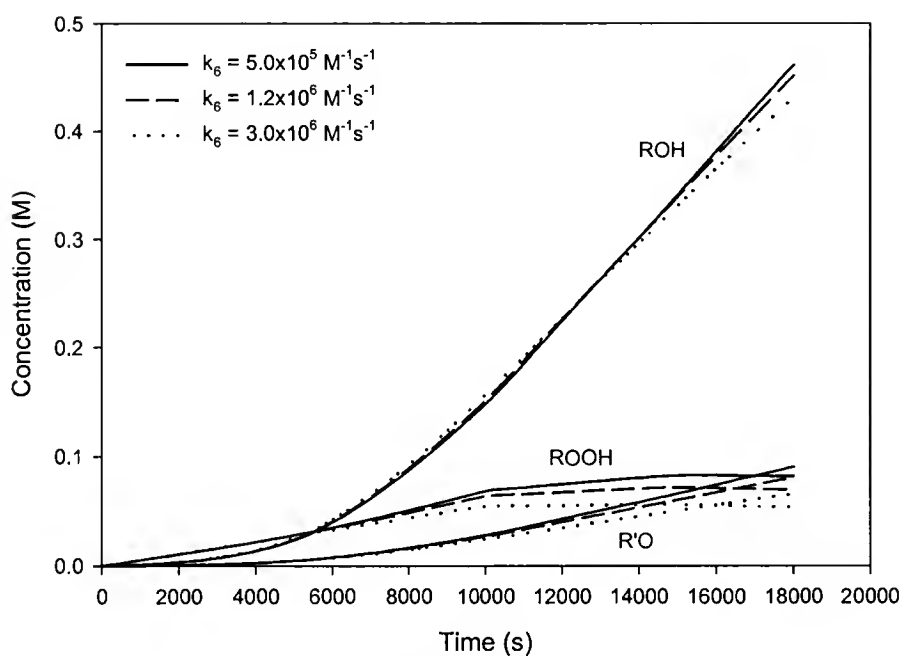


Figure A-6. Variation in k_6 ($\text{RO}\cdot + \text{ROOH} \rightarrow \text{ROH} + \text{ROO}\cdot$)

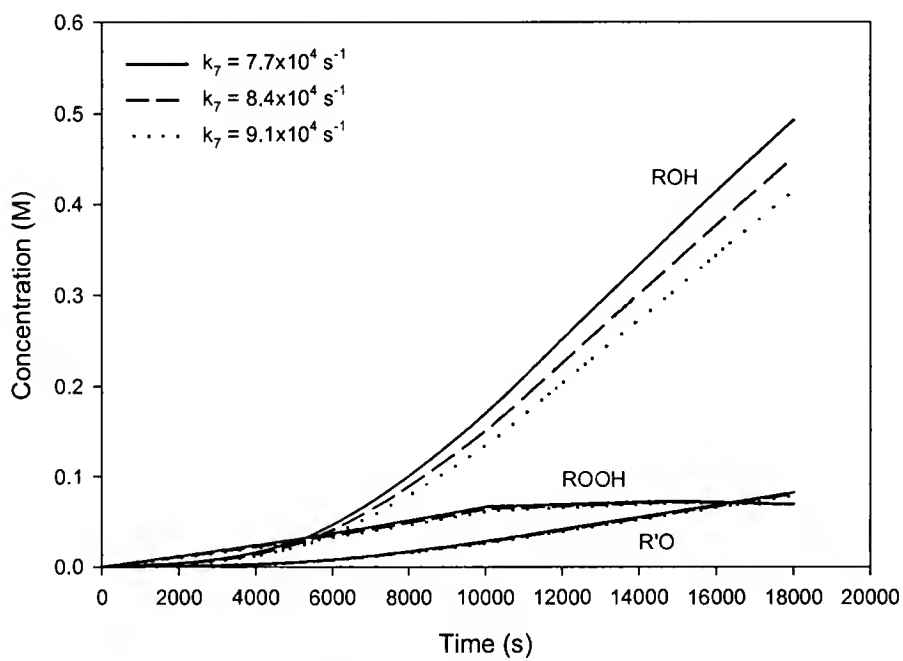


Figure A-7. Variation in k_7 ($\text{RO}\cdot \rightarrow \text{R}'\text{O} + \text{Me}\cdot$)

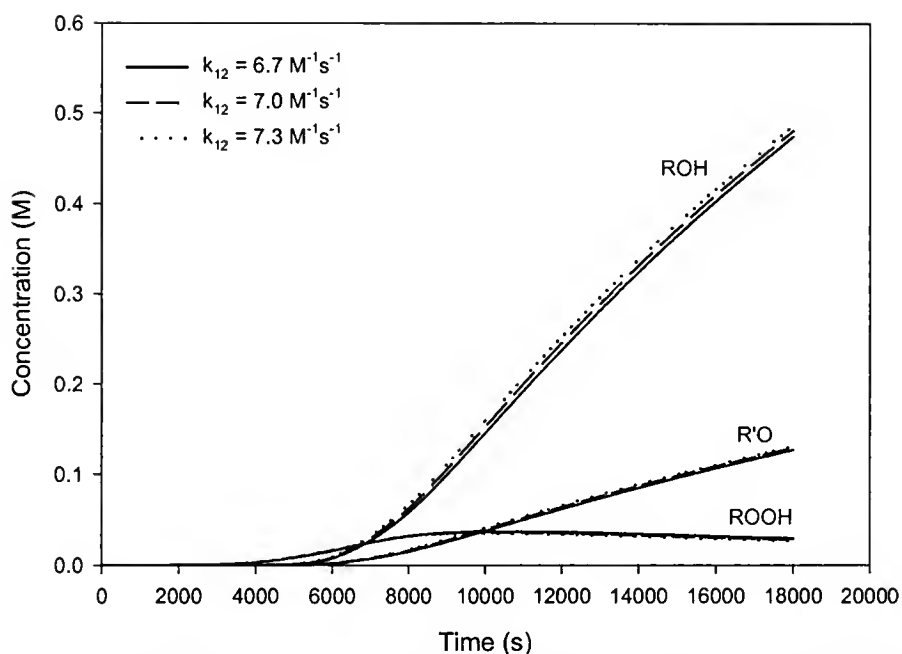


Figure A-8. Variation in k_{12} ($\text{ROOH} + \text{M}^{\text{III}} \rightarrow \text{ROO}\cdot + \text{H}^+ + \text{M}^{\text{II}}$). Catalytic step in peroxide decomposition step catalyzed by 2.

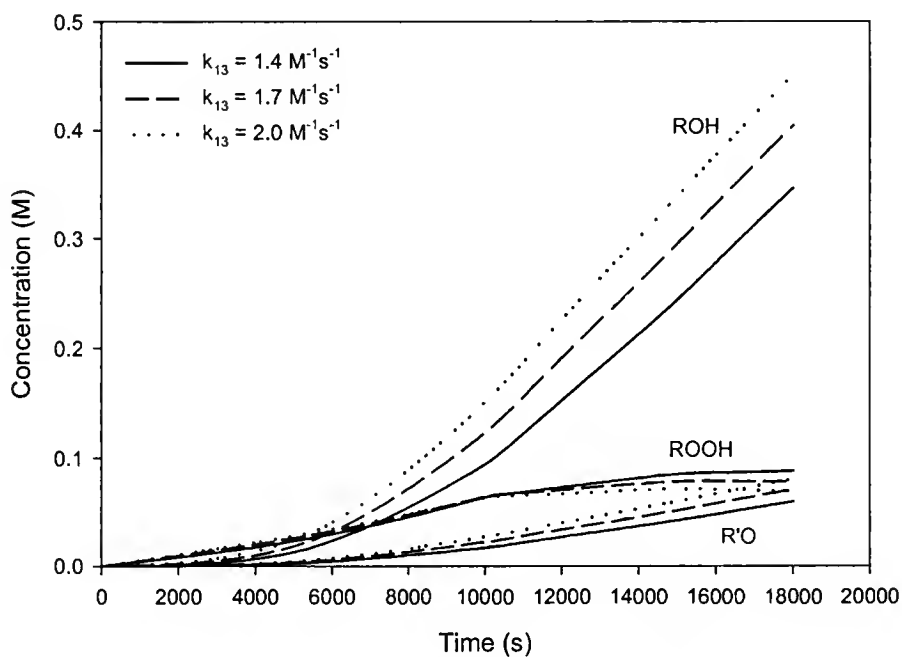


Figure A-9. Variation in k_{13} ($\text{ROOH} + \text{M}^{\text{II}} \rightarrow \text{RO}\cdot + \text{HO}^- + \text{M}^{\text{III}}$). Catalytic step in peroxide decomposition step catalyzed by 1.

LIST OF REFERENCES

- (1) Sheldon, R. A., Kochi, J. K. *Metal-Catalyzed Oxidations of Organic Compounds*; Academic Press: New York, 1981.
- (2) Shilov, A. E., Shul'pin, G. B. *Activation and Catalytic Reactions of Saturated Hydrocarbons in the Presence of Metal Complexes*; Kluwer Academic Publishers: Boston, 2000.
- (3) Backstrom, H. L. J. *J. Am. Chem. Soc.* **1927**, *49*, 1460.
- (4) Farmer, E. H., Sundralingham, A. *J. Chem. Soc.* **1942**, 121.
- (5) Parshall, G. W. *Homogeneous catalysis: The applications and chemistry of catalysis by soluble transition metal complexes*; John Wiley & Sons: New York, 1980.
- (6) Kamiya, Y., Ingold, K. U. *Can. J. Chem* **1964**, *42*, 1027.
- (7) Kamiya, Y., Ingold, K. U., Lafortun, A., Beaton, S. *Can. J. Chem* **1963**, *41*, 2034.
- (8) Hiatt, R., Irwin, K. C., Gould, C. W. *J. Org. Chem.* **1968**, *33*, 1430.
- (9) Helfin, B., Schwartz, G. A., U.S. 3,530,185, **1970**.
- (10) Bhaduri, S., Mukesh, D. *Homogeneous catalysis: mechanisms and industrial applications*; Wiley-Interscience: New York, 2000.
- (11) Reich, L., Stivala, S. S. *Autoxidation of Hydrocarbons and Polyolefins; Kinetics and Mechanisms*; Marcel Dekker, INC.: New York, 1969.
- (12) Howard, J. A., Ingold, K. U. *Can. J. Chem.* **1968**, *46*, 2655.
- (13) Ellis, P. E., Lyons, J. E. *Coord. Chem. Rev.* **1990**, *105*, 181.
- (14) Wijesekera, T. P., Lyons, J. E., Ellis, P. E. *Catal. Lett.* **1996**, *36*, 69.
- (15) Lyons, J. E., Ellis, P. E. *Catal. Lett.* **1991**, *8*, 45.
- (16) Grinstaff, M. W., Hill, M. G., Labinger, J. A., Gray, H. B. *Science* **1994**, *264*, 1311.

- (17) Labinger, J. A. *Catal. Lett.* **1994**, *26*, 95.
- (18) Koenig, T., Owens, J. M. *J. Am. Chem. Soc.* **1974**, *96*, 4054.
- (19) Barton, D. H. R., Doller, D. *Acc. Chem. Res.* **1992**, *25*, 504.
- (20) Barton, D. H. R., Beviere, S. D., Chavasiri, W., Csuhai, E., Doller, D., Liu, W. G. *J. Am. Chem. Soc.* **1992**, *114*, 2147.
- (21) Celenligil-Cetin, R., Staples, R. J., Stavropoulos, P. *Inorg. Chem.* **2000**, *39*, 5838.
- (22) Kiani, S., Tapper, A., Staples, R. J., Stavropoulos, P. *J. Am. Chem. Soc.* **2000**, *122*, 7503.
- (23) Schuchardt, U., Jannini, J. D. M., Richens, D. T., Guerreiro, M. C., Spinace, E. V. *Tetrahedron* **2001**, *57*, 2685.
- (24) Singh, B., Long, J. R., de Briani, F. F., Gatteschi, D., Stavropoulos, P. *J. Am. Chem. Soc.* **1997**, *119*, 7030.
- (25) Tanaka, K. *Chemtech* , 555. 1974.
- (26) Vaska, L. *Science* **1963**, *140*, 809.
- (27) Tsang, P. K. S., Sawyer, D. T. *Inorg. Chem.* **1990**, *29*.
- (28) Porniewicz, L. M., Kulczycki, A., Weselucha-Birczynska, A., Majcherczyk, H., Nakamoto, K. *New. J. Chem.* **1999**, *8*.
- (29) Itoh, S., Taki, M., Nakao, H., Holland, P. L., Tolman, W. B., Que, L., Fukuzumi, S. *Angew. Chem. Int. Ed.* **2000**, *39*, 398.
- (30) Schoenecker, B., Zheldakova, T., Liu, Y., Motteritzsch, M., Gunther, W., Gorls, H. *Angew. Chem. Int. Ed.* **2003**, *42*, 3240.
- (31) Blain, I., Giorgi, M., DeRiggi, I., Reglier, M. *Eur. J. Inorg. Chem.* **2000**, 393.
- (32) Arends, I. W. C. E., Sheldon, R. A. *Topics in Catalysis* **2002**, *19*, 133.
- (33) Notari, B. *Catal. Today* **1993**, *18*, 163.
- (34) Herrmann, W. A., Fischer, R. W., Marz, D. W. *Angew. Chem. Int. Ed.* **1991**, *30*, 1638.
- (35) Herrmann, W. A., Kratzer, R. M., Ding, H., Thiel, W. R., Gras, H. J. *Organometall. Chem.* **1998**, *555*, 293.
- (36) Coperet, C., Adolfsson, H., Sharpless, K. B. *Chem. Comm.* **1997**, 1565.

- (37) Groves, J. T., Nemo, T. E. *J. Am. Chem. Soc.* **1983**, *105*, 5786.
- (38) Powel, M. F., Pai, E. F., Bruice, T. C. *J. Am. Chem. Soc.* **1984**, *106*, 3277.
- (39) Meunier, B., Guilmet, E., De Carvalho, M. E., Poilblanc, R. *J. Am. Chem. Soc.* **1984**, *106*, 6676.
- (40) Lee, W. A., Bruice, T. C. *J. Am. Chem. Soc.* **1985**, *107*, 513.
- (41) Battioni, P., Renaud, J. P., Bartoli, J. F., Reina-Artiles, M., Fort, M., Mansuy, D. *J. Am. Chem. Soc.* **1988**, *110*, 8462.
- (42) Zhang, W., Jacobson, E. N. *J. Am. Chem. Soc.* **1990**, *112*, 2801.
- (43) Zhang, W., Jacobson, E. N. *J. Org. Chem.* **1991**, *56*, 2296.
- (44) Palucki, M., McCormick, G. J., Jacobson, E. N. *Tet. Lett.* **1995**, *36*, 5457.
- (45) Pietikainen, P. *Tetrahedron* **1998**, *54*, 4319.
- (46) Yao, H., Richardson, D. E. *J. Am. Chem. Soc.* **2000**, *122*, 3220.
- (47) Lane, B. S., Vogt, M., Deroose, V. J., Burgess, K. *J. Am. Chem. Soc.* **2002**, *124*, 11946.
- (48) Richardson, D. E., Yao, H. R., Frank, K. M., Bennett, D. A. *J. Am. Chem. Soc.* **2000**, *122*, 1729.
- (49) Wijesekera, T. P., Lyons, J. E., Ellis, P. E. *Catal. Lett.* **1996**, *36*, 69.
- (50) Ellis, P. E., Lyons, J. E. *Catal. Lett.* **1989**, *3*, 389.
- (51) Lyons, J. E., Ellis, P. E., Myers H.K. *J. Catal.* **1995**, *155*, 59.
- (52) MacFaul, P. A., Arends, I. W. C. E., Ingold, K. U., Wayner, D. D. M. *J. Chem. Soc., Perkin Trans. 2* **1997**, *2*, 135.
- (53) Bottcher, A., Birnbaum, E. R., Day, M. W., Gray, H. B., Grinstaff, M. W., Labinger, J. A. *J. Mol. Catal., A:Chem.* **1997**, *117*, 229.
- (54) Grinstaff, M. W., Hill, M. G., Birnbaum, E. R., Schaefer, W. P., Labinger, J. A., Gray, H. B. *Inorg. Chem.* **1995**, *34*, 4896.
- (55) Xu, C. Ph.D., University of Florida, Gainesville, Fl., **1999**.
- (56) Richardson, D. E., Xu, C., Abboud, K. A., U.S. 6,258,981, **2001**.
- (57) Richardson, D. E., Xu, C., Abboud, K. A., Weakley, G. K., U.S. 6,307,100, **2001**.

- (58) Weakley, G. K. Ph.D., University of Florida, Gainesville, Fl., **2002**.
- (59) Liu, C., Xingkai, Y., Ruiyun, Z., Wu, Y. *J. Mol. Catal. ,A:Chem.* **1996**, *112*, 15.
- (60) Sobkowiak, A., Narog, D., Sawyer, D. T. *J. Mol. Catal. ,A:Chem.* **2000**, *159*, 247.
- (61) Sahle-Demessie, E., Gonzalez, M. A., Enriquez, J., Zhao, Q. *Ind. Eng. Chem. Res.* **2000**, *39*, 4858.
- (62) Kamiya, Y. *Bull. Chem. Soc. Jap.* **1970**, *43*, 830.
- (63) Fukuzumi, S., Ono, Y. *Bull. Chem. Soc. Jap.* **1979**, *52*, 2255.
- (64) Blanchard, H. S. *J. Am. Chem. Soc.* **1960**, *82*, 2014.
- (65) Tsodikov, M. V., Kugel, V. Y., Slivinskii, E. V., Bondarenko, G. N., Maksimov, Y. V., Alvarez, M. A., Hidalgo, M. C., Navio, J. A. *Appl. Catal. ,A-Gen.* **2000**, *193*, 237.
- (66) Hsu, Y. F., Cheng, C. P. *J. Mol. Catal. ,A:Chem.* **1997**, *120*, 109.
- (67) Hsu, Y. F., Cheng, C. P. *J. Mol. Catal. ,A:Chem.* **1998**, *136*, 1.
- (68) He, Y., Wang, R., Liu, Y., Chang, Y., Wang, Y., Xia, C., Suo, S. *J. Mol. Catal. ,A:Chem.* **2000**, *159*, 109.
- (69) Ellis, P. E., Lyons, J. E. *J. Chem. Soc.* **1989**, 1189.
- (70) Moore, K. T., Horvath, I. T., Therien, M. J. *Inorg. Chem.* **2000**, *39*, 3125.
- (71) Middleton, B. S., Ingold, K. U. *Can. J. Chem.* **1967**, *45*, 191.
- (72) Thomas, J. R. *J. Am. Chem. Soc.* **1967**, *89*, 4872.
- (73) Evans, S., Smith, J. R. L. *J. Chem. Soc. ,Perkin Trans. 2* **2000**, *2*, 1541.
- (74) Pohorecki, R., Baldyga, J., Moniuk, W., Podgorska, W., Zdrojkowski, A., Wierzchowski, P. T. *Chem. Eng. Sci.* **2001**, *56*, 1285.
- (75) Hendry, D. G., Russell, G. A. *J. Am. Chem. Soc.* **1964**, *86*, 2368.
- (76) Fujiwara, T., Matsuda, K., Yamamoto, Y. *Inorg. Nucl. Chem. Lett.* **1980**, *16*, 301.
- (77) Gillard, R. D. *Inorg. Chim. Acta* **1979**, *37*, 103.
- (78) Luo, Y. *Handbook of bond dissociation energies in organic compounds*; CRC Press: New York, 2003.

- (79) Beigee, A., Howard, J. A., Scaiano, J. C., Stewart, L. C. *J. Am. Chem. Soc.* **1983**, *105*, 6120.
- (80) Birnbaum, E. R., Grinstaff, M. W., Labinger, J. A., Bercaw, J. E., Gray, H. B. *J. Mol. Catal. ,A:Chem.* **1995**, *104*, L119.
- (81) Schlesener, C. J., Amatore, C., Kochi, J. K. *J. Am. Chem. Soc.* **1984**, *106*, 3567.
- (82) Hage, J. P., Powel, J. A., Sawyer, D. T. *J. Am. Chem. Soc.* **1995**, *117*, 12897.
- (83) Durham, B., Wilson, S. R., Hodgson, D. J., Meyer, T. J. *J. Am. Chem. Soc.* **1980**, *102*, 600.
- (84) Konig, E. *Coord. Chem. Rev.* **1968**, *3*, 471.
- (85) Konig, E., Ritter, G., Madeja, K. *J. inorg. nucl. Chem.* **1981**, *43*, 2273.
- (86) Fox, D. B., Hall, J. R., Plowman, R. A. *Aust. J. Chem.* **1962**, *15*, 235.
- (87) Gallois, B., Real, J., Hauw, C., Zarembowitch, J. *Inorg. Chem.* **1990**, *29*, 1152.
- (88) Figg, D. C., Herber, R. H., Potenza, J. A. *Inorg. Chem.* **1992**, *31*, 2111.
- (89) Comprehensive Coordination Chemistry; Wilkinson, G., ed. Pergamon Press: New York, 1987.
- (90) Parton, R. F., Neys, P. E., Jacobs, P. A., Sosa, R. C., Rouxhet, P. G. *J. Catal.* **1996**, *164*, 341.
- (91) Parton, R. F., Peere, G. J., Neys, P. E., Jacobs, P. A., Claessens, R., Baron, G. V. *J. Mol. Catal. ,A:Chem.* **1996**, *113*, 445.
- (92) Nam, W., Ho, R., Valentine, J. S. *J. Am. Chem. Soc.* **1991**, *113*, 7052.
- (93) Zang, Y., Kim, J., Dong, Y., Wilkinson, E. C., Appleman, E. H., Que, L. *J. Am. Chem. Soc.* **1997**, *119*, 4197.
- (94) Duelund, L., Hazell, R., McKenzie, C. J., Nielsen, L. P., Toftlund, H. *J. Chem. Soc. , Dalton Trans.* **2001**, 152.
- (95) Simaan, J., Dopner, S., Banse, F., Bourcier, S., Boucchoux, G., Boussac, A., Hilderbrand, P., Girerd, J. J. *Eur. J. Inorg. Chem.* **2000**, 1627.
- (96) Kim, J., Larka, E., Wilkinson, E. C., Que, L. *Angew. Chem. Int. Ed.* **1995**, *34*, 2048.
- (97) Kim, J., Harrison, R. G., Kim, C., Que, L. *J. Am. Chem. Soc.* **1996**, *118*, 4373.

- (98) MacFaul, P. A., Ingold, K. U., Wayner, D. D. M., Que, L. *J. Am. Chem. Soc.* **1997**, *119*, 10594.
- (99) MacFaul, P. A., Arends, I. W. C. E., Ingold, K. U., Wayner, D. D. M. *J. Chem. Soc., Perkin Trans. 2* **1997**, *2*, 135.
- (100) Klopstra, M., Hage, R., Kellogg, R. M., Feringa, B. L. *Tet. Lett.* **2003**, *44*, 4581.
- (101) Menage, S., Vincent, J. M., Lambeaux, C., Chottard, G., Grand, A., Fontecave, M. *Inorg. Chem.* **1993**, *32*, 4766.
- (102) Menage, S., Wilkinson, E. C., Que, L., Fontecave, M. *Angew. Chem. Int. Ed.* **1995**, *34*, 203.
- (103) Bennett, D. A. Ph.D., University of Florida, Gainesville, FL, **2002**.
- (104) Palucki, M., Pospisil, P. J., Zhang, W., Jacobson, E. N. *J. Am. Chem. Soc.* **1994**, *116*, 12135.
- (105) Larrow, J. F., Jacobson, E. N. *Org. Synth., Vol 75* **1998**, *75*, 1.
- (106) Campbell, K. A., Lashley, M. R., Wyatt, J. K., Nantz, M. H., Britt, R. D. *J. Am. Chem. Soc.* **2001**, *123*, 5710.
- (107) Cavallo, L., Jacobsen, H. *Angew. Chem. Int. Ed.* **2000**, *39*, 589.
- (108) Palucki, M., Finney, N. S., Pospisil, P. J., Guler, M. L., Ishida, T., Jacobson, E. N. *J. Am. Chem. Soc.* **1998**, *120*, 948.
- (109) Palucki, M., Pospisil, P. J., Zhang, W., Jacobson, E. N. *J. Am. Chem. Soc.* **1994**, *116*, 9333.
- (110) Hughes, D. L., Smith, G. B., Liu, J., Dezeny, G. C., Senanayake, C. H., Larsen, R. D., Verhoeven, T. R., Reider, P. J. *J. Org. Chem.* **1997**, *62*, 2222.
- (111) Collin, J. P., Sauvage, J. P. *Inorg. Chem.* **1986**, *25*, 135.
- (112) Hagen, K. S. *Inorg. Chem.* **2000**, *39*, 5867.
- (113) Schilt, A. A. *J. Am. Chem. Soc.* **1960**, *82*, 3000.
- (114) Konig, E., Madeja, K. *Inorg. Chem.* **1967**, *6*, 48.
- (115) Wu, R., Poyraz, M., Sowrey, F. E., Anson, C. E., Wocadlo, S., Powell, A. K., Jayasooriya, U. A., Cannon, R. D., Nakamoto, T., Katada, M., Sano, H. *Inorg. Chem.* **1998**, *37*, 1913.

BIOGRAPHICAL SKETCH

The author was born August 19th, 1974 in Split, Croatia. She is the second child of Ivan and Duska Bitanga. At the age of 12 Ana and her family immigrated to the United States. She resided in Fort Lee, New Jersey for the first 12 years of living in America. In 1998 Ana graduated from Kean University with a BS degree in chemistry. The following year Ana worked in industry, first with International Specialty Products followed by a position at Union Carbide working on Ziegler-Natta polymerization catalysts. During the summer of 1999 Ana married Elon Ison and together they moved to Gainesville, Florida to pursue a graduate career at the University of Florida. In December of 1999 Ana gave birth to a beautiful baby girl Mya and continued to pursue her doctorate. Under the advisement of Dr. David Richardson, Ana completed her Ph.D. in Spring 2004. She is looking forward to a rewarding career in teaching and research.

I certify that I have read this study and that in my opinion it conforms to acceptable standards of scholarly presentation and is fully adequate, in scope and quality, as a dissertation for the degree of Doctor of Philosophy.



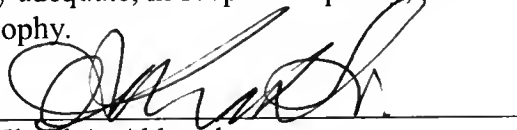
David E. Richardson, Chairman
Professor of Chemistry

I certify that I have read this study and that in my opinion it conforms to acceptable standards of scholarly presentation and is fully adequate, in scope and quality, as a dissertation for the degree of Doctor of Philosophy.



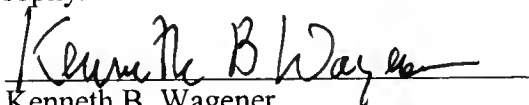
Daniel R. Talham
Professor of Chemistry

I certify that I have read this study and that in my opinion it conforms to acceptable standards of scholarly presentation and is fully adequate, in scope and quality, as a dissertation for the degree of Doctor of Philosophy.



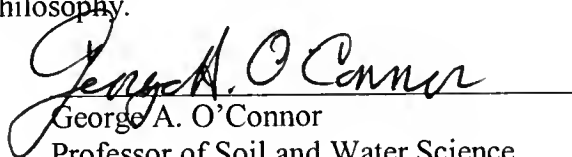
Khalil A. Abboud
Associate Research Scientist of Chemistry

I certify that I have read this study and that in my opinion it conforms to acceptable standards of scholarly presentation and is fully adequate, in scope and quality, as a dissertation for the degree of Doctor of Philosophy.



Kenneth B. Wagener
Professor of Chemistry

I certify that I have read this study and that in my opinion it conforms to acceptable standards of scholarly presentation and is fully adequate, in scope and quality, as a dissertation for the degree of Doctor of Philosophy.



George A. O'Connor
Professor of Soil and Water Science

This dissertation was submitted to the Graduate Faculty of the Department of Chemistry in the College of Liberal Arts and Sciences and to the Graduate School and was accepted as partial fulfillment of the requirements for the degree of Doctor of Philosophy.

August, 2004



Dean, Graduate School



.I 85

